RESEARCH

Utah Department of Transportation - Research Division
Keeping Utah Moving
4501 South 2700 West - P.O. Box 148410 - SLC,UT 84114-8410

Report No. UT-17.23

EVALUATION OF CURVE FITTING TECHNIQUES FOR ESTIMATING END OF PRIMARY CONSOLIDATION SETTLEMENT: Provo Westside Connector Project, Utah

Prepared For:

Utah Department of Transportation
Research Division

Submitted By:

Brigham Young University
Construction Management

Authored By:

Clifton B. Farnsworth, Ph.D., P.E
Christopher Pister

March 2017
Final Report

DISCLAIMER

The authors alone are responsible for the preparation and accuracy of the information, data, analysis, discussions, recommendations, and conclusions presented herein. The contents do not necessarily reflect the views, opinions, endorsements, or policies of the Utah Department of Transportation or the U.S. Department of Transportation. The Utah Department of Transportation makes no representation or warranty of any kind, and assumes no liability therefore.

TECHNICAL REPORT ABSTRACT

1. Report No. UT-17.23	2. Government Accession No. N/A	3. Recipient's Catalog No. N/A	
4. Title and Subtitle EVALUATION OF CURVE FITTING TECHNIQUES FOR ESTIMATING END OF PRIMARY CONSOLIDATION SETTLEMENT: Provo Westside Connector Project, Utah		5. Report Date March 2017	
		6. Performing Organization Code N/A	
7. Author(s) Clifton B. Farnsworth, Christopher Pister		8. Performing Organization Report No. N/A	
9. Performing Organization Name and Address Construction Management Program Brigham Young University 230 SNLB Provo, Utah 84602		10. Work Unit No. 5H07615H	
		11. Contract or Grant No. 15-8263	
12. Sponsoring Agency Name and Address Utah Department of Transportation 4501 South 2700 West P.O. Box 148410 Salt Lake City, UT 84114-8410		13. Type of Report & Period Covered Final August 2014 – March 2017	
		14. Sponsoring Agency Code PIC UT13.404	
15. Supplementary Notes Prepared in cooperation with the Utah Department of Transportation and the U.S. Department of Transportation, Federal Highway Administration			

16. Abstract

This final report discusses the installation of magnet extensometer instrumentation associated with the Provo Westside Connector construction project in Utah County, Utah. The settlement monitoring instrumentation was installed in August of 2014, and embankment construction followed shortly thereafter. Maximum fill height was achieved in early December 2014. This report includes a summary of the installation, readings that were collected, and the modeling work regarding the settlement monitoring and end-of-primary settlement projections. Two different curve fitting techniques were evaluated in this research: using the standard primary consolidation equations and the finite difference equations for estimating the end of primary consolidation settlement. For the site investigated, the curve fitting techniques proved to be somewhat problematic because the soil layers had small magnitudes of settlement and the transition between primary and secondary settlement was not readily apparent during the evaluation of real time field data. Using the finite difference equations also proved somewhat problematic in trying to fit the full record of field data based on all of the different stages of loading.

17. Key Words Magnet Extensometers, Finite Difference, Primary Consolidation Settlement, Foundation Instrumentation	18. Distribution Statement Not restricted. Available through: UDOT Research Division 4501 South 2700 West P.O. Box 148410 Salt Lake City, UT 84114-8410 www.udot.utah.gov/go/research		23. Registrant's Seal N/A
19. Security Classification (of this report) Unclassified	20. Security Classification (of this page) Unclassified	21. No. of Pages 101	22. Price N/A

TABLE OF CONTENTS

LIST OF TABLES

LIST OF FIGURES

vi

UNIT CONVERSION FACTORS

SI* (MODERN METRIC) CONVERSION FACTORS

APPROXIMATE CONVERSIONS TO SI UNITS

Symbol	When You Know	Multiply By	To Find	Symbol
LENGTH				
in	inches	25.4	millimeters	mm
ft	feet	0.305	meters	m
yd	yards	0.914	meters	m
mi	miles	1.61	kilometers	km
AREA				
in^2	square inches	645.2	square millimeters	mm^2
ft^2	square feet	0.093	square meters	m^2
yd^2	square yard	0.836	square meters	m^2
ac	acres	0.405	hectares	ha
mi^2	square miles	2.59	square kilometers	km^2
VOLUME				
fl oz	fluid ounces	29.57	milliliters	mL
gal	gallons	3.785	liters	L
ft^3	cubic feet	0.028	cubic meters	m^3
yd^3	cubic yards	0.765	cubic meters	m^3
NOTE: volumes greater than 1000 L shall be shown in m^3				
MASS				
oz	ounces	28.35	grams	g
lb	pounds	0.454	kilograms	kg
T	short tons (2000 lb)	0.907	megagrams (or "metric ton")	Mg (or "t")
TEMPERATURE (exact degrees)				
^oF	Fahrenheit	5 (F-32)/9 or (F-32)/1.8	Celsius	^oC
ILLUMINATION				
fc	foot-candles	10.76	lux	lx
fl	foot-Lamberts	3.426	candela/m^2	cd/m^2
FORCE and PRESSURE or STRESS				
lbf	poundforce	4.45	newtons	N
lbf/in^2	poundforce per square inch	6.89	kilopascals	kPa

APPROXIMATE CONVERSIONS FROM SI UNITS

Symbol	When You Know	Multiply By	To Find	Symbol
LENGTH				
mm	millimeters	0.039	inches	in
m	meters	3.28	feet	ft
m	meters	1.09	yards	yd
km	kilometers	0.621	miles	mi
AREA				
mm^2	square millimeters	0.0016	square inches	in^2
m^2	square meters	10.764	square feet	ft^2
m^2	square meters	1.195	square yards	yd^2
ha	hectares	2.47	acres	ac
km^2	square kilometers	0.386	square miles	mi^2
VOLUME				
mL	milliliters	0.034	fluid ounces	fl oz
L	liters	0.264	gallons	gal
m^3	cubic meters	35.314	cubic feet	ft^3
m^3	cubic meters	1.307	cubic yards	yd^3
MASS				
g	grams	0.035	ounces	oz
kg	kilograms	2.202	pounds	lb
Mg (or "t")	megagrams (or "metric ton")	1.103	short tons (2000 lb)	T
TEMPERATURE (exact degrees)				
^oC	Celsius	1.8C+32	Fahrenheit	^oF
ILLUMINATION				
lx	lux	0.0929	foot-candles	fc
cd/m^2	candela/m^2	0.2919	foot-Lamberts	fl
FORCE and PRESSURE or STRESS				
N	newtons	0.225	poundforce	lbf
kPa	kilopascals	0.145	poundforce per square inch	lbf/in^2

*SI is the symbol for the International System of Units. (Adapted from FHWA report template, Revised March 2003)

EXECUTIVE SUMMARY

This final report discusses the installation of magnet extensometer instrumentation associated with the Provo Westside Connector construction project in Utah County, Utah. The settlement monitoring instrumentation was installed in August of 2014, and embankment construction followed shortly thereafter. Maximum fill height was achieved in early December 2014. This report includes a summary of the installation, readings that were collected, and the modeling work regarding the settlement monitoring and end-of-primary settlement projections. Two different curve fitting techniques were evaluated in this research including using the standard primary consolidation equations and the finite difference equations for estimating the end of primary consolidation settlement.

The following conclusions were developed from this research project: 1) having a good instrumentation program is an important element in being able to make critical decisions regarding the achievement of sufficient primary consolidation settlement. Magnet extensometer data is especially useful for being able to identify the compression associated with specific soil layers; 2) curve fitting techniques are somewhat problematic in that they currently do not accurately account for the transition between primary consolidation and secondary settlement; and 3) accounting for multiple stages of construction is somewhat problematic using the finite difference procedure. This problem seems to be enhanced for slower paced construction and smaller magnitudes of settlement achieved under a smaller embankment load. From this research it is recommended that for construction projects with potential critical subsurface settlements, construction teams should establish an open transparent approach to determining the end of primary consolidation. These effective channels of communication with all team members can minimize the effects associated with lengthy and/or "tricky-to-estimate" data. Discussions should also include the idea of risk and the potential effects of post-construction settlement (meaning the magnitude and rate) on the constructed facility.

1.0 INTRODUCTION

1.1 Problem Statement

A recently completed UDOT research project investigated the use of the finite difference technique in estimating consolidation settlement of foundation soils with horizontal drainage. This particular project demonstrated that the finite difference technique has potential to be used in conjunction with magnet extensometer data for projecting the end of primary consolidation settlement during construction of large earth embankments over soft saturated cohesive soils. The results of this research project are summarized in the UDOT Research Report No. UT-08.11 entitled *Evaluation of Methods for Determining Horizontal Drainage Properties of Soft Clayey Soils* (Farnsworth and Bartlett, 2009). However, this research study utilized pre-existing I-15 reconstruction data (from the Salt Lake Valley 1998-2002). Therefore, this subsequent research project was initiated to field verify the proposed finite difference technique during an actual construction project.

1.2 Objectives

This research had two principal objectives: first, utilize the finite difference technique to evaluate the consolidation settlement of embankment foundation soils using magnet extensometer data, and second, continue to evaluate the general use of magnet extensometer data for estimating the end of primary consolidation settlement of subsurface clay layers bounded by a magnet extensometer.

1.3 Scope

The construction project selected to perform this research on was the Provo Westside Connector project, a new roadway connecting interstate I-15 at University Avenue in Provo, Utah with the Provo municipal airport. This site was selected for the following reasons: 1) An extensive evaluation of consolidation settlement had previously been performed at this location in conjunction with the construction of the I-15 southbound access to University Avenue (i.e., the bridge over the interstate); 2) The current project design indicated that prefabricated vertical

(PV) drains would not penetrate to a sufficient depth to mitigate drainage of deeper clay layers, and for these reasons the upper layer would consolidate much more rapidly than the lower layers strictly due to drainage path; and 3) The construction project had elected to install a magnet extensometer as part of their settlement monitoring program, and therefore this research project benefitted from saving some of the cost associated with instrumentation installation.

The primary means of field instrumentation necessary to perform this research was a magnet extensometer. Magnet extensometers are especially useful in evaluating differences in consolidation rates for subsurface clay layers. The most common method currently used to project the end-of-primary consolidation settlement either from surface date or in conjunction with magnet data is the Asaoka technique (Asaoka, 1978). However, more recently the finite difference technique in conjunction with magnet extensometers has been demonstrated to be a useful technique in projecting time of consolidation settlement as field data is obtained (Farnsworth et al., 2014). This particular construction project was selected as an ideal location to field verify the results of the previous study and to evaluate the use of this methodology in real time.

This final report is the principal deliverable submitted in conjunction with this research project. This report includes a brief summary of the instrumentation installation, an overview of data collection, methods associated with modeling construction settlement, and analysis of methods for projecting end of primary consolidation.

1.4 Outline of Report

This report is organized in the following manner:

- Introduction
- Instrumentation Installation
- Research Modeling
- Conclusions

3

2.0 INSTRUMENTATION INSTALLATION

2.1 Overview

This Instrumentation Installation chapter includes an overview of the soil conditions encountered at the University Avenue Interchange, the magnet extensometers that were installed at this location, and the data collection procedures used for this research.

2.2 I-15 - University Avenue Interchange Soil Conditions

The Provo Westside Connector is located adjacent to the shoreline of Utah Lake along the North side of the Provo Bay. The subsurface soils are typical of the soils located in the center of the valleys along much of the Wasatch Front, including the soft thick Lake Bonneville Clay layers. Therefore, the alignment is located primarily upon clayey lacustrine and alluvium deposits (IGES, 2013). The largest new embankment on the project occurs at the Provo University Avenue Interchange where the Provo Westside Connector intersects I-15. Figure 2-1 shows the initial construction site from the interstate (looking to the west) during PV drain installation. At this location a large embankment (more than 20 ft tall), flanked by mechanically stabized earth (MSE) walls, was constructed.

Figure 2-1 Provo Westside Connector site during PV drain installation.

The geotechnical profile at this site can be found in project boring B-22 and cone penetrometer sounding CPT-07. These two profiles were obtained during the geotechnical investigation, were included in the project geotechnical report (IGES, 2013), and are the most proximate geotechnical information to the instrumentation for this project. These profiles were utilized in helping assemble the subsurface profile for the finite difference modeling performed with this research and are included within Appendix A.

The geotechnical reports indicated that primary consolidation settlements at this location could take between several months to several years, depending upon the construction techniques used to address the time dependent settlement behavior of the foundation soils (IGES, 2013). To speed up the time to achieve end-of-primary settlement, prefabricated vertical (PV) drains were used at this site, thus allowing radial drainage of the upper clay soils. However, drains were only installed to a depth of approximately 65 feet, and so any consolidation settlement initiated within the deeper clay layers would undergo vertical drainage.

2.3 Magnet Extensometer Installation

The Provo Westside Connector Project included the design and installation of two magnet extensometers at the research site, one in the center of the full height embankment and the other at the same project station adjacent to the MSE wall just outside the embankment boundary. Although project decisions were made independent of the research, the project team gave approval for the research team to assist them in the design and installation of the magnet extensometers for this research. Therefore, the design of the magnet elevations was made as a joint venture between Brigham Young University (BYU) and IGES. The elevations of the magnets were designed to correspond with the principal interface between major soil layers.

Magnet installation was subcontracted through the project team and the work performed by Bedke Engineering. Drilling for the first magnet extensometer began in early August 2014. Shortly after installation of the critical center extensometer, it was discovered that the elevation of two of the magnets had slipped during installation and therefore were not located at the soil layer boundaries as designed. The driller, therefore, drilled an adjacent hole about five feet away, and replaced these critical magnets. Attempting to correlate these two holes with each other has

5

made the interpretation of the data more challenging. Either way, these two holes serve as the principal source of data to be utilized for this research. Figure 2-2 shows a cone penetrometer (CPT) profile with the corresponding elevations of the magnets that were installed. Eight magnets (datum through 7) were installed in the initial hole (M-2) and four magnets (datum through 3) in the replacement hole (M-2A). Each magnet extensometer consists of standard installation, including a 1-inch diameter PVC center pipe with corresponding spider magnets.
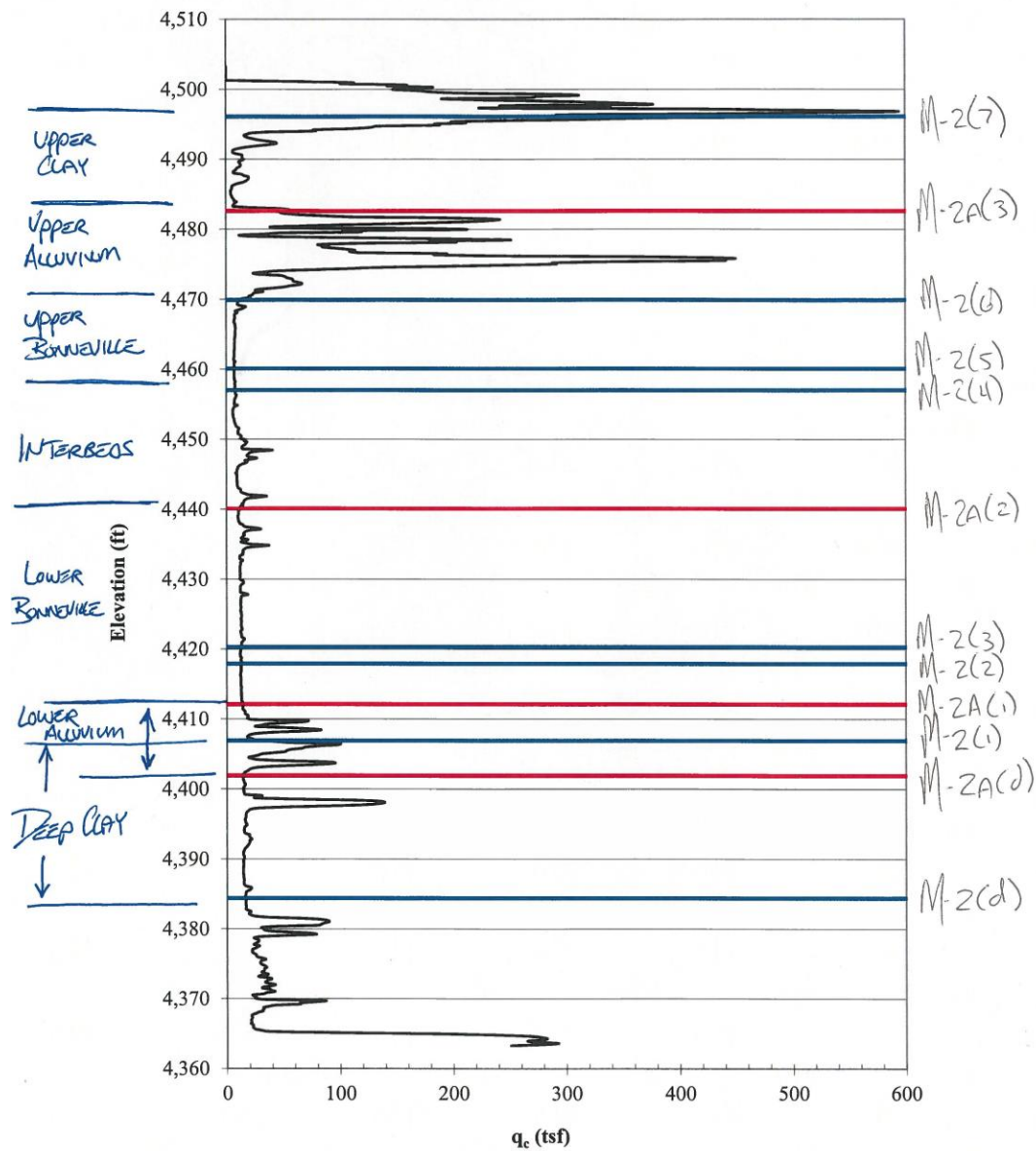
Figure 2-2 Elevations of the magnets compared with CPT layer profile.

Construction of the embankment and MSE walls began in mid-August 2014, following final installation of the instrumentation. It should be noted that although not used for this research project, additional project instrumentation included an additional magnet extensometer outside of the construction footprint adjacent to the north face of the MSE wall, tube-type settlement manometers, vibrating wire settlement sensors, and vibrating wire piezometers. Embankment construction was halted several times over the course of the next several months, to ensure that stability of the foundation soils was maintained. Therefore, full-height embankment and surcharge (approximately 23.3 ft) was not reached until mid-December 2014. Figure 2-3 shows the protective concrete barriers that housed each of the two extensometers within the center of the embankment fill. Similarly, Figure 2-4 shows the full height MSE wall and surcharge along the south face of the new roadway. It is at this point during construction (meaning full-height) where the settlement data for modeling is most useful.

Figure 2-3 Location of the magnet extensometers in the center of the embankment.

Figure 2-4 Full-height MSE wall and surcharge along the south side of the new roadway.

2.4 Magnet Extensometer Data

Each spider magnet consisted of an upper and lower magnet, with a slight gap between them. Therefore, three different readings were obtained for each magnet: the deepest reading (corresponding with the bottom of the lower magnet when the probe is first triggered), a center reading (the average depth of the "gap between the beeps"), and the shallowest reading (corresponding with the top of the upper magnet when the probe sensor switches off). Although only one complete set of these readings was needed for this research, obtaining all three readings provided redundancy in the data and helped minimize erroneous readings.

Data gathering commenced immediately upon completion of the magnet extensometer installation. IGES began taking readings on August 14, 2014, and upon the initiation of the research project BYU began gathering readings on September 9, 2014. IGES chose to read the extensometers only once a week for project purposes. However, to ensure a richer dataset,

especially during the early steep portion of the primary consolidation settlement curve, BYU chose to supplement the dataset by reading multiple days each week. The initial intention was to combine these two datasets. However, it was soon discovered that the two probes being used actually measured the top and bottom of the magnets differently. To account for this difference, a couple of simultaneous tests using both probes were performed, so that all of the magnet readings could be correlated with each other and the early part of the settlement curve could be established. Thereafter, only the BYU data was utilized to eliminate the potential introduction of any additional error into the dataset by differences in the two probes. Unfortunately, the BYU probe broke late in the data collection, and had to be sent back to the manufacturer for repairs. Therefore, the latter part of the settlement curve has also been supplemented with the IGES data. The complete set of raw IGES and BYU data for both extensometers is included in Appendix B. Figure 2-5 and Figure 2-6 show plots of the interpreted settlement data for both extensometers.
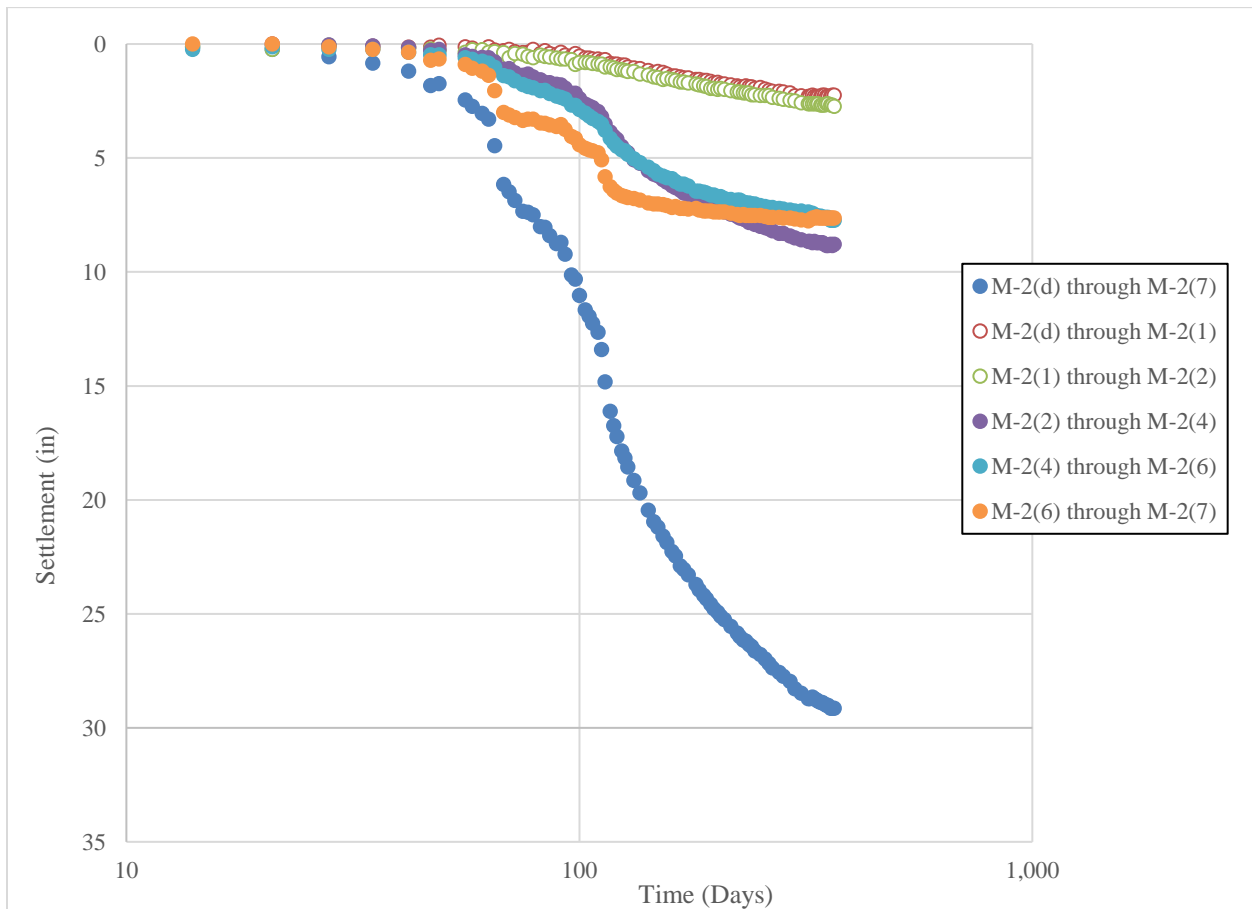
Figure 2-5 Magnet extensometer M-2 settlement data.

9
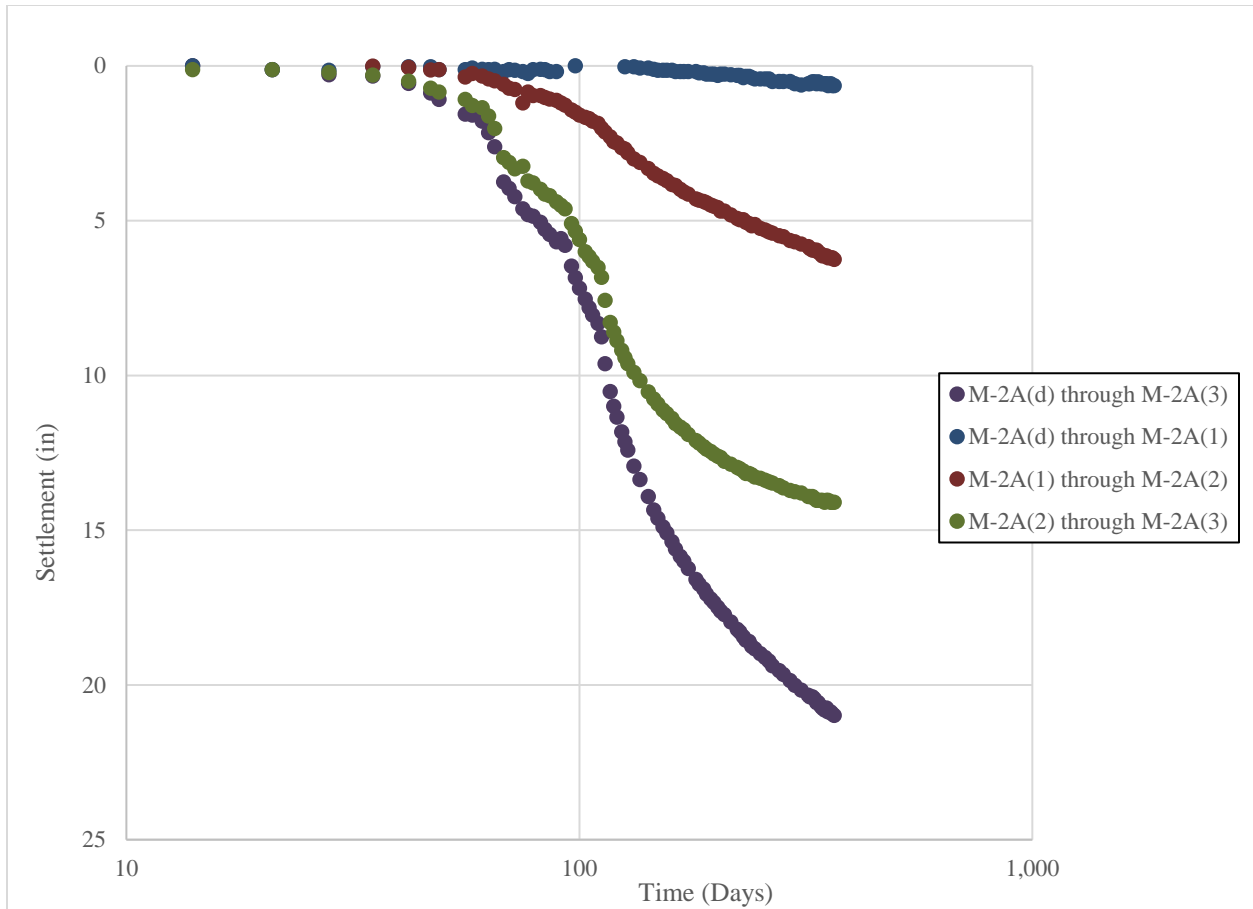
Figure 2-6 Magnet extensometer M2-A settlement data.

The settlement data shown in Figures 2-5 and 2-6 has been divided into layers and shows the compression occurring between adjacent magnets. Tables 2-1 and 2-2 identify which magnet layers generally correspond with which subsurface clay layers, based on the information shown in Figure 2-2. These layers generally consist of (from top to bottom) upper clay, upper alluvium, upper Lake Bonneville clay, interbedded sands and silts, lower Lake Bonneville clay, lower alluvium, and deep clay layers. Figure 2-5 shows that the total settlement between the upper and lower magnets within the profile is approximately 30 total inches, essentially a composite settlement of all the other layers. Additionally, the majority of the subsurface compression occurred (with a nearly equal split) between the upper clay and both Lake Bonneville clay layers. Note that in PV drains extended through each of these three clay layers. The deeper clay layers had significantly less settlement, presumably due to lower induced stresses and perhaps higher preconsolidation pressures. The symbols used for the lower two layers in Figure 2-5 have been

10

left unshaded to indicate vertical drainage occurring due to the installation depth of the PV drains discontinuing within the lower Lake Bonneville clay layer (above these layers). Figure 2-6 follows a similar trend, although with very different layer boundary conditions. The principal challenge associated with this research is noted in Figure 2-5 and Figure 2-6; each of the curves appears to have essentially reached a log-linear state, i.e. achieved end-of-primary consolidation and exhibiting secondary settlement. However, each is further showing very different rates of compression along the log-linear portion of the curve. These challenges will be further discussed in later sections of this report.

Table 2-1 Magnet extensometer and soil layers for M-2.

Magnet Layers	Corresponding Layers
M-2(d) through M-2(7)	complete settlement profile
M-2(d) through M-2(1)	deep clay, lower alluvium
M-2(1) through M-2(2)	lower alluvium, lower Bonneville clay
M-2(2) through M-2(4)	lower Bonneville clay, interbeds, upper Bonneville clay
M-2(4) through M-2(6)	upper Bonneville clay
M-2(6) through M-2(7)	upper alluvium, upper clay

Table 2-2 Magnet extensometer and soil layers for M-2A.

Magnet Layers	Corresponding Clay Layer
M-2A(d) through M-2A(3)	lower alluvium through upper Bonneville clay
M-2A(d) through M-2A(1)	lower alluvium
M-2A(1) through M-2A(2)	lower Bonneville clay, interbeds
M-2A(2) through M-2A(3)	interbeds, upper Bonneville clay, upper alluvium

3.0 RESEARCH MODELING

3.1 Overview

This Research Modeling chapter includes a brief background regarding the settlement conditions encountered at this site, the research efforts for using curve fitting techniques in conjunction with the Asaoka projection method, and the research efforts for using the finite difference technique.

3.2 Background

When constructing large embankments over thick, soft, clay soils, the resulting consolidation settlement of those foundation soils can be very large. Figure 3-1 shows that the magnitude of settlement for the Westside embankment of the existing Provo University Avenue interchange, constructed in 1999, was just under 60 inches of construction and post-construction settlement (Farnsworth and Bartlett, 2012). Note the significant rate and corresponding magnitude of secondary settlement observed at this location – approximately six inches over a seven year post-construction period.
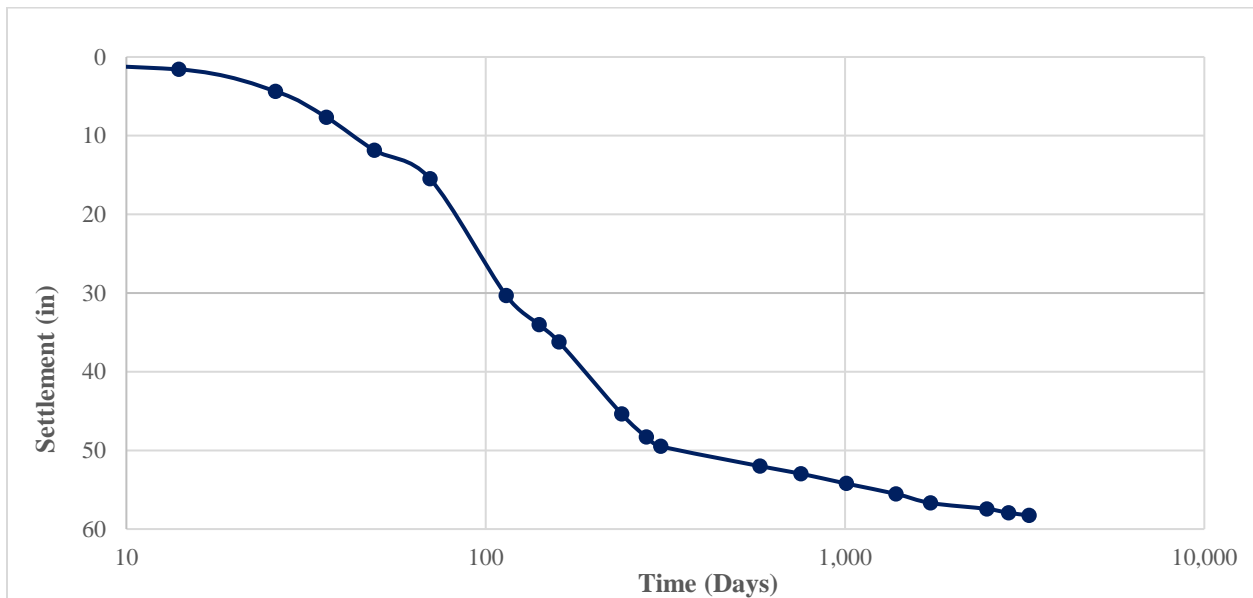
Figure 3-1 Earlier University Avenue embankment construction settlement.

The fill and surcharge height for the proposed embankment evaluated in this research was not nearly as tall as the University Avenue bridge; however, the settlement was still projected to be on the order of 24 inches (IGES, 2013). To reduce the waiting time associated with primary consolidation settlement, vertical drains are often installed within the foundation soils to allow for horizontal drainage of the excess pore water pressures. Unfortunately, at this location the PV drains were only installed to a depth of about 65 ft, thus the upper layers should consolidate under radial consolidation conditions while the lower layers will consolidate under vertical consolidation conditions. Farnsworth and Bartlett (2009) describe the similarities and differences between radial and vertical consolidation.

3.3 Asaoka Projections and Curve Fitting Data

Field performance data of primary consolidation settlement plotted versus lapsed time can be used to identify when primary consolidation has essentially been completed. However, field performance data is often used in conjunction with the Asaoka projection method (Asaoka, 1978) to provide an estimate of the end of primary settlement and the time for primary consolidation for each settlement period. This technique is particularly useful where the settlement data does not provide a definitive assessment of the completion of primary consolidation on log-time vs. settlement plots. Estimating the end of primary consolidation with field data using the Asaoka method is described in Farnsworth and Bartlett (2009). This method is also useful for projecting end of primary consolidation for individual layers when used in conjunction with magnet extensometer data (Farnsworth et al., 2014). This method was one of the principal methods utilized by the geotechnical consultant on the Provo Westside Connector project.

Performing Asaoka projections requires a couple of key assumptions. First, the compression is based on a constant load. To account for this, the settlement for the maximum loading case begins only once the maximum load is reached. An ideal consolidation curve would be achieved if the load was placed instantaneously; however, loads are placed in sequential manner, one lift at a time. The faster this process occurs, the more closely the resultant settlement curve will resemble the theoretical consolidation curve. Unfortunately, the rate of construction is not always rapid. In many cases, foundation stability will also affect the speed

13

with which embankment construction can occur. Second, the Asaoka projection method requires that readings be taken at equivalent time intervals (for example every seven days). For both of these reasons, curve fitting methods are typically used to match a theoretical consolidation curve with the actual field data.

The theoretical curve is typically a plot of the one-dimensional consolidation curve for either the vertical or radial drainage case, respectively. The radial equation (Barron, 1948; Sridharan et al., 1996) is used for layers undergoing consolidation with PV drains and can be represented by:

Equation 3-1: $\qquad U_r = 1 - e^{-8T_r/F(n)}$

where U_r is the degree of consolidation with radial drainage. T_r is the dimensionless time factor for consolidation with radial drainage, and is a function of the coefficient of radial (or horizontal) consolidation, c_h, the drainage path length, H, and the time of consolidation, t. The parameter $F(n)$ can be found using the following equation:

Equation 3-2: $\qquad F(n) = ln(n)*[n^2/(n^2\text{-}1)] - [(3n^2\text{-}1)/(4n^2)]$

where n is the drain spacing ratio defined by:

Equation 3-3: $\qquad n = d_e / d_w$

where d_e is the diameter of influence and d_w is the diameter of the drain. The diameter of influence is essentially two times the effective radial drainage path. For this research, a drain spacing ratio, n, of 30 was used. Farnsworth et al. (2009) further demonstrate and describe how to calculate the drain spacing ratio parameter. To calculate the average degree of consolidation with vertical drainage, or U_v, for the vertical consolidation case (clay layers lying below the influence of the PV drains), the equation given by Siviram and Swamee (1977) for U_{av} varying from 0 to 100% (Das 1983) is used:

Equation 3-4: $\qquad U_{av}\% = 100*[(4T_v/\pi)^{0.5}] / [1+(4T_v/\pi)^{2.8}]^{0.179}$

where T_v is the dimensionless time factor for two-way vertical drainage. This factor is a function of the coefficient of vertical consolidation, c_v, the drainage path length, H, and the time of consolidation, t.

3.3.1 Curve Fitting Application

Curve fitting is best achieved by using four different parameters to define the curve and match the existing field data: the time that constant load was achieved, the corresponding value of settlement at the start of constant load, an estimated value of total settlement, and a partial term from the dimensionless time parameter T_v or T_r (c_v/H^2 within the parameter T_v or c_h/d_e^2 within the parameter T_r, respectively). The estimated value of total settlement serves as the ending anchor point for the curve, and the coefficient of consolidation to distance squared ratio essentially controls the curvature of the resulting plot. The latter two values are adjusted until the theoretical settlement curve closely fits the field data. Figure 3-2 shows an example of the radial curve fit to the compression data between magnet 6 and 7 for magnet extensometer M2.
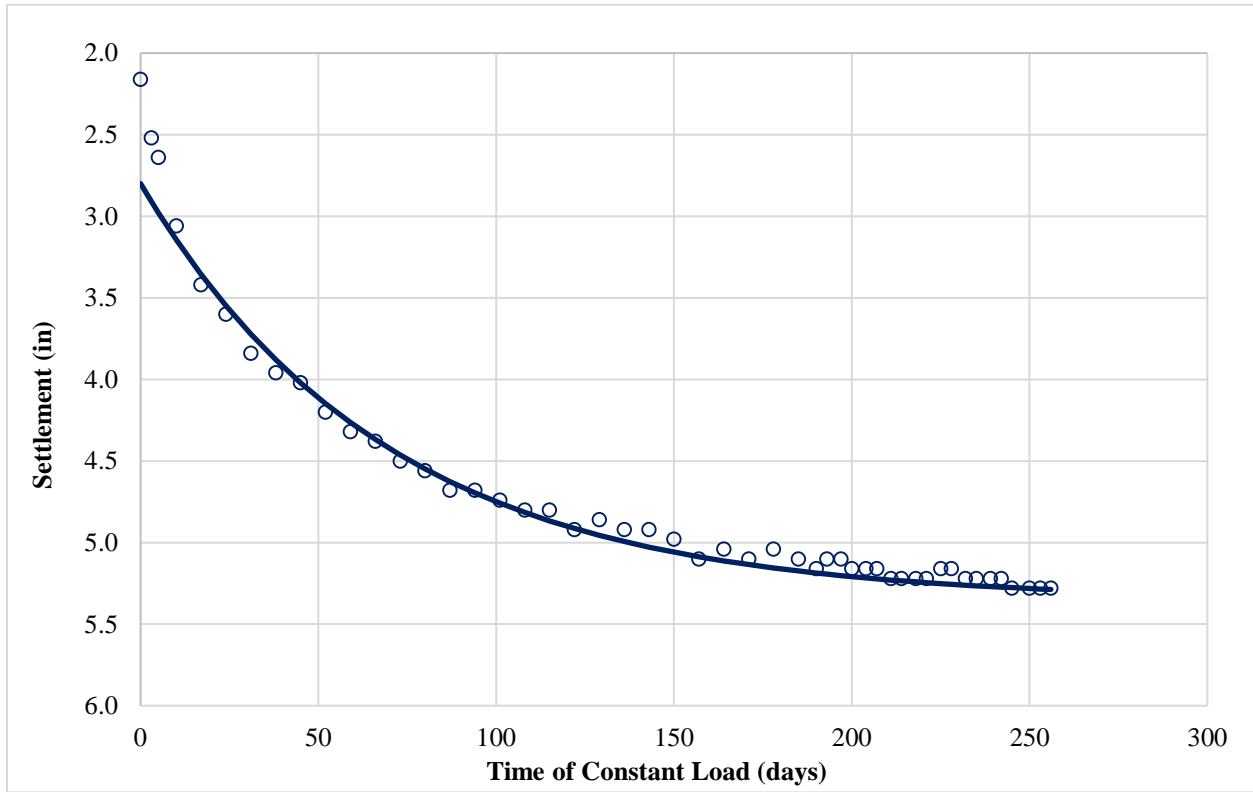
Figure 3-2 Fitted radial curve for the compression data between magnets 6 and 7.

15

Note that Figure 3-2 is shown with a linear time scale, although a semi log scale can also be used. For this dataset, the constant maximum load was placed at day 109. This point in the dataset became the time zero, as shown on the plot. The beginning anchor point for the fitted curve (settlement at the time of constant load) was 2.8 inches, and the ending anchor point for the fitted curve (estimated total settlement) was 5.35 inches. The value of c_h/d_e^2 was 0.0048. Although the values may vary slightly, individuals performing this curve fitting technique typically come up with similar values. The ending value from the curve then essentially provides an estimate of the total settlement expected. In this case, the project total settlement is 5.35 inches and the current settlement is 5.28 inches, thus projecting another 0.07 inches of consolidation settlement. Both the Asaoka (1978) procedure and extrapolating the fitted curve further can provide an estimate of the time remaining to reach end of consolidation settlement.
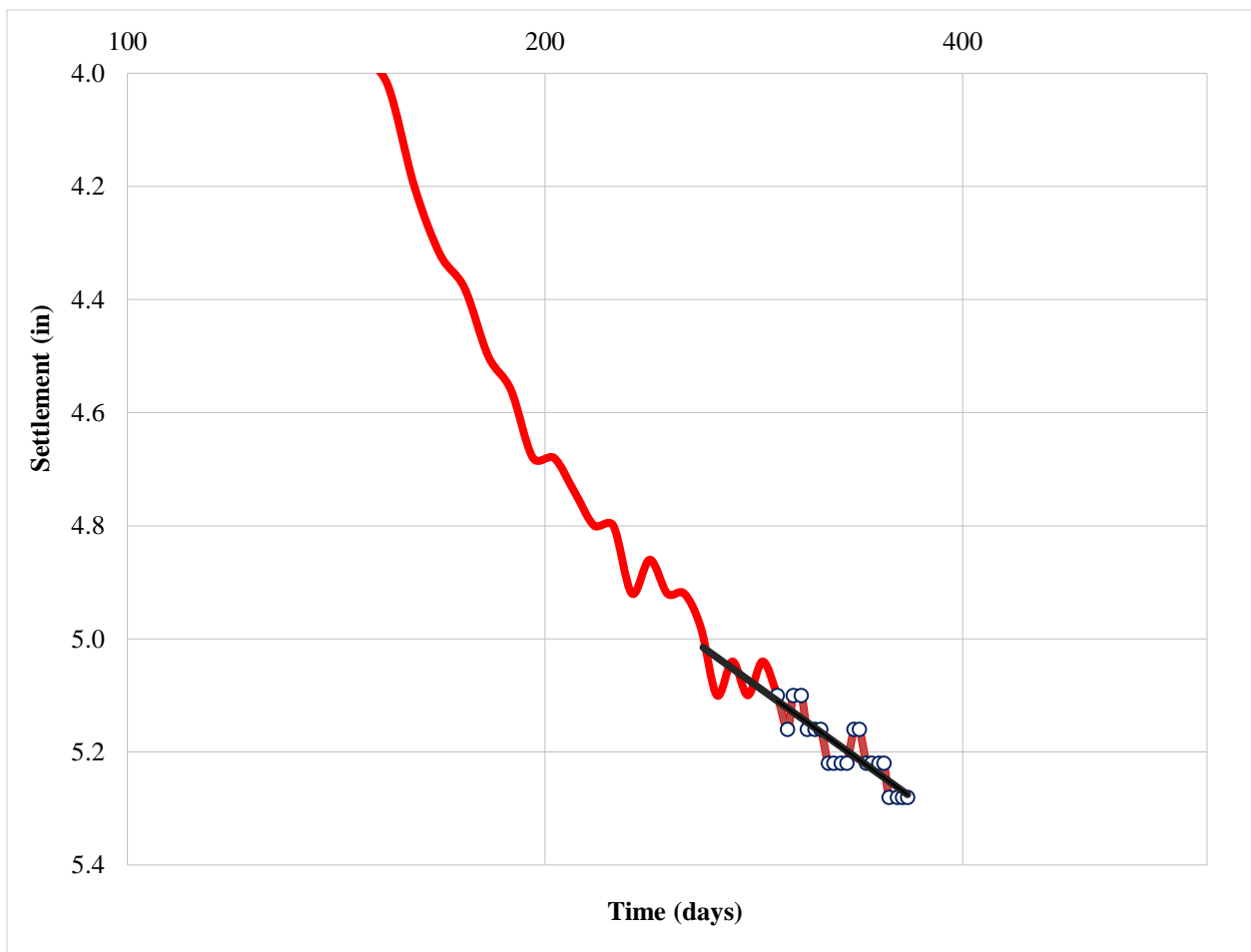
Figure 3-3 Apparent log-linear behavior in the latter portion of fitted radial curve for the compression data between magnets 6 and 7.

An interesting observation was made during this research regarding the curve fitting technique utilized. Although the numbers utilized in this curve fitting exercise provide a reasonable fit with the field data, this process assumed that the end of primary consolidation settlement was not yet reached. However, upon closer investigation of the data (see Figure 3-3), it appears that the latter portion of the data has reached a log-linear trend, thus, indicative of having reached the end of primary consolidation and initiating secondary (or creep) settlement. This is a little tricky to identify and interpret with a great deal of accuracy because of the resolution of accuracy with which the magnet probe can read. However, when zoomed in on the dataset, the curve does appear to have reached a log-linear state of compression. Additional data would help to verify this particular phenomena; however, when making real time data projections, time may not be practical.
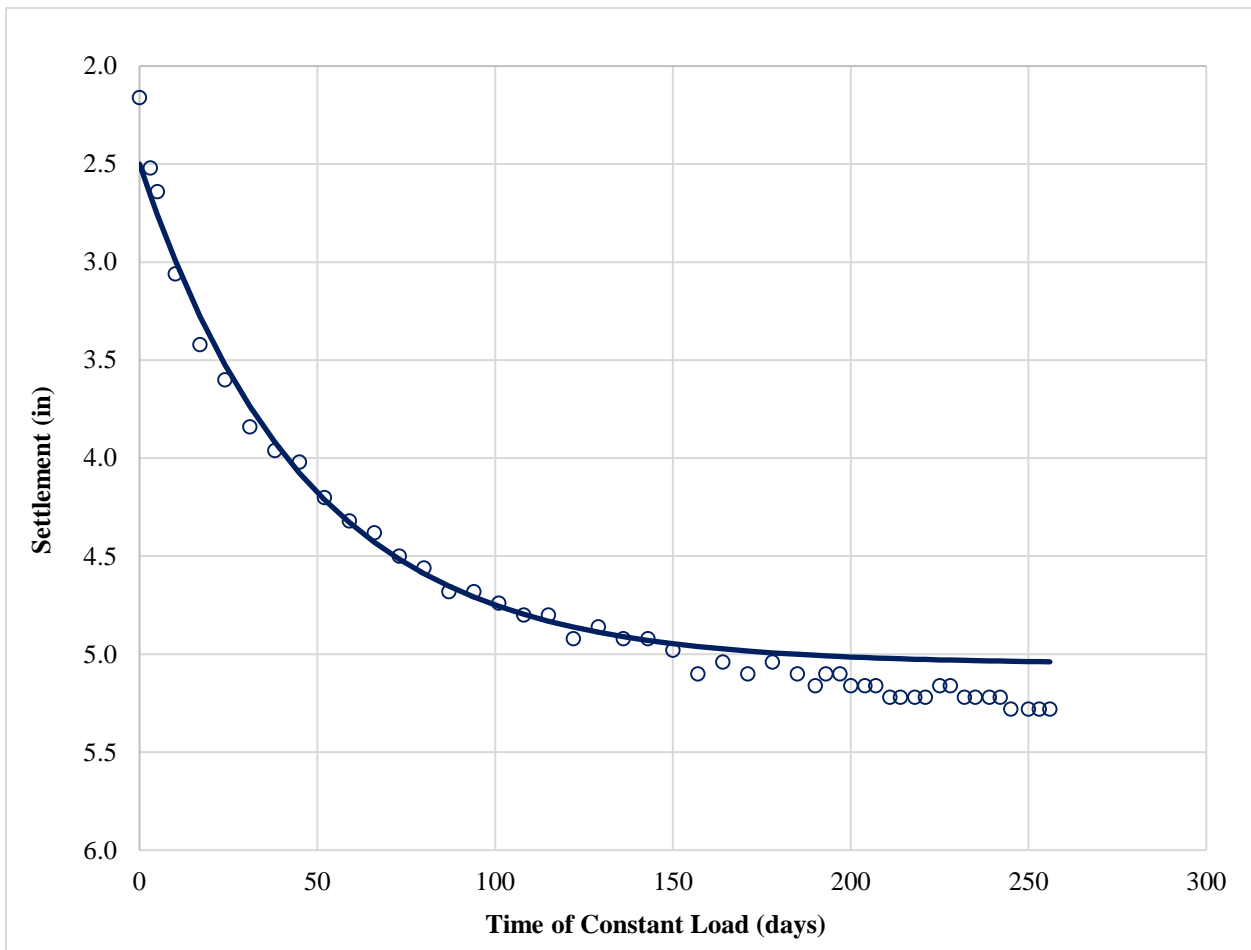
Figure 3-4 Updated fitted curve for the compression data between magnets 6 and 7 assuming end of primary consolidation settlement has already been reached.

17

If this particular curve has indeed reached the end of primary consolidation settlement and is now undergoing secondary settlement, the initial curve fitting would be incorrect. For this example, a log-linear trend line was fitted to the latter portion of the dataset (Figure 3-3), thus identifying the approximate location of end of primary settlement. Using this point as the ending anchor point, and the curve fitting procedure repeated. Figure 3-4 shows these results. The starting point for the constant load remained 109 days, since this value was a function of the fill placement. The parameters used to fit this curve included a beginning anchor point of 2.50 inches, a value of estimated total settlement of 5.05 inches, and a coefficient of consolidation to distance squared ratio of 0.0071. Note that the beginning anchor point fits the dataset better now.

This example demonstrates that the curve fitting technique being used in conjunction with the Asaoka (1978) projection method must carefully consider whether the end of primary consolidation settlement has been reached or not. In the initial part of the example, an estimate suggesting that the end of primary consolidation settlement had not yet been reached was provided. This in turn suggests that additional time is still required to reach the desired level (percentage) of primary settlement. However, the latter half of the example demonstrates that as the soil layers transition from primary consolidation settlement to secondary creep settlement, the curve fitting becomes tricky until sufficient data has been gathered indicating that the data has become log-linear in nature. It should further be noted that two different log-linear portions of the curve develop: the initial linear portion during the heart of primary consolidation and the latter linear portion as the primary consolidation settlement transitions over to post-construction creep settlement. Although only a single example is shown within the body of this report, all of the radial drainage layers within this research exhibited this phenomenon (see the figures shown Appendix C). It should further be noted that the vertical drainage curves (for the deeper clay layers) exhibited the log-linear trend within the early part of the data, as shown within Appendix C. Because of the complexities involved in identifying which portion of the curve is being dealt with, multiple types of instrumentation are necessary to make a truly informed decision regarding the end of primary consolidation settlement. In this case, piezometer data within the clay layers helped support the idea that primary consolidation settlement had been reached, even though the initial curve fitting process was suggesting otherwise.

There are a couple additional observations from this research that need to be acknowledged. The curve fitting process uses equations that completely flatten out when the end of consolidation occurs. In essence, the curve fitting procedure does not have a process that effectively accounts for the shape of the transition between primary consolidation and secondary compression. Rather than flattening, an ideal curve would need to transition to a slope matching the log-linear rate of secondary compression. For large magnitudes of primary settlement (e.g. three to five feet of primary settlement, as explored in previous research on Bonneville Clay deposits) this differential does not appear to be as pronounced. However, for smaller magnitudes of settlement, as seen in the example above, this phenomenon appears to be more pronounces. With regard to this phenomenon, the following conditions may provide situations where curve fitting techniques become more complicated and thus additional caution may be warranted. First, soils expected to consolidate rapidly, especially undergoing radial drainage, would exhibit a more rapid transition from primary consolidation settlement to secondary settlement. Second, for soils where the construction of the embankment is slow and thus takes place over a lengthy period of time, a theoretical consolidation curve assuming immediate loading conditions may not fit the field data as readily. Finally, fitting a curve to field data for clay layers that exhibit smaller magnitudes of settlement can be somewhat problematic.

3.4 Finite Difference Projections

As demonstrated in Farnsworth and Bartlett (2009) and Farnsworth et al. (2014), the finite difference technique can also be used for both design and construction estimation of the time-rate of settlement of foundation soils. The finite difference technique is a more rigorous approach to curve fitting a theoretical curve with measured field data. However, this method can only be used for a location where sufficient characterization of the subsurface settlement and drainage properties has been performed. As with the other curve fitting methods discussed, this method also finds significant benefit in being able to project the settlement for multi-layered systems, where the time and settlement magnitude are projected for individual layers using magnet extensometer data. Although this method may be more rigorous than the traditional curve fitting approach coupled with the Asaoka (1978) method, the principal benefit of this approach is

the potential to account for changes in loading conditions during construction, as opposed to looking only at the data once the maximum loading condition is reached.

The basic finite difference equation for the solution of dissipation of excess pore water pressure for one-dimensional consolidation of a soil layer, considering two-way vertical drainage, can be expressed as:

Equation 3-5: $u_{0,t+\Delta t} = (\Delta t / (\Delta z)^2) * (u_{1,t} + u_{2,t} - 2_{u0,t}) + u_{0,t}$

where u is the excess pore water pressure, Δt is a factor equal to the coefficient of vertical consolidation, c_v, multiplied by the change in time, Δt, and Δz is the change in depth (Das, 1983). In the vertical consolidation equation, node 0 represents the selected node, node 1 represents the adjacent node directly above the selected node, and node 2 represents the adjacent node directly below the selected node. With this equation a linear set of vertical nodes can be used to establish an estimate for the dissipation of excess pore pressures within the subsurface profile, considering vertical drainage. Scott (1963) noted that the value of $\Delta t / (\Delta z)^2$ must remain less than 0.5 for convergence of the solution to take place and that the best approximation of the solution is achieved when the value of $\Delta t / (\Delta z)^2$ is equal to the ratio of 1/6.

The finite difference method can also be used to estimate the dissipation of excess pore pressures for the radial drainage case, as would develop with the use of PV drains. The basic finite difference solution for one-dimensional consolidation considering only radial drainage can be expressed as:

Equation 3-6: $u_{0,t+\Delta t} = (\Delta t / (\Delta r)^2) * \{u_{3,t} + u_{4,t} + [(u_{4,t} - u_{3,t})/2(r/\Delta r)] - 2u_{0,t}\} + u_{0,t}$

where u is the excess pore water pressure, Δt is a factor equal to the coefficient of horizontal consolidation, c_h, multiplied by the change in time, Δt, r is the radius of drainage influence for the PV drain, and Δr is the change in radius (Das, 1983). As with the previous equation, node 0 represents the selected node. However, in this case node 3 represents the adjacent node directly to the left of the selected node, and node 4 represents the adjacent node directly to the right of the selected node. This equation can be used to establish a linear set of horizontal nodes and estimate the dissipation of excess pore pressures within the subsurface profile considering only horizontal drainage. When PV drains are installed both vertical and horizontal drainage occurs. However,

for very thick clay layers (~15 ft) the vertical drainage which would occur only at the upper and lower interfaces can be considered negligible. As identified previously, the value of $\Delta t / (\Delta r)^2$ must remain less than 0.5 for convergence of the solution to take place, with the best approximation of the solution again occurring for $\Delta t / (\Delta r)^2$ equal to the ratio of 1/6.

Because consolidation is a highly nonlinear process, it is important to subdivide relatively thick layers into smaller sublayers. One approach is to simply divide the layer into equal sublayers. Another approach involves using thinner sublayers near the boundaries of the layer, as this is where the settlement occurs the soonest. In either case, the clay layer should be divided into smaller sublayers of approximately 1 ft. Furthermore, an appropriate effective vertical stress should be applied to each sublayer, considering the geometry of the loading condition and layering of the bearing soils. For this research the 1 ft sublayer recommendation was used.

When considering vertical drainage for untreated soils, a vertical one-dimensional finite mesh is established for the complete soil profile. On the other hand, for radial drainage for PV drain treated soils, a horizontal one-dimensional finite mesh is established for each individual sublayer. The appropriate horizontal coefficient of consolidation for each sublayer should be used. The use of back-calculated magnet extensometer data is especially insightful for this situation, because it provides an average horizontal coefficient of consolidation for specific clay layers and also accounts for the smear zone created during PV drain installation (Farnsworth et al., 2014). If this type of data is not available, an assumption has to be made about the smear effects to the horizontal coefficient of consolidation. The horizontal coefficient of consolidation can either be directly adjusted or else a stiffer zone can be placed within the finite difference mesh adjacent to the PV drain to account for the smear effects. In either case, without in situ measurements, the effects must be assumed. For this research, the radial finite difference formula was used in conjunction with magnet extensometer data for the PV drain treated zone to account for radial consolidation occurring in the upper clay layers.

The finite different method is used to generate the dissipation of the excess pore water pressure from the applied loading condition for any given time increment. The effective stress of the soil at each time step then becomes the sum of average dissipated excess pore water pressure through the sublayer and the original in situ effective stress for hydrostatic conditions. Therefore,

the change in void ratio for virgin compression during each time increment can be calculated using the following equation:

Equation 3-7:$\qquad \Delta e = c_c \log (\sigma_{v't+\Delta t} / \sigma_{v(t)})$

For recompression of overconsolidated soils, the same equation can be used, except that c_r (recompression index) is substituted for c_c (compression index). The vertical strain for each sublayer is calculated using:

Equation 3-8:$\qquad \varepsilon_{vi} = \Delta e / (1 + e_o)$

where e_o is the initial void ratio for recompression, or the void ratio at the preconsolidation stress for virgin compression. The settlement for each sublayer is calculated by multiplying the vertical strain of each sublayer by the height of each sublayer, H_i, as given by:

Equation 3-9:$\qquad S_{vi} = \varepsilon_{vi} * H_i$

All of the individual sublayer settlement values can be summed together to produce the total settlement at each calculated time increment, defined by the following equation:

Equation 3-10:$\qquad S_{v\text{-total}} = \sum S_{vi}$

Utilization of this technique is valuable during the design phase, for initial estimation of the anticipated time-rate of settlement. The use of the finite difference technique provides the ability to generate more accurate time estimates for multiple layers consolidating at different rates. It should be noted that it is impractical to consider that loading conditions are instantaneous. The easiest way to account for the time associated with loading is to use an average loading condition over the duration of loading, and then adjust the finite difference model to the complete load at the completion of the loading sequence. This is especially useful for considering the rate of construction and for staged embankment construction utilized to maintain stability of the foundation soils. The finite difference model can be adjusted to account for multiple loading sequences.

Although the finite difference technique can be utilized in design, using it during construction can also be of importance. This research focuses on this application. The finite

difference generated data can be fitted with the actual field settlement data, while accounting for the actual loading conditions (meaning geometry and time). This results in both an estimate of the time to end of primary consolidation settlement and the associated magnitude of settlement. For strictly surface settlement data, a number of assumptions have to be made about the differing consolidation behavior of the various layers. However, for magnet extensometer data, the finite difference method can be utilized to fit the finite difference model with the specific settlement data for each sublayer. This research was based upon that very premise, and serves as a case study in performing this technique during a construction project.

3.4.1 Finite Difference Modeling

This section describes the finite difference model that was set up for this research and describes how the finite difference method was utilized for both radial and vertical drainage attempting to fit field data and further predict the time remaining to end of primary consolidation settlement. The first step is to establish the stress distribution that is applied at the various sublayers based on the geometry of the constructed embankment. The general stress distribution for an embankment load is based on the Boussinesq solution (Das, 1983) for a long embankment, with the geometry shown in Figure 3-5. Width B1 represents the width of the full height portion of the embankment from the centerline of the roadway to the beginning of the embankment slope. Width B2 represents the width of the embankment slope. For this research project, both sides of the embankment were contained by MSE walls. Therefore, the sloped embankment portion shown in Figure 3-5 was not necessary and was not included. The geometric width of the load was then essentially half of the roadway width, with the stress distribution calculated directly beneath the center of the embankment (i.e., beneath the center line, CL).
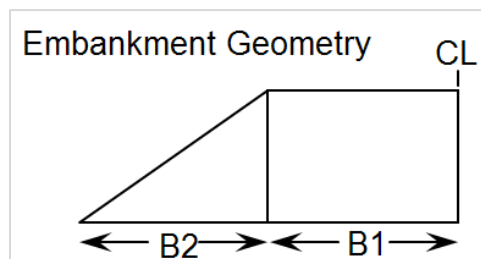
Figure 3-5 Basic geometry of the embankment load to determine stress distribution beneath the constructed embankment.

23

The total stress, q, imposed at the centerline directly beneath the newly constructed full height embankment is calculated using the following formula:

Equation 3-11: $q = \gamma h$

where the height of the embankment, h, is the difference between the top and bottom elevations of the embankment and γ is the unit weight of the embankment material. Figure 3-6 shows an example of the parameters included in the finite difference spreadsheet developed for this research. As shown, other basic parameters necessary for calculating the stress distribution at each sublayer include the elevation of the groundwater table, the unit weight of water, γ_w, and the thickness, Δz, of the subsurface layers to be analyzed (Figure 3-6).

	Bottom Elevation	Top Elevation	Width, B1	Width, B2	γ	q
Embankment Fill	ft	ft	ft	ft	lb/ft^3	psf
	4500.0	4505.5	40.0	0.0	120.0	660.0

	Elevation		$\gamma_w =$	62.4	lb/ft^3
Water Table	ft				
	4498.0		$\Delta z =$	1.0	ft

Figure 3-6 Example of parameters necessary for determining stress distribution beneath the constructed embankment.

The next step within the finite difference modeling technique involves constructing the soil profile. The finite difference model will only be as accurate as the information utilized to construct the soil profile. Therefore, high quality investigation data is necessary for effective modeling. Figure 3-7 shows an example of the top two soil layers (upper alluvium and upper Bonneville clay) included in the finite difference spreadsheet developed for this research. The first principle layer in the soil profile is the Upper Alluvium (Figure 2-2). Because this layer is granular the entire layer is lumped into one sublayer. The next principal layer in the in the soil profile is the Upper Clay layer (Figure 2-2). This is one of the critical clay settlement layers and so it is broken down into individual sublayers with a thickness of 1 ft. The other parameters necessary for the modeling include the soil properties moist unit weight, γ (for soils above the

water table), saturated unit weight, γ_{sat} (for soils below the water table), compression index, c_c, the recompression index, c_r, the initial void ratio, e_o, and the overconsolidation ratio (OCR). These soil parameters should initially come from actual investigation data whenever possible. For this research, these soil parameters were obtained from the geotechnical investigation and laboratory report for this project (IGES, 2013). Table 3-1 shows all of the different soil layer parameters used for the finite difference modeling performed in this research. Note that the OCR is not shown in Figure 3-7, but rather is incorporated later into the spreadsheet in Figure 3-8.

Layer	Sublayer	Bottom Elevation ft	Top Elevation ft	γ lb/ft^3	γ_{sat} lb/ft^3	c_r	c_c	e_o	
Upper Alluvium	1	4494.0	4500.0	110.0	120.0				Magnet
Upper Clay	A1	4493.0	4494.0		115.0	0.0100	0.1000	1.300	7
Upper Clay	A2	4492.0	4493.0		115.0	0.0100	0.1000	1.300	
Upper Clay	A3	4491.0	4492.0		115.0	0.0100	0.1000	1.300	
Upper Clay	A4	4490.0	4491.0		115.0	0.0100	0.1000	1.300	
Upper Clay	A5	4489.0	4490.0		115.0	0.0100	0.1000	1.300	
Upper Clay	A6	4488.0	4489.0		115.0	0.0100	0.1000	1.300	
Upper Clay	A7	4487.0	4488.0		115.0	0.0100	0.1000	1.300	
Upper Clay	A8	4486.0	4487.0		115.0	0.0100	0.1000	1.300	
Upper Clay	A9	4485.0	4486.0		115.0	0.0100	0.1000	1.300	
Upper Clay	A10	4484.0	4485.0		115.0	0.0100	0.1000	1.300	
Upper Clay	A11	4483.0	4484.0		115.0	0.0100	0.1000	1.300	
Upper Clay	A12	4482.0	4483.0		115.0	0.0100	0.1000	1.300	
Upper Clay	A13	4481.0	4482.0		115.0	0.0100	0.1000	1.300	
Upper Clay	A14	4480.0	4481.0		115.0	0.0100	0.1000	1.300	6

Figure 3-7 Example of soil profile for upper soil layers used in this research.

Table 3-1 Magnet extensometer and PV drain treated soil layers for M-2.

Soil Layer	Bottom Elevation (ft)	Top Elevation (ft)	γ (pcf)	γ_{sat} (pcf)	c_r	c_c	e_o	OCR
Upper Alluvium	4494	4500	110	120	-	-	-	1
Upper Clay	4480	4494	-	115	0.01	0.10	1.30	1.70
Granular Interbed	4470	4480	-	120	-	-	-	1
Upper Bonneville Clay	4460	4470	-	115	0.20	0.65	1.30	1.70
Lower Bonneville Clay	4418	4460	-	115	0.03	0.30	1.27	1.32

The next step involves determining the stress distribution throughout the entire soil profile and the resulting compression for each sublayer. Figure 3-8 shows the example spreadsheet for the top two layers (alluvium and upper clay layer), corresponding with the previous figures. Note that the values shown are calculated for the midheight of each sublayer. The first column, σ'_{v1i}, is used to calculate the initial vertical effective stress at the midheight of each sublayer prior to the embankment loading. This is performed with Equation 3-11, accumulating the weight of each sublayer throughout the profile, and using effective stress parameters for sublayers beneath the groundwater table. The thickness column gives the height of each sublayer, and the z_i column gives the depth to the midheight of each sublayer.

σ'_{v1i} (midheight)	Thickness	z_i	$\Delta\sigma/q$ (midheight)	$\Delta\sigma'_{vi}$ (midheight)	σ'_{v2i}	*OCR	σ'_{pi}	Δe Calcs	Δe	$\Delta\varepsilon$	Δh	
psf	ft	ft		psf	psf		psf				ft	
277.6	6.0	3.0	1.000	659.9	937.5	1	277.6	0.000	0.000	0.000	0.000	INCHES
476.7	1.0	6.5	0.998	658.8	1135.5	1.70	810.4	0.017	0.017	0.007	0.007	0.48
529.3	1.0	7.5	0.997	658.2	1187.5	1.70	899.8	0.014	0.014	0.006	0.006	
581.9	1.0	8.5	0.996	657.5	1239.4	1.70	989.2	0.012	0.012	0.005	0.005	
634.5	1.0	9.5	0.995	656.5	1291.0	1.70	1078.7	0.010	0.010	0.004	0.004	
687.1	1.0	10.5	0.993	655.3	1342.4	1.70	1168.1	0.008	0.008	0.004	0.004	
739.7	1.0	11.5	0.991	653.9	1393.6	1.70	1257.5	0.007	0.007	0.003	0.003	
792.3	1.0	12.5	0.988	652.4	1444.7	1.70	1346.9	0.005	0.005	0.002	0.002	
844.9	1.0	13.5	0.986	650.5	1495.4	1.70	1436.3	0.004	0.004	0.002	0.002	
897.5	1.0	14.5	0.983	648.5	1546.0	1.70	1525.8	0.003	0.003	0.001	0.001	
950.1	1.0	15.5	0.979	646.2	1596.3	1.70	1615.2	0.002	0.002	0.001	0.001	
1002.7	1.0	16.5	0.975	643.7	1646.4	1.70	1704.6	0.002	0.002	0.001	0.001	
1055.3	1.0	17.5	0.971	641.0	1696.3	1.70	1794.0	0.002	0.002	0.001	0.001	
1107.9	1.0	18.5	0.967	638.1	1746.0	1.70	1883.4	0.002	0.002	0.001	0.001	
1160.5	1.0	19.5	0.962	634.9	1795.4	1.70	1972.9	0.002	0.002	0.001	0.001	

Figure 3-8 Example of stress distribution and compression calculations.

The $\Delta\sigma/q$ column is used to calculate the Boussinesq stress distribution throughout the soil profile based on the embankment geometry previously discussed. The ratio of stress reduction at the midheight of each sublayer is given by:

Equation 3-12: $\Delta\sigma/q = 2 * 1/\pi * [((B_1+B_2)/B_2)*(\alpha_1+\alpha_2)-(B_1/B_2)*(\alpha_2)]$

where α_1 and α_2 are calculated in radians with:

Equation 3-13: $\alpha1 = \tan^{-1}((B_1+B_2)/z) - \tan^{-1}(B_1/z)$

Equation 3-14: $\alpha2 = \tan^{-1}(B_1/z)$

where B_1 and B_2 have been defined in Figure 3-5, and z is equal to the depth to the layer midheight. Note Equation 3-12 includes a factor of 2 to account for both contributing sides of the embankment load acting above the roadway center line.

The $\Delta\sigma'_{vi}$ column uses the reduction ratio calculated with Equation 3-12 multiplied by the embankment stress, q, to calculate the change in stress at the midheight of each sublayer. The σ'_{v2i} column then adds the initial stress, σ'_{v1i}, with the increase from the embankment stress, $\Delta\sigma'_{vi}$, to provide the final effective vertical stress at the midheight of each sublayer upon reaching equilibrium. The OCR column is used to enter an overconsolidation ratio for each sublayer. These values are then multiplied by the initial stress, σ'_{v1i}, to provide the preconsolidation pressure, σ'_{pi}. The change in void ratio, Δe, is calculated with the following:

Equation 3-15: $\qquad \Delta e = c_r * \log(\sigma'_{v2i} / \sigma'_{v1i})$ $\qquad\qquad\qquad$ for $\sigma'_{v2i} < \sigma'_{pi}$

Equation 3-16: $\qquad \Delta e = c_r * \log(\sigma'_{pi} / \sigma'_{v1i}) + c_c * \log(\sigma'_{v2i} / \sigma'_{pi})$

$\qquad\qquad\qquad\qquad\qquad\qquad\qquad\qquad\qquad\qquad\qquad\qquad$ for $\sigma'_{v2i} \geq \sigma'_{pi}$

where the parameters have been previously defined. The change in vertical strain, $\Delta\varepsilon$, is calculated with the following:

Equation 3-17: $\qquad \Delta\varepsilon = \Delta e / (1 + e_o)$

The corresponding change in height, or primary consolidation settlement for each individual sublayer, is then calculated by:

Equation 3-18: $\qquad \Delta\varepsilon * \Delta h$

The total settlement for each layer is the summation of the calculated individual compression of each sublayer. For the loading conditions shown in the example (Figures 3-16 – 3.18) the total expectant primary consolidation settlement for the upper clay layer is 0.48 inches.

For the case of staged construction, a separate spreadsheet page is used for calculating each loading sequence. The previous figures show the loading scenario for construction stage 1, building to an embankment height of 5.5 ft. These stages must match the construction

sequencing. The corresponding values in the second sheet (for stage 2) should appropriately reflect any changes that may have occurred between the first and second stages. For example, where the preconsolidation pressure was exceeded at each sublayer due to stage one loading, the overconsolidation ratio should be adjusted to a value of 1.0 for the second stage.

The finite difference spreadsheet for this research was set up to include only radial drainage. As indicated previously, some vertical drainage would also occur near the upper and lower granular boundaries of the clay layer. However, for very thick clay layers, the vertical drainage can be considered negligible. With strictly radial drainage occurring, the drainage and subsequent settlement of each soil layer becomes independent of any other soil layers consolidating within the soil profile. The finite difference calculations for radial drainage follow the method described by Das (1983). Several additional parameters must be input into the finite difference calculation sheet. Das (1983) describes using arbitrary reference values (u_R, t_R, and r_R) to enable the user to scale the calculations for pore pressure, $\underline{u}$, time increment, $\Delta\underline{time}$, or radial node increment, $\Delta\underline{r}$. However, for this research these values were set at 1.0.

The parameters necessary to perform the finite difference method include the radius of drainage, r (the drainage path length), Δr (the distance between the finite difference nodes), and Δt (the time step between the finite difference calculations). The horizontal coefficient of consolidation, c_h, for each layer must also be given. A lumped parameter is used in the finite difference equation and is given as:

Equation 3-19: $\Delta\underline{t} / (\Delta\underline{r})^2 = (c_h * \Delta\underline{time} / r_R^2) / (\Delta\underline{r})^2$

For the finite difference calculations to converge, the value of this lumped parameter must be less than 0.5. However, the best solution is found when the value of this lumped parameter is equal to 0.167. Because the solution for each sublayer accumulates for the final settlement results, the time increment must be the same for each of the primary layers. However, because a different value of c_h is used for each of the layers, the resulting lumped parameters will each be different, but should approximate the value of 0.167 as best as possible. The complete explanation for the finite difference method followed for this research can be found in Das (1983). An example of the spreadsheet parameters used in the finite difference analysis for this research is shown in Figure 3-9. Note that the final values of c_h used in the modeling for this

research were 0.001, 0.0005, and 0.0008 in^2/min for magnet layers 6-7, 4-6, and 2-4, respectively.
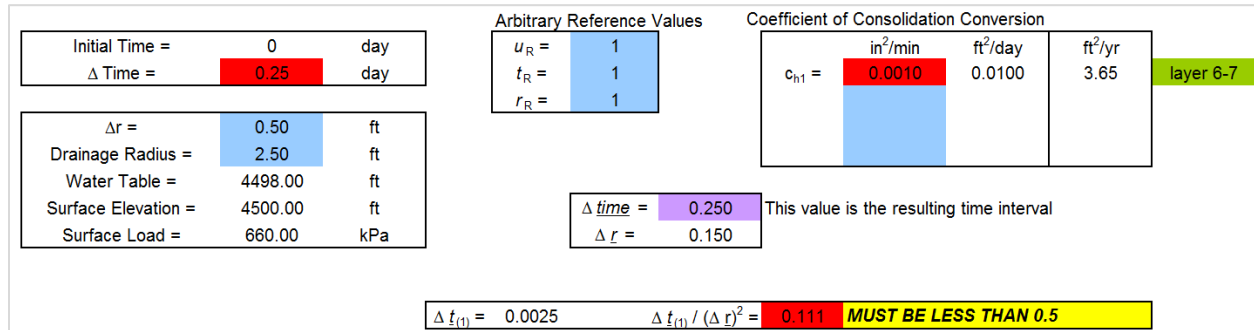
Figure 3-9 Example of finite difference parameters used in this research.

The sublayer parameters necessary to complete the finite difference calculations include the change in load, the initial vertical effective stress, the layer thickness, and the preconsolidation pressure. These values were calculated previously (see Figure 3-8). The finite difference calculations are shown in Figure 3-10 based on the radial drainage finite difference equation (Equation 3-6). The node radius is the width of the drainage path, and the corresponding change in radius for each of the subsequent nodes. The node distance is then the distance of each of the nodes from the drainage boundary to the vertical drain. The parameter r is the node distance adjusted by the arbitrary reference value for the radial adjustment (1.0 - no scaling adjustment made in this research). The finite difference method calculations will provide the same percentage of dissipation of excess pore pressure regardless of the initial value used. Therefore, a value of 100% is used for the load at each node. These percentages are later converted back to the actual excess pore pressure values for each sublayer. The parameter u is the excess pore pressure value adjusted by the arbitrary reference value for the pore pressure adjustment (again 1.0 - no scaling adjustment made in this research). The initial condition line represents 100% excess pore pressure at each node, except for the drainage boundary, where the value becomes 0, or complete dissipation. This occurs at time step 0. The finite difference calculations continue at each node for the given time increment, and the resulting pore pressure dissipation is shown in Figure 3-10 through day 4.

	Δ$t_{(4)}$ / (Δr)² =	0.111	Excess Pore Pressure % Dissipation						
			Finite Difference Based on Excess Pore Pressure						
	Node Radius	ft	2.50	2.00	1.50	1.00	0.50	0.00	
	Node Distance	ft	0.00	0.50	1.00	1.50	2.00	2.50	
	r		0.000	0.500	1.000	1.500	2.000	2.500	
	% Load at Node	%	100.00	100.00	100.00	100.00	100.00	100.00	% Avg
0	u	%	100.00	100.00	100.00	100.00	100.00	100.00	Dissipation
	Initial Condition		0	100.00	100.00	100.00	100.00	100.00	
0.25			0	90.56	100.00	100.00	100.00	100.00	2.10
0.50			0	83.21	99.03	100.00	100.00	100.00	3.95
0.75			0	77.37	97.52	99.90	100.00	100.00	5.60
1.00			0	72.64	95.73	99.66	99.99	100.00	7.11
1.25			0	68.73	93.83	99.28	99.95	100.00	8.49
1.50			0	65.45	91.90	98.79	99.89	99.99	9.77
1.75			0	62.65	90.00	98.19	99.78	99.97	10.98
2.00			0	60.22	88.17	97.51	99.63	99.92	12.11
2.25			0	58.11	86.41	96.77	99.44	99.86	13.19
2.50			0	56.24	84.74	95.99	99.20	99.77	14.21
2.75			0	54.57	83.15	95.18	98.92	99.64	15.19
3.00			0	53.07	81.65	94.34	98.61	99.48	16.13
3.25			0	51.71	80.23	93.50	98.25	99.29	17.04
3.50			0	50.47	78.88	92.66	97.86	99.06	17.91
3.75			0	49.33	77.61	91.81	97.44	98.79	18.76
4.00			0	48.29	76.40	90.97	97.00	98.49	19.58

Figure 3-10 Example of finite difference calculations for change in percent excess pore pressure.

It should be noted that at the furthest distance away from the radial drain (node distance of 2.5 ft), a no drainage boundary condition occurs. The left side of the finite difference equation is mirrored to represent the non-existing right side. When Equation 3-6 is used at this boundary condition it then reduces to the following equation:

Equation 3-20: $u_{0,t+\Delta t} = (\Delta t/(\Delta r)^2)*(2*u_{3,t} - 2u_{0,t}) + u_{0,t}$

The average dissipation of excess pore pressure is the weighted average of pore pressure dissipation across the entire subsurface layer (i.e., the weighted average of pore pressure dissipation at each of the finite difference nodes). This dissipation value is that which is used later for the settlement calculations.

The next step in the estimation of the time-rate of settlement calculations is converting the percentage of excess pore pressure dissipation to the actual value of excess pore pressure dissipation for each time step. This must be performed for each individual sublayer, because each sublayer has a different applied stress since the applied stress decreases with depth. Figure 3-11 shows an example of this for the first seven sublayers of the upper clay layer. These values correspond with the four days' worth of dissipation shown in Figure 3-10. It should also be noted

that in the staged construction process, any remaining excess pore pressure not completely dissipated during the previous stage must be carried over into the next stage. This is simply the addition of the remaining excess pore pressure and the additional excess pore pressure generated from the additional load. The dissipation of excess pore pressure for subsequent stages of construction follow the same finite difference calculations described above.

			EFFECTIVE STRESS CALCULATIONS						
		Sublayer	A1	A2	A3	A4	A5	A6	A7
% Avg		Change Effective Stress	658.84	658.23	657.45	656.49	655.32	653.95	652.36
Dissipation									
2.10			13.83	13.81	13.80	13.78	13.75	13.72	13.69
3.95			26.00	25.98	25.95	25.91	25.86	25.81	25.75
5.60			36.91	36.88	36.83	36.78	36.71	36.64	36.55
7.11			46.82	46.78	46.72	46.65	46.57	46.47	46.36
8.49			55.94	55.88	55.82	55.74	55.64	55.52	55.39
9.77			64.40	64.34	64.26	64.17	64.06	63.92	63.77
10.98			72.32	72.26	72.17	72.07	71.94	71.79	71.61
12.11			79.80	79.72	79.63	79.51	79.37	79.20	79.01
13.19			86.88	86.80	86.70	86.57	86.42	86.23	86.02
14.21			93.63	93.54	93.43	93.29	93.13	92.93	92.71
15.19			100.08	99.99	99.87	99.72	99.55	99.34	99.10
16.13			106.28	106.18	106.05	105.90	105.71	105.49	105.23
17.04			112.24	112.14	112.01	111.84	111.65	111.41	111.14
17.91			118.01	117.90	117.76	117.59	117.38	117.13	116.85
18.76			123.58	123.47	123.32	123.14	122.92	122.67	122.37
19.58			128.99	128.87	128.72	128.53	128.31	128.04	127.72

Figure 3-11 Example of converting percent dissipation to change in effective stress (in psf).

The final step is the calculation of settlement for each sublayer at each time step based on the dissipation of excess pore pressures. The settlement based on the loading conditions prior to exceeding the preconsolidation pressure is calculated using Equation 3-15 with Equations 3-17 and 3-18, as previously discussed. Although three different equations are listed, these calculations were all performed in a single spreadsheet cell. The settlement after the preconsolidation pressure has been exceeded is calculated using Equation 3-16 with Equations 3-17 and 3-18. Figure 3-11 shows an example of the settlement calculations, corresponding to the same four days' worth of finite difference data presented in Figures 3.10 and 3.11. The settlement value of 0.000054 ft (upper left cell) represents the expected settlement occurring in sublayer A1 of the upper clay layer at time interval 0.25 days. The total settlement for the entire upper clay layer would then simply be the accumulation of the settlement values for each of the individual sublayers, calculated for each time step.

Sublayer	A1	A2	A3	A4	A5	A6	A7
Original Load	476.70	529.30	581.90	634.50	687.10	739.70	792.30
Thickness	1.00	1.00	1.00	1.00	1.00	1.00	1.00
Pp	810.39	899.81	989.23	1078.65	1168.07	1257.49	1346.91
Settlement	0.000054	0.000049	0.000044	0.000041	0.000037	0.000035	0.000032
	0.000100	0.000090	0.000082	0.000076	0.000070	0.000065	0.000060
	0.000141	0.000127	0.000116	0.000106	0.000098	0.000091	0.000085
	0.000177	0.000160	0.000146	0.000134	0.000124	0.000115	0.000107
	0.000210	0.000190	0.000173	0.000159	0.000147	0.000137	0.000128
	0.000239	0.000217	0.000198	0.000182	0.000168	0.000157	0.000146
	0.000267	0.000242	0.000221	0.000203	0.000188	0.000175	0.000163
	0.000292	0.000265	0.000242	0.000223	0.000206	0.000192	0.000179
	0.000316	0.000287	0.000262	0.000241	0.000224	0.000208	0.000195
	0.000339	0.000307	0.000281	0.000259	0.000240	0.000223	0.000209
	0.000360	0.000327	0.000299	0.000276	0.000255	0.000238	0.000223
	0.000380	0.000345	0.000316	0.000291	0.000270	0.000252	0.000235
	0.000399	0.000363	0.000332	0.000307	0.000284	0.000265	0.000248
	0.000418	0.000380	0.000348	0.000321	0.000298	0.000278	0.000260
	0.000435	0.000396	0.000363	0.000335	0.000311	0.000290	0.000271
	0.000452	0.000411	0.000377	0.000348	0.000323	0.000301	0.000282

Figure 3-12 Example of settlement calculations (measured in ft) based on excess pore pressure dissipation.

One of the principal purposes of this research was to explore the possibility of using the finite difference method with real time settlement data during a construction project to project the end of consolidation settlement. Previous research (Farnsworth et al., 2014) had demonstrated reasonable accuracy in using the finite difference approach with a two stage settlement plot. Figure 3-13 shows a plot of the settlement data for the consolidation of the clay between magnets 4 and 6 of magnet extensometer M-2 (same data shown in Figure 2-5). Construction of the embankment on this construction project was somewhat sporadic. The raw field data indicates that there are five basic stages where embankment construction has halted, for whatever reason. These transition points between the five different stages occurred at day 28, 61, 96, and 110 (as seen in Figure 3-13). At each one of these points a peak fill height was reached and construction temporarily halted, therefore, initiating a new settlement curve.
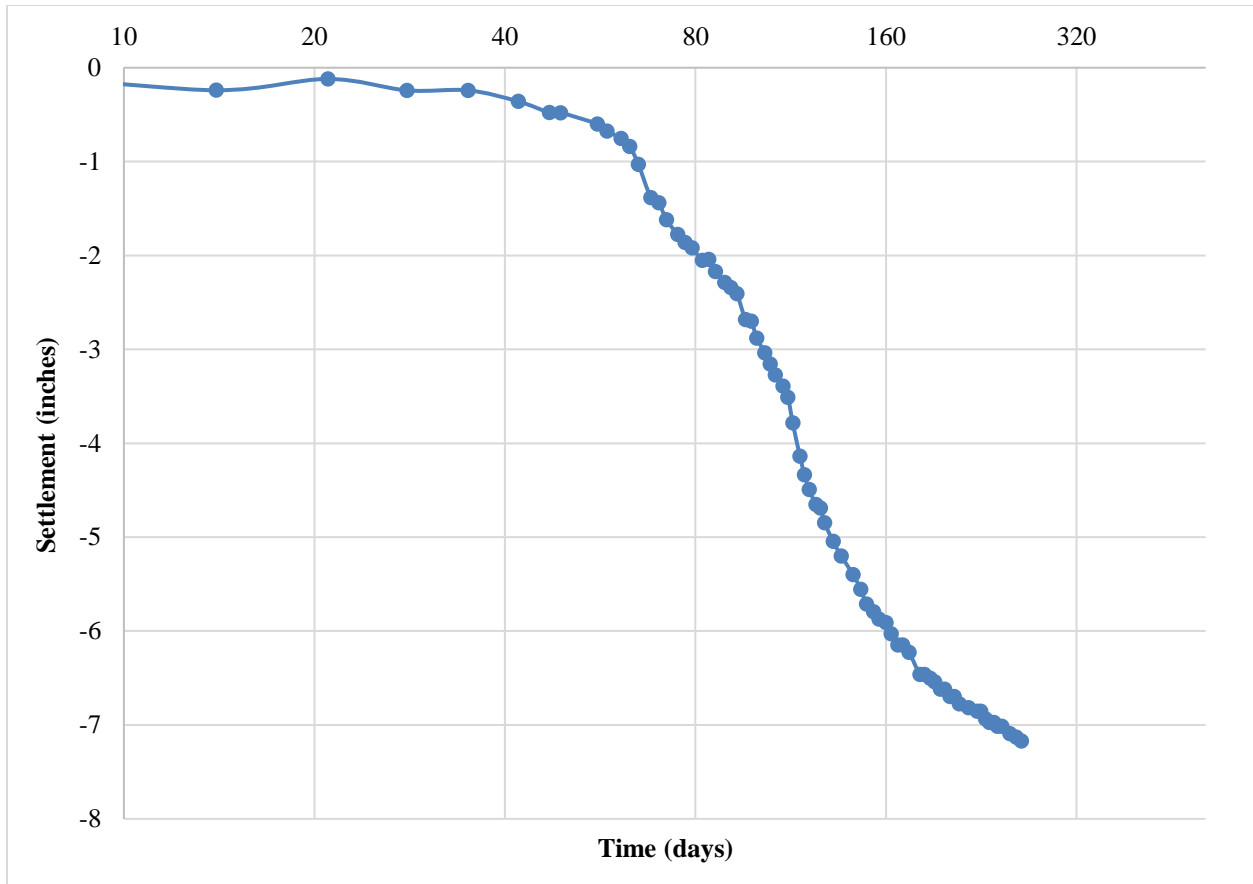
Figure 3-13 Field data for settlement occurring between magnets 4 and 6 (M-2).

The finite difference spreadsheet used in this research was set up using the transition points indicated above as the change in loading conditions. Although the actual embankment placement and corresponding change in loading conditions would have occurred over a multiple day period, for modeling purposes the assumption was made that the next staged load occurred immediately, rather than attempt to model the load placement. This would have required an additional "loading" stage being added between each sustained full height load. The final approach included linking each of the sheets together so that the final accumulated settlement would correspond with the field data, and then modifying the input parameters in the finite difference model until the finite difference generated curves matched the field data. Figure 3-14 shows the results for the settlement data between magnets 4 and 6 of magnet extensometer M-2. This was the best fit that was achieved during the finite difference modeling. All three finite difference generated data is shown in Appendix D.
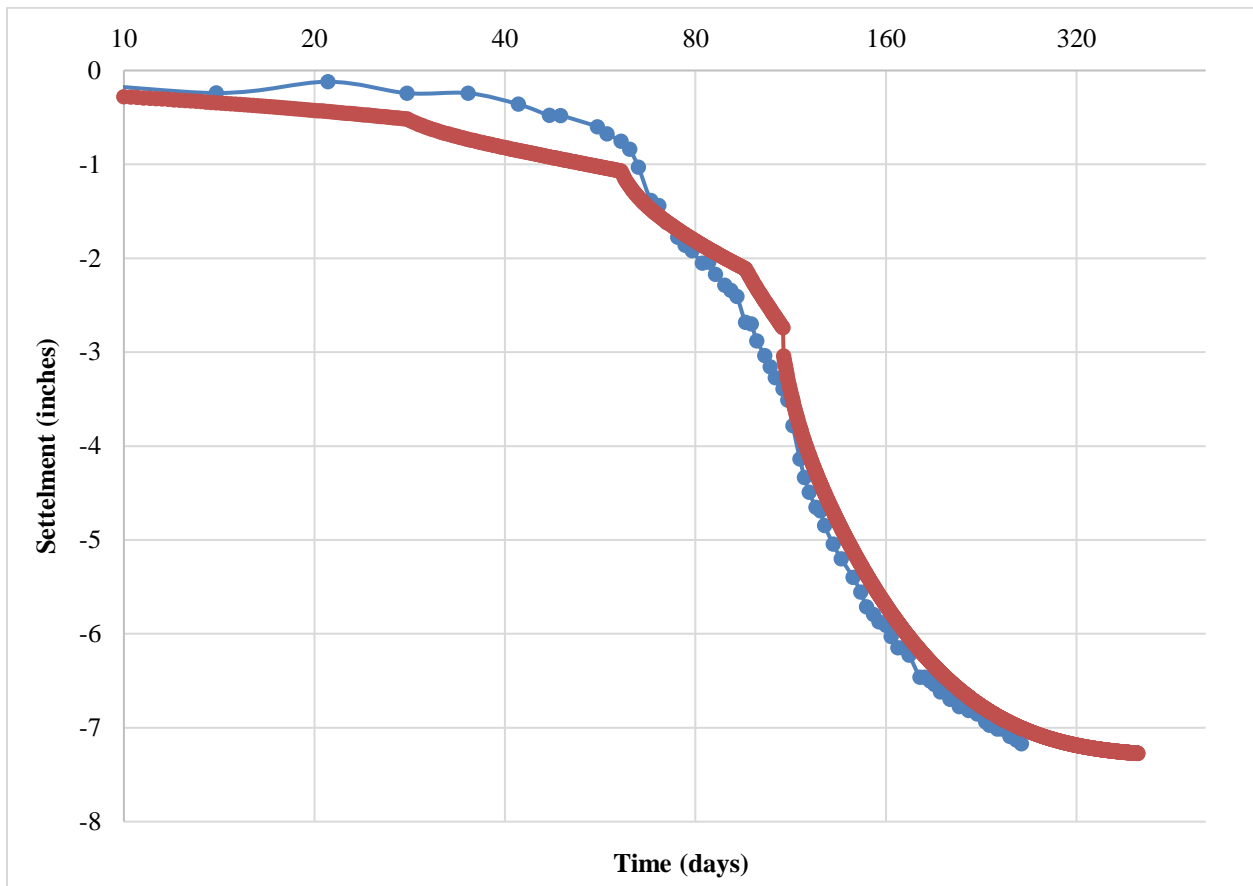
Figure 3-14 Finite difference fitted curves with field data for settlement occurring between magnets 4 and 6 (M-2).

It should be noted that the finite difference modeling was initially developed early in this research and despite the author's best efforts to get the data to fit, the model just didn't seem to want to cooperate. It soon became apparent that many of the same difficulties discussed previously during the curve fitting section of this research became paramount during the modeling portion of the research as well. These problems include using equations that flatten at end of primary consolidation as well as the time of construction occurring between stages and difficulty fitting multiple consolidation curves synchronously. Regarding the shape of the finite difference radial drainage curve, the theoretical curve does not account for the transition that occurs between primary consolidation to secondary creep settlement and the sloped nature of creep settlement (Figure 3-15). On this research project this seems to have been exasperated by soil layers that reached the end of primary consolidation accompanied by quite large rates of secondary settlement, as discussed previously.

Figure 3-15 shows a single finite difference curve fitted with field data for only the final fill stage (i.e. full height embankment). This figure is similar to the data shown in Figure 3-4, except that the finite difference equation was used to fit the data rather than the standard radial consolidation equation. For this particular loading case, the preconsolidation pressure would have been exceeded, and therefore an overconsolidation ratio (OCR) of 1 was used. The other two parameters used in fitting this curve were $c_c = 0.53$ and $c_h = 0.0015$ in^2/min. There are several observations that can be made from this figure. First, it is much easier (and quite possible) to fit a single finite difference curve with a single series of field data, as opposed to attempting to fit the entire loading scenario and complete settlement data (Figure 3-14). Although this latter case is theoretically possible, it appears that fitting the entire range of actual construction data, considering multiple stages of loading, with typical geotechnical design and construction data, may not be practical. However, fitting a single curve, or maybe even two as demonstrated in previous research, is feasible. This seems to be greatly influenced by the rate of construction. Unfortunately, this figure also demonstrates the challenges associated with the theoretical curves that flatten at the end of primary consolidation as opposed to transitioning to a sloped secondary settlement portion of the curve. For early portions of the settlement data this is not nearly as problematic, but does become an issue once the end of primary consolidation is reached. Other research has focused on accurately estimating the rate of secondary settlement. However, the transition zone from primary consolidation settlement to secondary settlement is still not readily defined for the Bonneville soils. Without a defined way to accurately account for this transition zone, curve fitting procedures, especially with the finite difference method, will continue to be somewhat problematic for soils without a well-defined primary consolidation shape (i.e., small magnitudes of settlement and rapid consolidation).
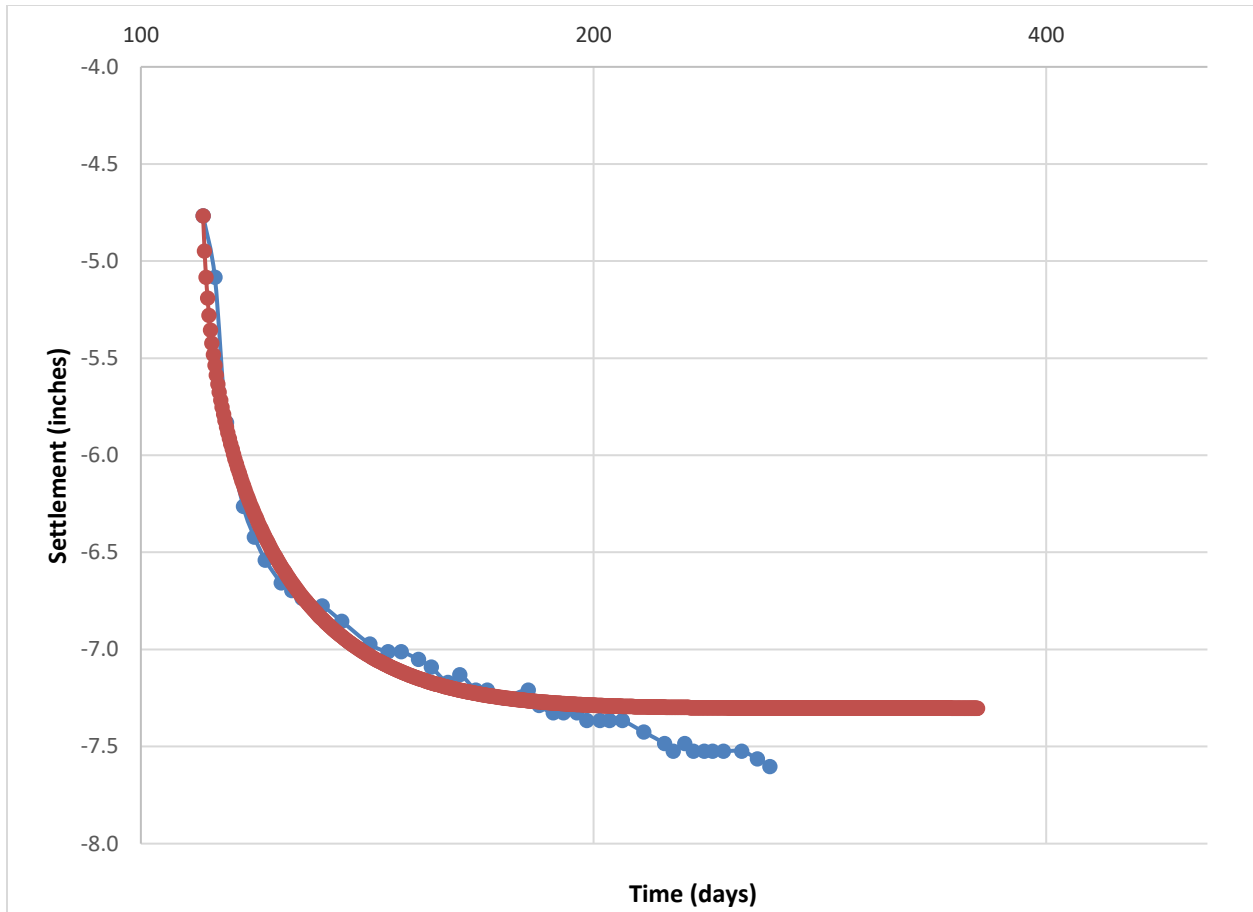
Figure 3-15 Single finite difference fitted curves with field data for settlement occurring between magnets 6 and 7 (M-2) at final fill stage.

Figure 3-1 is the most complete record of field data identifying this transition for the Bonneville soils and indicates that there is a distinct log-linear curve that develops for secondary settlement. The time of construction was critical for the data shown in Figure 3-1. Additionally, a large surcharge was used at this location to reduce the effects of long-term (secondary) settlement. This surcharge was released once the log-linear portion of the consolidation curve began to flatten, thus causing the abrupt transition between primary and secondary settlement near shown in the figure. For this research, it seems that the transition between primary and secondary settlement occurred more naturally, and therefore is not nearly as readily identifiable. This appears to be the most critical dilemma still facing this estimation process. Unfortunately, this research was unable to provide any specific solutions for readily identifying when that transition point is reached, except that perhaps once sufficient secondary settlement has occurred the log-linear trend becomes more discernible. There is one final caution associated with the data

presented in this research that should be noted. Long-term monitoring, and truly being able to establish the secondary settlement rates, was not able to happen in this research because construction related activities removed the magnet extensometers once it was determined by the project team that sufficient primary consolidation settlement of the complete profile had been achieved. This further meant that the true final rate of secondary settlement was unable to be established after pulling the surcharge and constructing the final pavement section a year later.

4.0 CONCLUSIONS

4.1 Summary

The Provo Westside Connector Interchange project was a good construction project to use for evaluating the curve fitting techniques coupled with field data for estimating the end of primary consolidation settlement. On previous research projects, the settlement data has typically been associated with larger embankments, hence causing larger magnitudes of settlement. However, for this research project, a smaller embankment was constructed in an area of virgin soil compression, and provided an ideal scenario for evaluating the use of curve fitting techniques with real time construction data to evaluate the various techniques. Unfortunately, in this case, the research did not provide any conclusive results. Rather the curve fitting process ended up being somewhat problematic, and there was a great deal of debate amongst project team members about whether sufficient consolidation settlement had taken place. However, this in turn has led to several critical observations that should be considered in the future as these techniques continue to be utilized.

4.2 Findings

The following conclusions were developed during this research project and have been discussed throughout this report:

1) Having a good instrumentation program is an important element in being able to make critical decisions regarding the achievement of sufficient primary consolidation settlement. Magnet extensometer data is especially useful for being able to identify the compression associated with specific soil layers. In this project this was especially true for soil layers consolidating with different rates including the upper soil layers treated with PV drains allowing radial drainage and lower soil layers beneath the PV drain treated soil undergoing vertical drainage. Although not detailed in this report since it wasn't part of the research instrumentation, piezometers measuring pore pressure were also used by the project team to help facilitate the decision making for releasing surcharge for pavement construction. A solid instrumentation plan should be part of

38

every construction site over soft soils where ground settlements affect construction schedule.

2) Curve fitting techniques are somewhat problematic in that they currently do not accurately account for the transition between primary consolidation and secondary settlement. This is especially true for both the vertical and radial standard consolidation and finite difference equations that flatten at the end of primary consolidation rather than transitioning to the sloped condition of secondary settlement. This phenomenon was somewhat exasperated on this project because of small magnitudes of primary consolidation settlement, rapid rates of primary consolidation due to PV drain installation, and fairly steep rates of secondary settlement.

3) The principal benefit of using the finite difference method is being able to account for the complete loading scenario and staged construction. However, on this project the construction sequencing was fairly slow and multiple stages of construction occurred. The more stages of construction that occur, the more difficult it becomes to provide an accurate estimate of settlement using the finite difference procedure. For this research five different stages of construction were identified, without a well-defined loading rate between stages. Matching the actual field data was much easier for layers and stages that had not yet exceeded the preconsolidation pressure of the sublayer. Unfortunately, once the preconsolidation pressure had been exceeded, it became more difficult to accurately fit the composite settlement curve with the actual field data. The finite difference approach can still provide reasonable estimates for single staged construction, such as once the peak loading has occurred. Previous research has indicated that reasonable estimates for two consecutive stages with rapid loading between can be achieved using this procedure. Unfortunately, this method appears to be somewhat impractical for multiple stages of construction. This problem appeared to be somewhat enhanced by the slower construction pace, smaller magnitudes of settlement achieved under a smaller embankment, and most certainly the fact that the transition between primary and secondary settlement is not accounted for in the standard finite difference equations.

4.3 Limitations and Challenges

One potential limitation for this research may be using typical one-dimensional equations for real world three-dimensional primary consolidation. These effects were not explored during this research, but it is apparent that maybe they should be. Rather, this research focused on techniques that are currently being utilized on projects, with typical types of geotechnical investigation data and construction related instrumentation. These techniques coupled with additional minor modifications may provide more accurate results with more substantial investigational data (such as providing a better estimate of the rate of secondary settlement, the time associated with radial consolidation, or other radial consolidation parameters). Although the research did not provide any substantial validation of these curve fitting techniques, the techniques continue to be used in industry. However, this research did provide some additional insight into the actual problems associated with using these techniques for estimating the end of primary consolidation.

4.4 Recommendations

Based on this research, the following specific recommendations are given:

1) An open transparent approach to determining the end of primary consolidation and effective channels of communication with all team members can minimize the effects associated with lengthy and/or "tricky-to-estimate" data. Discussions should also include the idea of risk, and the potential effects of post-construction settlement (meaning the magnitude and rate) on the constructed facility.

2) Continue to implement effective instrumentation programs on projgects with potentially critical subsurface settlements. Magnet extensometers should be included in projects with multiple soft compressible clay layers anticipated to consolidate at different rates. This is especially true for sites where PV drains do not extend to a sufficient depth to allow radial drainage in deeper clay layers with anticipated appreciable settlement.

3) Caution should be used when employing any of the curve fitting techniques that do not appropriately account for secondary settlement. Underestimating the percent of

consolidation settlement that has occurred will allow for larger than expected and potentially significant post-construction settlements.

4.5 Further Research

Further research should continue to build upon this work. Estimating the end of primary consolidation is critical for several reasons. First, construction contracts involving time-rate of consolidation challenges typically require that contractors be flexible in waiting until sufficient consolidation settlement has been reached. This can be problematic for construction scheduling and sequencing when accurate estimates cannot be provided. Second, for time critical construction projects, the risk of releasing the embankment for final pavement construction increases. Third, if an embankment is released for final pavement construction early, whether due to misunderstanding the settlement data or for a rushed project, post-construction settlements may exceed tolerable magnitudes. This may be more problematic for embankments that abut next to bridges. Despite the challenges associated with performing this research, several important observations were identified. In turn, this information can ultimately contribute as words of caution and recommendation for those seeking to provide reasonable and accurate estimates of the end of primary consolidation settlement for the Lake Bonneville clay deposits.

5.0 REFERENCES

Asaoka, A. (1978). "Observational Procedure of Settlement Prediction." *Soils and Foundations*, Japan. 18(4), 87-101.

Barron, R. A. (1948). "Consolidation of Fine-Grained Soils by Drain Wells." *Transactions, Volume 113*, American Society of Civil Engineers, Washington D.C., 718-742.

Das, B. M. (1983). Advanced Soil Mechanics, Hemisphere Publishing Corporation, New York.

Farnsworth, C.B. and Bartlett, S.F. (2009). "Evaluation of Methods for Determining Horizontal Drainage Properties of Soft Clayey Soils." *UDOT Research Report No. UT-08.11*, Utah Department of Transportation, Salt Lake City, Utah.

Farnsworth, C.B. and Bartlett, S.F. (2012). "I-15 Reconstruction Long-Term Embankment Monitoring Study – Final Report." *UDOT Research Report No. UT-12.18*, Utah Department of Transportation, Salt Lake City, Utah.

Farnsworth, C.B., Bartlett, S.F., and Lawton, E.C. (2014). "Estimation of Time-Rate of Settlement for Multilayered Clays Undergoing Radial Drainage." *Transportation Research Record: Journal of the Transportation Research Board*, No. 2363, 3-11.

IGES (2013). Geotechnical Report, F-LC49(129) Provo Westside Connector Project, Utah Department of Transportation, Salt Lake City, Utah.

Scott, R. F. (1963). "Principles of Soil Mechanics." Addison-Wesley, Reading, Massachusetts.

Sridharan, A., Prakash, K., and Asha, S. R. (1996) "Consolidation Behavior of Clayey Soils under Radial Drainage." *Geotechnical Testing Journal, Vol. 19, No. 4*, ASTM, Philadelphia, PA, 421-431.

Siviram, B., and Swamee, P. (1977). A Computational Method for Consolidation Coefficient, *Soils and Foundations Journal, Vol. 17, No. 2*, JGS, Tokyo, Japan, 48-52.

APPENDIX A: GEOTECHNICAL PROFILES

This appendix contains the geotechnical investigation data for the Provo Westside Connector project, including the boring logs and CPT soundings nearest the instrumentation location.

DATE		
STARTED:	1/15/13	
COMPLETED:	1/17/13	
BACKFILLED:	1/18/13	

Geotechnical Investigation
Provo
Utah County, Utah
Project Number   00285-042

IGES Rep: JG
Rig Type: CME Track Rig
Boring Type: Mud Rotary

BORING NO:
B-22
Sheet 1 of 6

LOCATION
NORTHING 246,376.77   EASTING 595,682.38   ELEVATION 4,493.40

Depth (Meters / Feet)	Samples	Water Level	Graphical Log	Unified Soil / AASHTO Classification	MATERIAL DESCRIPTION	N	N*	SPT BLOW COUNT	Dry Density (pcf)	Moisture Content %	Percent minus 200	Liquid Limit	Plasticity Index	Moisture Content and Atterberg Limits (Plastic Limit / Moisture Content / Liquid Limit)
0				ML	SILT - soft, moist, dark grey, organics, grading to light grey silt at 1.5'	1 3 3	4							
		▽		MH A-7-5	Elastic SILT - soft, very wet, light grey, organics	4 4 4 3	5			57.1	88.5	54	18	
5 ft				ML	SILT with sand - medium stiff, wet, grey, some dessicated clods, sand is fine	2 3 4 5	7							
				CL-ML A-4	Sandy Silty CLAY - soft, wet, grey, organics, sand is fine				95.0	28.8	58.2	27	5	
				ML	SILT - medium stiff, wet, greenish grey, some fine sand, trace organics	3 10 11 11	21							
10 ft														
15 ft				GW-GM	Well-Graded GRAVEL with silt and sand - dense, wet, grey with black and white gravel, gravel is angular and rounded	14 21 23	17			7.3	3.3			
20 ft				SM	Silty SAND - loose, wet, grey, sand is fine	5 4 2 4	6			28.7	27.4	NP	NP	
					- no recovery	1 0	5							

N - OBSERVED UNCORRECTED BLOW COUNT   * N - UNCORRECTED, EQUIVALENT SPT BLOW COUNT

SAMPLE TYPE
- 2" O.D./1.38" I.D. SPLIT SPOON SAMPLER
- 3.25" O.D./2.42" I.D. U SAMPLER
- 3" O.D. THIN-WALLED SHELBY SAMPLER
- GRAB SAMPLE
- Modified California Sampler

NOTES:

WATER LEVEL
▼ - MEASURED   ▽ - ESTIMATED

Plate
B-21a

IGES
Copyright (c) 2013, IGES, INC.

DATE		
STARTED:	1/15/13	
COMPLETED:	1/17/13	
BACKFILLED:	1/18/13	

Geotechnical Investigation
Provo
Utah County, Utah
Project Number   00285-042

IGES Rep: JG
Rig Type: CME Track Rig
Boring Type: Mud Rotary

BORING NO:
B-22
Sheet 2 of

LOCATION

NORTHING   EASTING   ELEVATION 4,493.40
246,376.77   595,682.38

Moisture Content and Atterberg Limits

DEPTH														Moisture Content and Atterberg Limits
METERS	FEET	SAMPLES	WATER LEVEL	GRAPHICAL LOG	UNIFIED SOIL/ AASHTO CLASSIFICATION	MATERIAL DESCRIPTION	N	N*	SPT BLOW COUNT 10 20 30 40 50 60 70 80 90	Dry Density (pcf)	Moisture Content %	Percent minus 200	Liquid Limit	Plasticity Index	Plastic Limit / Moisture Content / Liquid Limit 10 20 30 40 50 60 70 80 90

- 25 ft / ~7.6 m — N = 7
- ~9 m / 30 ft — ML, A-6 — **SILT** - very soft, wet, grey with black streaks, 1/8" black sand seams every 3 to 4", sand is fine, organic odor — N = 0,0,0,1; N* = 1; Moisture Content % = 45.9; Percent minus 200 = 97.3; Liquid Limit = 38; Plasticity Index = 11
- ~35 ft — CL — **Lean CLAY** - soft, wet, grey with black streaks, organic odor — Dry Density = 75.5; Moisture Content % = 45.9; Percent minus 200 = 99.0
- ~12 m / 40 ft — CL — **Lean CLAY** - soft, wet, dark grey with black streaks, increasing plasticity with depth — N = 2,2,3; N* = 4; Moisture Content % = 46.2; Liquid Limit = 48; Plasticity Index = 22
- ~45 ft — CL — **Lean CLAY** - soft, wet, dark grey — Dry Density = 75.3; Moisture Content % = 46.8
- ~15 ft / 15 m — CL — **Sandy Lean CLAY** - medium stiff, wet, grey, alternating Clay and — N = 5,7; N* = 10; Moisture Content % = 29.4; Liquid Limit = 35; Plasticity Index = 13

N - OBSERVED UNCORRECTED BLOW COUNT   * N - UNCORRECTED, EQUIVALENT SPT BLOW COUNT

SAMPLE TYPE
- 2" O.D./1.38" I.D. SPLIT SPOON SAMPLER
- 3.25" O.D./2.42" I.D. U SAMPLER
- 3" O.D. THIN-WALLED SHELBY SAMPLER
- GRAB SAMPLE
- Modified California Sampler

NOTES:

WATER LEVEL
▼ - MEASURED   ▽ - ESTIMATED

Plate
B-21b

DATE		
STARTED:	1/15/13	
COMPLETED:	1/17/13	
BACKFILLED:	1/18/13	

Geotechnical Investigation
Provo
Utah County, Utah
Project Number   00285-042

IGES Rep: JG
Rig Type: CME Track Rig
Boring Type: Mud Rotary

BORING NO:
B-22
Sheet 3 of 6

LOCATION

NORTHING 246,376.77   EASTING 595,682.38   ELEVATION 4,493.40

DEPTH (METERS / FEET)	SAMPLES	WATER LEVEL	GRAPHICAL LOG	UNIFIED SOIL / AASHTO CLASSIFICATION	MATERIAL DESCRIPTION	N	N*	SPT BLOW COUNT 10 20 30 40 50 60 70 80 90	Dry Density (pcf)	Moisture Content %	Percent minus 200	Liquid Limit	Plasticity Index	Moisture Content and Atterberg Limits 10 20 30 40 50 60 70 80 90
50	X				Clayey Sand layers, 3" Clayey Sand layers every 6" throughout sample	10								
16 / 55														
17														
18 / 60				CL	Lean CLAY - medium stiff, wet, grey, slight organic odor, Silt seam suspected bottom 4"				88.4	32.8				●
19 / 65														
20 / 70				CH	Fat CLAY - medium stiff, wet, grey, with black streaks, slight organic odor				44.6		52	27		⊢●⊣
21 / 22														

N - OBSERVED UNCORRECTED BLOW COUNT   * N - UNCORRECTED, EQUIVALENT SPT BLOW COUNT

Moisture Content and Atterberg Limits
Plastic Limit ⊢ Moisture Content ● Liquid Limit ⊣

SAMPLE TYPE
- 2" O.D./1.38" I.D. SPLIT SPOON SAMPLER
- 3.25" O.D./2.42" I.D. U SAMPLER
- 3" O.D. THIN-WALLED SHELBY SAMPLER
- GRAB SAMPLE
- Modified California Sampler

NOTES:

WATER LEVEL
▼ - MEASURED   ▽ - ESTIMATED

Plate
B-21c

Geotechnical Investigation
Provo
Utah County, Utah
Project Number 00285-042

IGES Rep: JG
Rig Type: CME Track Rig
Boring Type: Mud Rotary

BORING NO:
B-22
Sheet 4 of

LOCATION

NORTHING 246,376.77 EASTING 595,682.38 ELEVATION 4,493.40

Moisture Content and Atterberg Limits

DEPTH		SAMPLES	WATER LEVEL	GRAPHICAL LOG	UNIFIED SOIL / AASHTO CLASSIFICATION	MATERIAL DESCRIPTION	N	N*	SPT BLOW COUNT 10 20 30 40 50 60 70 80 90	Dry Density (pcf)	Moisture Content %	Percent minus 200	Liquid Limit	Plasticity Index	Plastic Limit / Moisture Content / Liquid Limit 10 20 30 40 50 60 70 80 90
METERS	FEET														
23	75														
24	80				CH	Fat CLAY - soft, wet, black, organic odor				73.5	45.0		58	33	●(plotted)
25															
26	85														
27					ML A-4	SILT with sand - medium stiff, wet, grey, sand is fine	11 12 22	13	●	30.3	82.1		NP	NP	●(plotted)
28	90														
29	95														
30					CL	Lean Clay - medium stiff, wet, grey									●(plotted)

N - OBSERVED UNCORRECTED BLOW COUNT   * N - UNCORRECTED, EQUIVALENT SPT BLOW COUNT

SAMPLE TYPE
- 2" O.D./1.38" I.D. SPLIT SPOON SAMPLER
- 3.25" O.D./2.42" I.D. U SAMPLER
- 3" O.D. THIN-WALLED SHELBY SAMPLER
- GRAB SAMPLE
- Modified California Sampler

NOTES:

WATER LEVEL
▼ - MEASURED ▽ - ESTIMATED

IGES®
Copyright (c) 2013, IGES, INC.

Plate
B-21d

LOCATION

NORTHING 246,376.77 EASTING 595,682.38 ELEVATION 4,493.40

DEPTH		SAMPLES	WATER LEVEL	GRAPHICAL LOG	UNIFIED SOIL/ AASHTO CLASSIFICATION	MATERIAL DESCRIPTION	N	N*	SPT BLOW COUNT 10 20 30 40 50 60 70 80 90	Dry Density (pcf)	Moisture Content %	Percent minus 200	Liquid Limit	Plasticity Index	Moisture Content and Atterberg Limits 10 20 30 40 50 60 70 80 90
METERS	FEET														
	00				CH	Fat CLAY - stiff, wet, light grey mottled with grey, gastropod				88.1	32.2		49	25	
31															
32	05														
33						Fat CLAY - medium stiff, wet, grey mottled with black	2 3 6	6			41.4		50	25	
	10				CH										
34															
35	15														
36															
	20				SP	Poorly Graded SAND - loose, wet, black, sand is coarse									
37					CL A-6	Lean CLAY - stiff, wet, light grey				93.4	28.4	99.2	38	14	
38															

N - OBSERVED UNCORRECTED BLOW COUNT   * N - UNCORRECTED, EQUIVALENT SPT BLOW COUNT

Geotechnical Investigation
Provo
Utah County, Utah
Project Number   00285-042

IGES Rep: JG
Rig Type: CME Track Rig
Boring Type: Mud Rotary

BORING NO:
B-22
Sheet 6 of

LOCATION

NORTHING	EASTING	ELEVATION 4,493.40
246,376.77	595,682.38	

Moisture Content and Atterberg Limits

Plastic Limit	Moisture Content	Liquid Limit
	—————•—————	
10 20 30 40 50 60 70 80 90		

DEPTH METERS	FEET	SAMPLES	WATER LEVEL	GRAPHICAL LOG	UNIFIED SOIL / AASHTO CLASSIFICATION	MATERIAL DESCRIPTION	N	N*	SPT BLOW COUNT 10 20 30 40 50 60 70 80 90	Dry Density (pcf)	Moisture Content %	Percent minus 200	Liquid Limit	Plasticity Index	Moisture Content and Atterberg Limits 10 20 30 40 50 60 70 80 90
	125														
39															
	130				ML	SILT - medium stiff, wet, light grey - blow counts elevated, silt flowed into sampler prior to sampling.	17 17 45	13	•		32.8	90.8			•
40															
41	135														
42						- boring abandoned increased flow of artesian water to surface, backfilled with Portland cement Bottom of Boring @ 137 Feet									
43	140														
44	145														
45															

N - OBSERVED UNCORRECTED BLOW COUNT   * N - UNCORRECTED, EQUIVALENT SPT BLOW COUNT

SAMPLE TYPE
- 2" O.D./1.38" I.D. SPLIT SPOON SAMPLER
- 3.25" O.D./2.42" I.D. U SAMPLER
- 3" O.D. THIN-WALLED SHELBY SAMPLER
- GRAB SAMPLE
- Modified California Sampler

NOTES:

WATER LEVEL
▼ - MEASURED   ▽ - ESTIMATED

Plate
B-21f

CPT-07 — PROVO WEST CONNECTOR

Sounding: CPT-07
Cone: 332:T1500F15U500
Job No: 12-399
Date: 09:24:12 10:04
Site: PROVO WEST CONNECTOR

CONETEC IGES

SBT: Lunne, Robertson and Powell, 1997
Coords: Lat 40.206967 Long: -111.660917
● Equilibrium Pore Pressure from Dissipation

File: 12-399CPT-07.COR
Unit Wt: SBT Chart Soil Zones

Max Depth: 42.700 m / 140.09 ft
Depth Inc: 0.050 m / 0.164 ft
Avg Int: 0.150 m

IGES | **ConeTec**

Job No: 12-399
Date: 09:24:12 10:04
Site: PROVO WEST CONNECTOR

Sounding: CPT-07
Cone: 332:T1500F15U500

SBT: Lunne, Robertson and Powell, 1997
Coords: Lat: 40.206967 Long:-111.660917
● Equilibrium Pore Pressure from Dissipation

File: 12-399CPT-07.COR
Unit Wt: SBT Chart Soil Zones

Max Depth: 42.700 m / 140.09 ft
Depth Inc: 0.050 m / 0.164 ft
Avg Int: 0.150 m

APPENDIX B: RAW MAGNET EXTENSOMETER DATA

This appendix contains the actual readings taken for both of the magnet extensometers used in this research.

Table B-1 IGES raw data (measured in feet) for M-2.

	EXT	Datum Magnet	Mag 1	Mag 2	Mag 3	Mag 4	Mag 5	Mag 6	Mag 7
8/14/14	0	115.29	92.75	81.75	79.4	42.625	39.5	29.79	3.595
8/20/14	2.935	118.215	95.68	84.69	82.33	45.56	42.44	32.72	6.53
8/27/14	2.935	118.21	95.675	84.68	82.33	45.55	42.43	32.72	6.53
9/3/14	2.935	118.21	95.68	84.68	82.33	45.55	42.44	32.725	6.53
9/10/14	2.935	118.195	95.66	84.67	82.32	45.55	42.43	32.72	6.53
9/17/14	2.935	118.17	95.64	84.65	82.3	45.53	42.42	32.71	6.53
9/24/14	2.935	118.14	95.605	84.62	82.27	45.51	42.4	32.69	6.53
10/1/14	5.772	120.91	98.38	87.39	85.05	48.3	45.15	35.495	9.36
10/8/14	5.772	120.85	98.33	87.345	85	48.27	45.16	35.475	9.355
10/15/14	5.772	120.78	98.255	87.275	84.935	48.21	45.11	35.44	9.355
10/22/14	9.702	124.435	101.925	90.95	88.61	51.935	48.84	39.21	13.27
10/27/14	9.702	124.35	101.845	90.88	88.54	51.88	48.8	39.19	13.265
10/31/14	9.702	124.34	101.83	90.87	88.53	51.875	48.79	39.19	13.265
11/5/14	11.716	126.31	103.805	92.845	90.51	53.865	50.79	41.19	15.28
11/12/14	11.716	126.245	103.745	92.79	90.455	53.83	50.765	41.18	15.28
11/19/14	11.716	126.11	103.615	92.67	90.34	53.745	50.685	41.12	15.27
11/26/14	15.743	130.01	107.52	96.58	94.255	57.69	54.645	45.11	19.29
12/3/14	15.743	129.87	107.39	96.455	94.13	57.61	54.57	45.055	19.275
12/5/14	17.758	131.74	109.29	98.36	96.035	59.535	56.5	47	21.28
12/10/14	17.758	131.59	109.13	98.21	95.885	59.43	56.405	46.94	21.275
12/17/14	17.758	131.465	109.01	98.1	95.78	59.38	56.365	46.925	21.28
12/24/14	17.758	131.38	108.93	98.02	95.71	59.33	56.32	46.905	21.27
12/31/14	17.758	131.29	108.85	97.96	95.64	59.29	56.295	46.89	21.26
1/7/15	17.758	131.22	108.785	97.9	95.585	59.265	56.27	46.88	21.26
1/14/15	17.758	131.155	108.73	97.845	95.54	59.23	56.25	46.86	21.25
1/21/15	17.758	131.1	108.67	97.8	95.49	59.2	56.22	46.85	21.245
1/28/15	17.758	131.045	108.63	97.76	95.455	59.18	56.21	46.845	21.24
2/4/15	17.758	131	108.59	97.725	95.425	59.165	56.195	46.84	21.24
2/11/15	17.758	130.965	108.56	97.7	95.4	59.15	56.185	46.84	21.24
2/18/15	17.758	130.93	108.525	97.67	95.37	59.14	56.175	46.83	21.24
2/25/15	17.758	130.895	108.495	97.65	95.35	59.13	56.165	46.825	21.24
3/4/15	17.758	130.865	108.47	97.63	95.33	59.12	56.16	46.825	21.235
3/11/15	17.758	130.84	108.45	97.61	95.315	59.11	56.15	46.82	21.235

3/18/15	17.758	130.82	108.43	97.595	95.3	59.1	56.145	46.82	21.235
3/25/15	17.758	130.795	108.405	97.58	95.285	59.095	56.14	46.82	21.235
4/1/15	17.758	130.77	108.385	97.56	95.27	59.085	56.135	46.82	21.24
4/8/15	17.758	130.75	108.37	97.545	95.26	59.08	56.13	46.82	21.24
4/15/15	17.758	130.73	108.35	97.53	95.24	59.075	56.125	46.81	21.235
4/22/15	17.758	130.705	108.335	97.515	95.23	59.07	56.12	46.81	21.24
4/29/15	17.758	130.69	108.32	97.51	95.22	59.065	56.115	46.81	21.24
5/6/15	17.758	130.69	108.32	97.51	95.225	59.075	56.125	46.825	21.255
5/13/15	17.758	130.655	108.29	97.485	95.2	59.055	56.105	46.805	21.235
5/20/15	17.758	130.635	108.275	97.475	95.19	59.05	56.1	46.8	21.235
5/27/15	17.758	130.62	108.265	97.465	95.185	59.045	56.1	46.8	21.235
6/3/15	17.758	130.61	108.255	97.455	95.175	59.04	56.1	46.8	21.235
6/8/15	17.758	130.6	108.245	97.45	95.17	59.04	56.095	46.8	21.235
6/11/15	17.758	130.59	108.24	97.445	95.165	59.04	56.095	46.795	21.235
6/15/15	17.758	130.585	108.235	97.44	95.16	59.035	56.09	46.795	21.235
6/18/15	17.758	130.585	108.23	97.44	95.16	59.035	56.095	46.8	21.235
6/22/15	17.758	130.57	108.22	97.435	95.155	59.035	56.095	46.795	21.24
6/25/15	17.758	130.565	108.215	97.425	95.155	59.03	56.09	46.795	21.24
6/29/15	17.758	130.555	108.21	97.42	95.145	59.03	56.085	46.795	21.235
7/2/15	17.758	130.55	108.205	97.42	95.14	59.025	56.085	46.795	21.235
7/6/15	17.758	130.545	108.2	97.42	95.14	59.025	56.085	46.795	21.24
7/9/15	17.758	130.54	108.195	97.415	95.14	59.025	56.085	46.795	21.24
7/13/15	17.758	130.53	108.19	97.4	95.13	59.02	56.08	46.79	21.235
7/16/15	17.758	130.525	108.185	97.405	95.13	59.02	56.08	46.79	21.235
7/20/15	17.758	130.515	108.175	97.395	95.125	59.02	56.08	46.79	21.24
7/23/15	17.758	130.51	108.17	97.395	95.125	59.015	56.08	46.79	21.24
7/27/15	17.758	130.505	108.17	97.39	95.12	59.015	56.08	46.79	21.24
7/30/15	17.758	130.5	108.165	97.385	95.115	59.015	56.08	46.79	21.24
8/2/15	17.758	130.495	108.16	97.38	95.11	59.015	56.075	46.79	21.24
8/7/15	17.758	130.485	108.155	97.38	95.11	59.01	56.075	46.79	21.24
8/10/15	17.758	130.48	108.15	97.38	95.105	59.01	56.075	46.79	21.24
8/13/15	17.758	130.48	108.145	97.375	95.105	59.01	56.075	46.79	21.24

Table B-2 IGES raw data (measured in feet) for M-2A.

	EXT	Datum Magnet	Mag 1	Mag 2	Mag 3
8/14/14	0	98.41	88.16	60.16	17.73
8/20/14	3.1	101.5	91.25	63.25	20.82
8/27/14	3.1	101.5	91.24	63.25	20.82
9/3/14	3.1	101.49	91.235	63.25	20.82
9/10/14	3.1	101.48	91.23	63.25	20.82
9/17/14	3.1	101.455	91.21	63.25	20.82
9/24/14	3.1	101.43	91.18	63.21	20.81
10/1/14	5.293	103.4	93.15	65.19	22.82
10/8/14	5.293	103.35	93.11	65.14	22.805
10/15/14	5.293	103.28	93.035	65.09	22.785
10/22/14	9.254	107	96.76	68.835	26.66
10/27/14	9.254	106.92	96.685	68.78	26.645
10/31/14	9.254	106.91	96.67	68.77	26.645
11/5/14	11.271	108.89	98.65	70.76	28.66
11/12/14	11.271	108.855	98.595	70.72	28.65
11/19/14	11.271	108.72	98.465	70.61	28.62
11/26/14	15.318	112.66	102.4	74.57	32.64
12/3/14	15.318	112.53	102.27	74.46	32.595
12/5/14	17.329	114.42	104.165	76.37	34.55
12/10/14	17.329	114.27	104.01	76.24	34.52
12/17/14	17.329	114.16	103.905	76.16	34.5
12/24/14	17.329	114.09	103.83	76.11	34.49
12/31/14	17.329	114.01	103.76	76.05	34.48
1/7/15	17.329	113.945	103.705	76.015	34.48
1/14/15	17.329	113.885	103.65	75.97	34.46
1/21/15	17.329	113.83	103.595	75.94	34.45
1/28/15	17.329	113.79	103.55	75.91	34.44
2/4/15	17.329	113.75	103.52	75.89	34.44
2/11/15	17.329	113.72	103.49	75.87	34.44
2/18/15	17.329	113.69	103.465	75.85	34.435
2/25/15	17.329	113.665	103.44	75.835	34.43
3/4/15	17.329	113.64	103.415	75.82	34.43
3/11/15	17.329	113.62	103.395	75.81	34.43

3/18/15	17.329	113.6	103.375	75.8	34.43
3/25/15	17.329	113.58	103.36	75.79	34.43
4/1/15	17.329	113.56	103.34	75.78	34.425
4/8/15	17.329	113.54	103.325	75.765	34.425
4/15/15	17.329	113.525	103.305	75.755	34.425
4/22/15	17.329	113.51	103.295	75.75	34.42
4/29/15	17.329	113.495	103.285	75.745	34.42
5/6/15	17.329	113.485	103.27	75.74	34.425
5/13/15	17.329	113.465	103.255	75.73	34.42
5/20/15	17.329	113.455	103.245	75.72	34.415
5/27/15	17.329	113.44	103.235	75.72	34.415
6/3/15	17.329	113.43	103.225	75.71	34.415
6/8/15	17.329	113.42	103.215	75.71	34.415
6/11/15	17.329	113.415	103.21	75.705	34.415
6/15/15	17.329	113.41	103.21	75.705	34.415
6/18/15	17.329	113.41	103.205	75.7	34.41
6/22/15	17.329	113.4	103.2	75.7	34.41
6/25/15	17.329	113.4	103.19	75.695	34.41
6/29/15	17.329	113.39	103.185	75.695	34.41
7/2/15	17.329	113.385	103.18	75.69	34.41
7/6/15	17.329	113.38	103.18	75.69	34.41
7/9/15	17.329	113.375	103.175	75.685	34.41
7/13/15	17.329	113.365	103.165	75.68	34.41
7/16/15	17.329	113.365	103.165	75.68	34.41
7/20/15	17.329	113.36	103.155	75.68	34.41
7/23/15	17.329	113.355	103.15	75.675	34.405
7/27/15	17.329	113.35	103.15	75.675	34.405
7/30/15	17.329	113.35	103.145	75.675	34.405
8/2/15	17.329	113.345	103.145	75.675	34.405
8/7/15	17.329	113.34	103.14	75.67	34.41
8/10/15	17.329	113.335	103.135	75.67	34.41
8/13/15	17.329	113.33	103.13	75.665	34.405

Table B-3 BYU raw data (measured in meters) for M-2.

	EXT	Datum Magnet	Mag 1	Mag 2	Mag 3	Mag 4	Mag 5	Mag 6	Mag 7
9/10/14	0.895	36.148	29.267	25.901	25.181	13.999	13.057	10.086	2.100
9/17/14	0.895	36.140	29.259	25.896	25.175	13.995	13.052	10.082	2.099
9/24/14	0.895	36.131	29.251	25.888	25.166	13.989	13.047	10.079	2.099
9/29/14	1.759	36.979	30.099	26.737	26.017	14.841	13.900	10.934	2.963
10/10/14	1.759	36.955	30.076	26.715	25.995	14.826	13.886	10.924	2.962
10/13/14	1.759	36.947	30.070	26.709	25.989	14.821	13.882	10.921	2.962
10/17/14	2.957	38.106	31.229	27.870	27.151	15.987	15.051	12.094	4.157
10/20/14	2.957	38.061	31.185	27.827	27.109	15.952	15.017	12.068	4.155
10/24/14	2.957	38.043	31.168	27.811	27.092	15.940	15.006	12.062	4.155
10/27/14	2.957	38.031	31.157	27.801	27.082	15.933	15.001	12.059	4.155
11/3/14	3.571	38.628	31.755	28.400	27.683	16.537	15.384	12.670	4.769
11/7/14	3.571	38.625	31.752	28.399	27.682	16.539	15.611	12.675	4.776
11/10/14	3.571	38.608	31.736	28.384	27.667	16.526	15.599	12.665	4.768
11/14/14	3.571	38.596	31.725	28.374	27.657	16.520	15.594	12.662	4.768
11/17/14	3.571	38.571	31.701	28.351	27.635	16.503	15.579	12.652	4.766
11/21/14	4.798	39.774	32.904	29.557	28.840	17.715	16.792	13.869	5.992
11/24/14	4.798	39.756	32.888	29.541	28.825	17.705	16.783	13.863	5.990
11/26/14	4.798	39.749	32.881	29.534	28.818	17.700	16.780	13.861	5.990
11/28/14	4.798	39.741	32.874	29.528	28.813	17.696	16.776	13.860	5.990
12/1/14	4.798	39.731	32.864	29.519	28.804	17.691	16.772	13.858	5.990
12/3/14	4.798	39.712	32.847	29.502	28.788	17.680	16.762	13.850	5.990
12/5/14	5.412	40.283	33.417	30.075	29.361	18.261	17.344	14.438	6.597
12/8/14	5.412	40.247	33.385	30.043	29.330	18.238	17.323	14.424	6.594
12/10/14	5.412	40.231	33.370	30.029	29.316	18.229	17.316	14.420	6.594
12/12/14	5.412	40.220	33.359	30.020	29.306	18.223	17.312	14.418	6.595
12/15/14	5.412	40.204	33.344	30.005	29.293	18.216	17.305	14.415	6.595
12/17/14	5.412	40.195	33.335	29.997	29.285	18.213	17.302	14.413	6.594
12/19/14	5.412	40.185	33.327	29.990	29.278	18.208	17.299	14.412	6.594
12/23/14	5.412	40.167	33.310	29.973	29.262	18.199	17.290	14.408	6.591
12/27/14	5.412	40.153	33.297	29.963	29.252	18.193	17.286	14.406	6.591
1/2/15	5.412	40.133	33.279	29.946	29.236	18.184	17.279	14.402	6.590
1/6/15	5.412	40.120	33.268	29.937	29.226	18.179	17.275	14.401	6.590
1/9/15	5.412	40.114	33.261	29.931	29.221	18.175	17.273	14.401	6.590

1/13/15	5.412	40.104	33.252	29.924	29.214	18.172	17.271	14.400	6.590
1/16/15	5.412	40.093	33.243	29.914	29.205	18.165	17.265	14.395	6.586
1/20/15	5.412	40.084	33.236	29.908	29.199	18.163	17.263	14.394	6.587
1/23/15	5.412	40.076	33.228	29.901	29.192	18.158	17.258	14.392	6.584
1/27/15	5.412	40.066	33.219	29.894	29.186	18.154	17.256	14.391	6.585
1/30/15	5.412	40.061	33.215	29.890	29.182	18.153	17.255	14.390	6.584
2/3/15	5.412	40.055	33.209	29.885	29.177	18.150	17.252	14.389	6.584
2/10/15	5.412	40.043	33.199	29.876	29.169	18.144	17.249	14.389	6.583
2/13/15	5.412	40.038	33.194	29.872	29.165	18.143	17.247	14.388	6.584
2/17/15	5.412	40.033	33.190	29.869	29.162	18.142	17.247	14.388	6.585
2/20/15	5.412	40.028	33.185	29.865	29.159	18.140	17.246	14.387	6.584
2/24/15	5.412	40.021	33.179	29.861	29.154	18.137	17.243	14.386	6.583
2/27/15	5.412	40.016	33.176	29.858	29.151	18.136	17.241	14.385	6.583
3/3/15	5.412	40.012	33.171	29.854	29.148	18.134	17.240	14.385	6.583
3/6/15	5.412	40.008	33.169	29.851	29.145	18.134	17.240	14.385	6.583
3/10/15	5.412	40.004	33.165	29.848	29.143	18.132	17.239	14.385	6.583
3/17/15	5.412	39.997	33.159	29.843	29.139	18.130	17.237	14.384	6.583
3/24/15	5.412	39.989	33.152	29.838	29.134	18.127	17.234	14.382	6.583
3/27/15	5.412	39.986	33.150	29.836	29.132	18.127	17.234	14.382	6.584
3/31/15	5.412	39.981	33.146	29.833	29.129	18.125	17.233	14.382	6.583
4/3/15	5.412	39.981	33.144	29.831	29.127	18.124	17.232	14.382	6.584
4/7/15	5.412	39.977	33.141	29.828	29.125	18.124	17.232	14.382	6.584
4/10/15	5.412	39.974	33.138	29.827	29.122	18.122	17.230	14.381	6.583
4/14/15	5.412	39.969	33.135	29.824	29.122	18.122	17.229	14.381	6.583
4/21/15	5.412	39.966	33.131	29.821	29.119	18.121	17.229	14.382	6.584
4/27/15	5.412	39.961	33.128	29.818	29.116	18.119	17.228	14.381	6.584
5/2/15	5.412	39.956	33.124	29.814	29.113	18.117	17.227	14.380	6.584
5/7/15	5.412	39.950	33.119	29.811	29.110	18.116	17.225	14.379	6.583
5/16/15	5.412	39.945	33.114	29.807	29.107	18.115	17.224	14.379	6.583
5/22/15	5.412	39.941	33.111	29.805	29.104	18.113	17.223	14.378	6.583
6/1/15	5.412	39.935	33.106	29.801	29.101	18.112	17.222	14.378	6.583
6/8/15	5.412	39.927	33.101	29.797	29.098	18.110	17.220	14.377	6.583
6/18/15	5.412	39.922	33.096	29.794	29.095	18.109	17.220	14.376	6.583
6/29/15	5.412	39.916	33.091	29.790	29.091	18.107	17.218	14.375	6.583

Table B-4 BYU raw data (measured in meters) for M-2A.

	EXT	Datum Magnet	Mag 1	Mag 2	Mag 3
9/10/14	0.945	31.053	27.925	19.400	6.471
9/17/14	0.945	31.047	27.916	19.393	6.466
9/24/14	0.945	31.040	27.909	19.387	6.465
9/29/14	1.613	31.645	28.514	19.994	7.078
10/10/14	1.613	31.622	28.492	19.975	7.073
10/13/14	1.613	31.615	28.486	19.971	7.071
10/17/14	2.820	32.785	29.656	21.145	8.262
10/20/14	2.820	32.746	29.619	21.111	8.252
10/24/14	2.820	32.729	29.601	21.097	8.247
10/27/14	2.820	32.718	29.591	21.098	8.246
11/3/14	3.436	33.319	30.190	21.691	8.858
11/7/14	3.436	33.308	30.181	21.685	8.857
11/10/14	3.436	33.301	30.174	21.679	8.856
11/14/14	3.436	33.295	30.161	21.670	8.853
11/17/14	3.436	33.271	30.138	21.651	8.846
11/21/14	4.669	34.482	31.350	22.867	10.075
11/24/14	4.669	34.469	31.334	22.853	10.071
11/26/14	4.669	34.461	31.328	22.848	10.070
11/28/14	4.669	34.454	31.321	22.843	10.069
12/1/14	4.669	34.445	31.312	22.836	10.067
12/3/14	4.669	34.429	31.295	22.823	10.062
12/5/14	5.282	34.998	31.864	23.395	10.653
12/8/14	5.282	34.967	31.834	23.369	10.645
12/10/14	5.282	34.952	31.819	23.358	10.642
12/12/14	5.282	34.941	31.809	23.349	10.640
12/15/14	5.282	34.927	31.795	23.339	10.638
12/17/14	5.282	34.919	31.788	23.333	10.638
12/19/14	5.282	34.911	31.779	23.327	10.637
12/23/14	5.282	34.895	31.764	23.317	10.634
12/27/14	5.282	34.883	31.753	23.309	10.633
1/2/15	5.282	34.866	31.736	23.297	10.630
1/6/15	5.282	34.855	31.726	23.291	10.630
1/9/15	5.282	34.847	31.719	23.286	10.629

1/13/15	5.282	34.837	31.709	23.278	10.626
1/16/15	5.282	34.829	31.701	23.272	10.623
1/20/15	5.282	34.820	31.692	23.266	10.621
1/23/15	5.282	34.814	31.687	23.262	10.621
1/27/15	5.282	34.806	31.679	23.257	10.619
1/30/15	5.282	34.802	31.675	23.255	10.619
2/3/15	5.282	34.796	31.669	23.251	10.619
2/10/15	5.282	34.786	31.659	23.245	10.618
2/13/15	5.282	34.782	31.656	23.243	10.618
2/17/15	5.282	34.777	31.651	23.239	10.617
2/20/15	5.282	34.773	31.648	23.237	10.617
2/24/15	5.282	34.768	31.643	23.234	10.616
2/27/15	5.282	34.765	31.640	23.232	10.616
3/3/15	5.282	34.761	31.637	23.230	10.616
3/6/15	5.282	34.758	31.633	23.229	10.616
3/10/15	5.282	34.755	31.630	23.226	10.616
3/17/15	5.282	34.749	31.624	23.223	10.616
3/24/15	5.282	34.742	31.618	23.220	10.615
3/27/15	5.282	34.740	31.616	23.219	10.615
3/31/15	5.282	34.736	31.614	23.217	10.615
4/3/15	5.282	34.733	31.610	23.215	10.615
4/7/15	5.282	34.731	31.608	23.214	10.614
4/10/15	5.282	34.727	31.605	23.213	10.614
4/14/15	5.282	34.725	31.604	23.211	10.614
4/21/15	5.282	34.720	31.599	23.209	10.613
4/27/15	5.282	34.717	31.596	23.208	10.613
5/2/15	5.282	34.714	31.593	23.206	10.613
5/7/15	5.282	34.709	31.590	23.204	10.612
5/16/15	5.282	34.705	31.586	23.202	10.612
5/22/15	5.282	34.702	31.583	23.200	10.612
6/1/15	5.282	34.697	31.578	23.198	10.612
6/8/15	5.282	34.692	31.575	23.196	10.611
6/18/15	5.282	34.687	31.571	23.194	10.610
6/29/15	5.282	34.683	31.566	23.191	10.610

APPENDIX C: DATA AND FIGURES FROM CURVE FITTING

This appendix design variables used in the curve fitting portion of the research, and the corresponding fitted curves. These have been broken up for the radial and vertical portions of magnet extensometers M-2 and M-2A, respectively.

Table C-1 Radial drainage design variables for curve fitting field data for magnet extensometer M-2.

Magnet Interval	Day of Max Load	Settlement at start of curve (in)	Final settlement (in)	c_h/d_e^2
6-7 w/out end of consolidation	109	2.80	5.35	0.0048
6-7 w/ end of consolidation	109	2.50	5.05	0.0071
4-6 w/out end of consolidation	109	3.70	7.45	0.0049
4-6 w/ end of consolidation	109	3.20	7.00	0.0075
2-4 w/out end of consolidation	109	3.80	9.50	0.0035
2-4 w/ end of consolidation	109	3.50	8.60	0.0052
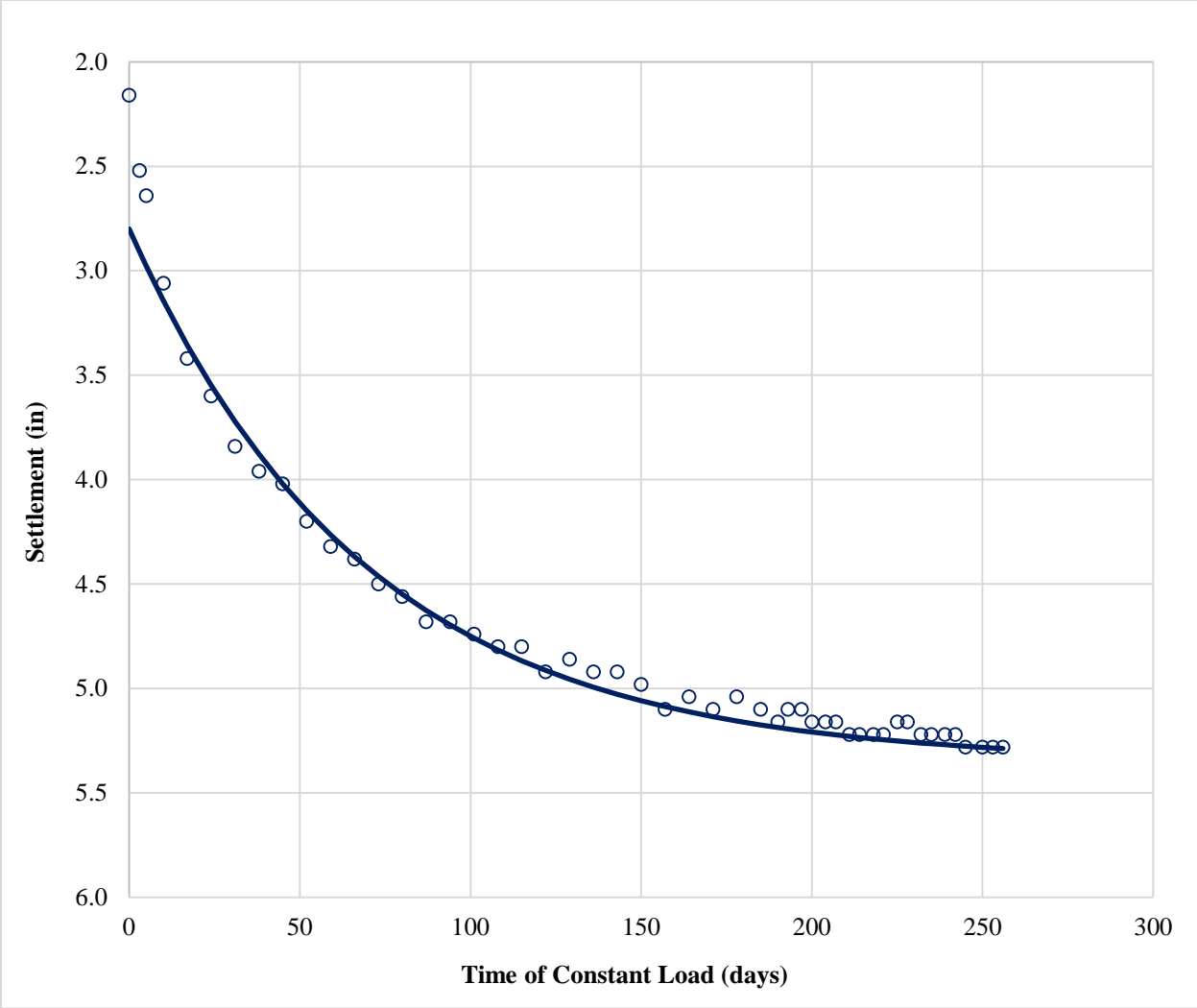
Figure C-1 Fitted radial curve for the compression data between magnets 6 and 7 (M-2).
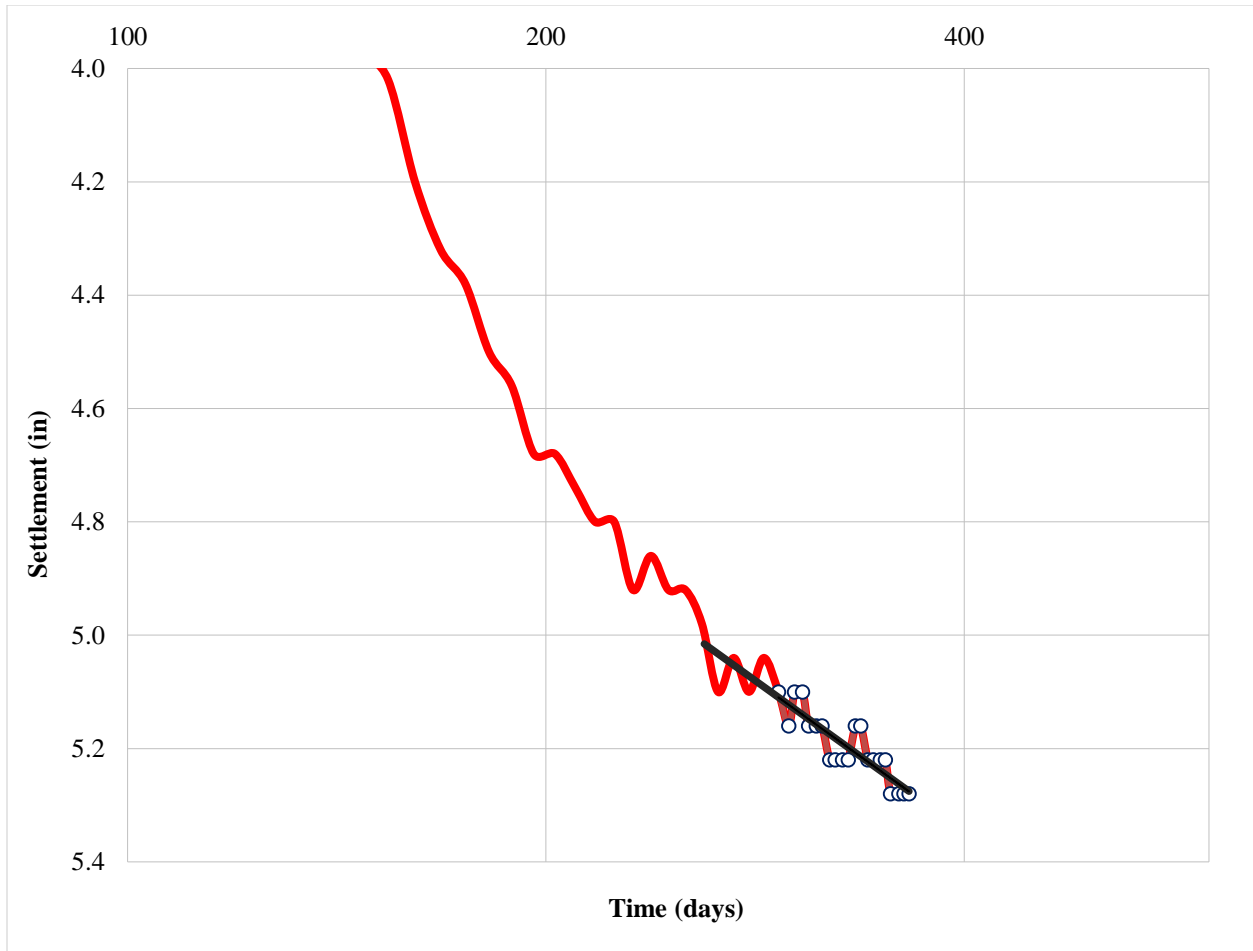
Figure C-2 Apparent log-linear behavior in the latter portion of fitted radial curve for the compression data between magnets 6 and 7 (M-2).
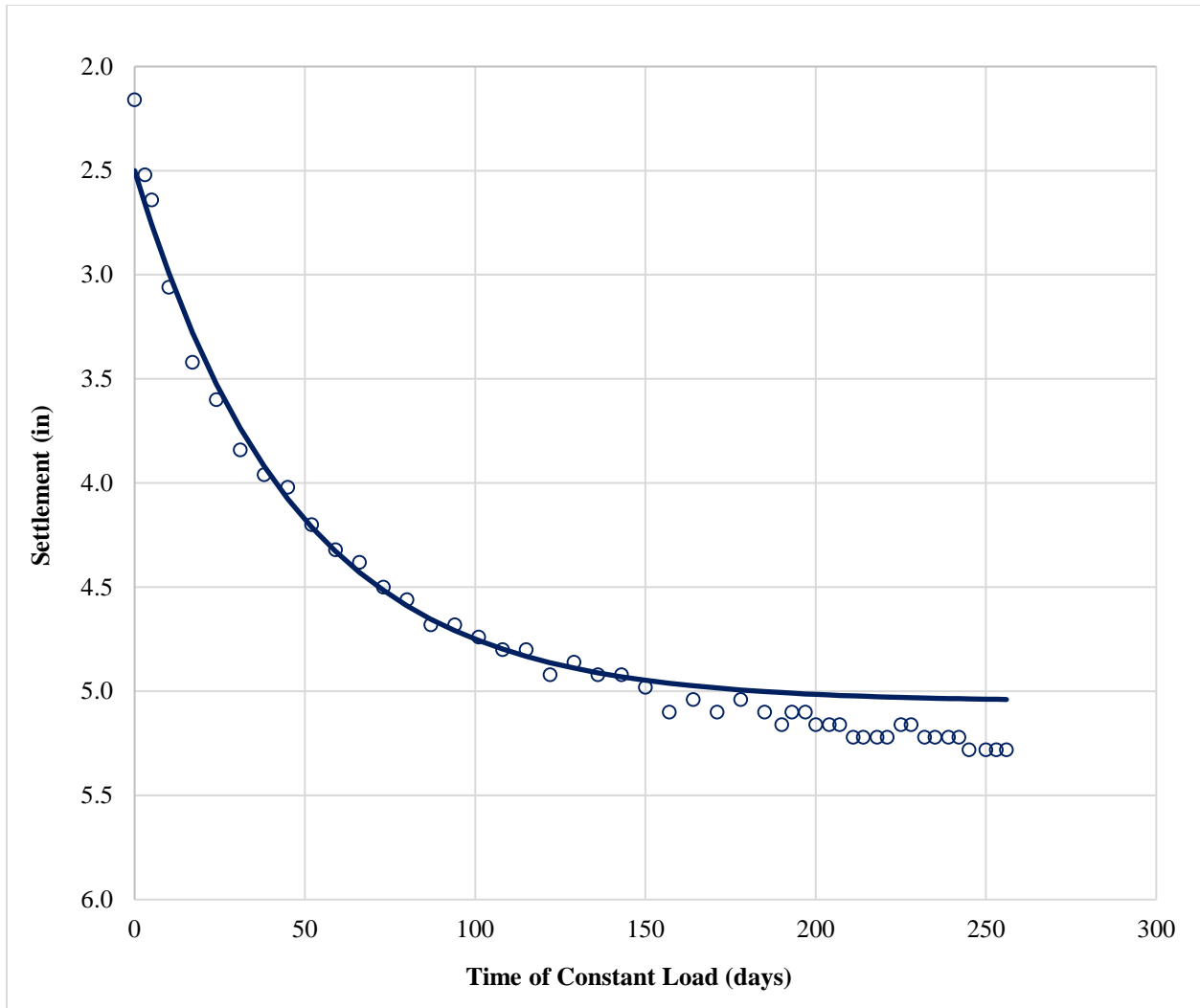
**Figure C-3 Updated fitted curve for the compression data between magnets 6 and 7 (M-2) assuming end of primary consolidation settlement has already been reached.**
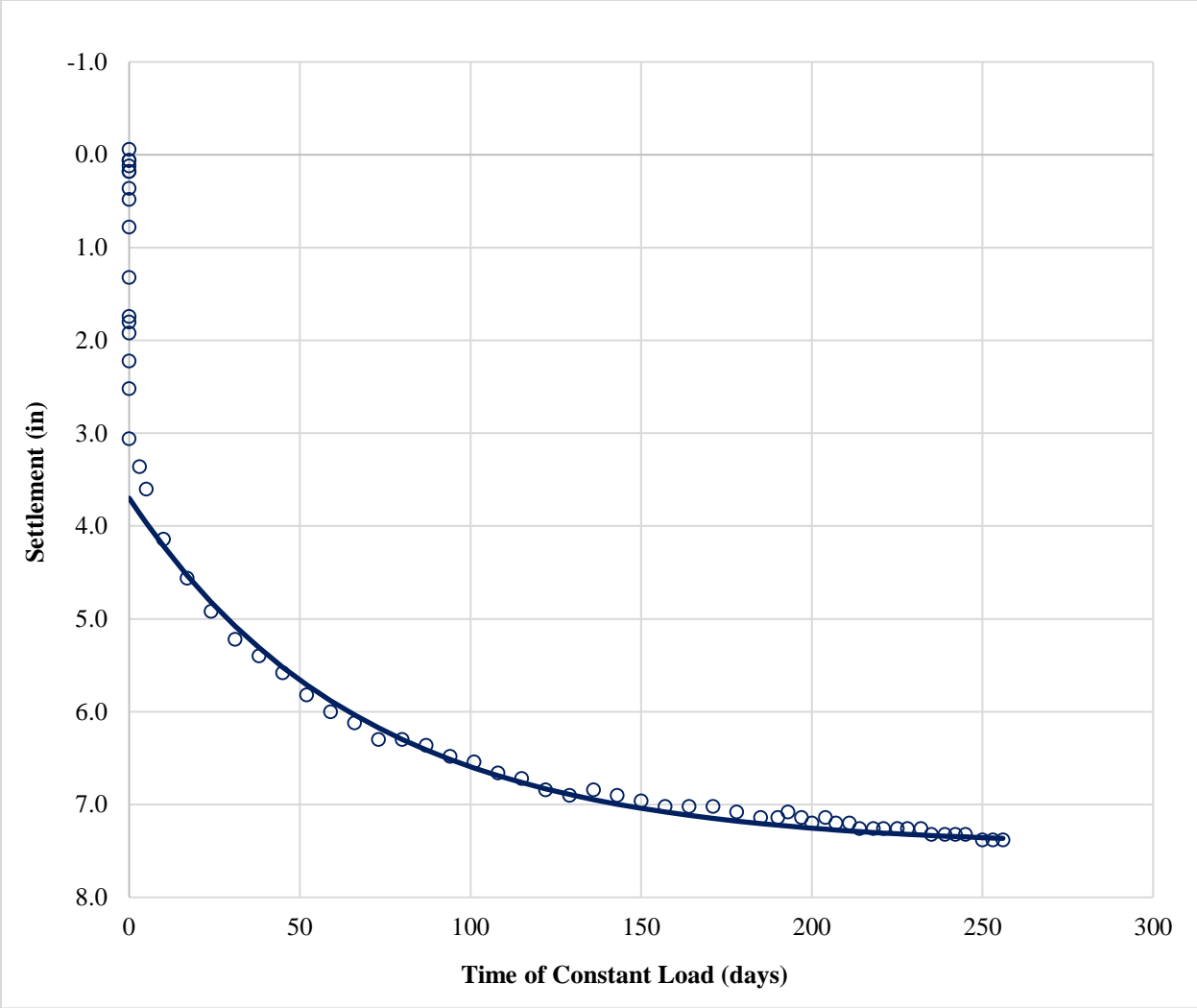
Figure C-4 Fitted radial curve for the compression data between magnets 4 and 6 (M-2).
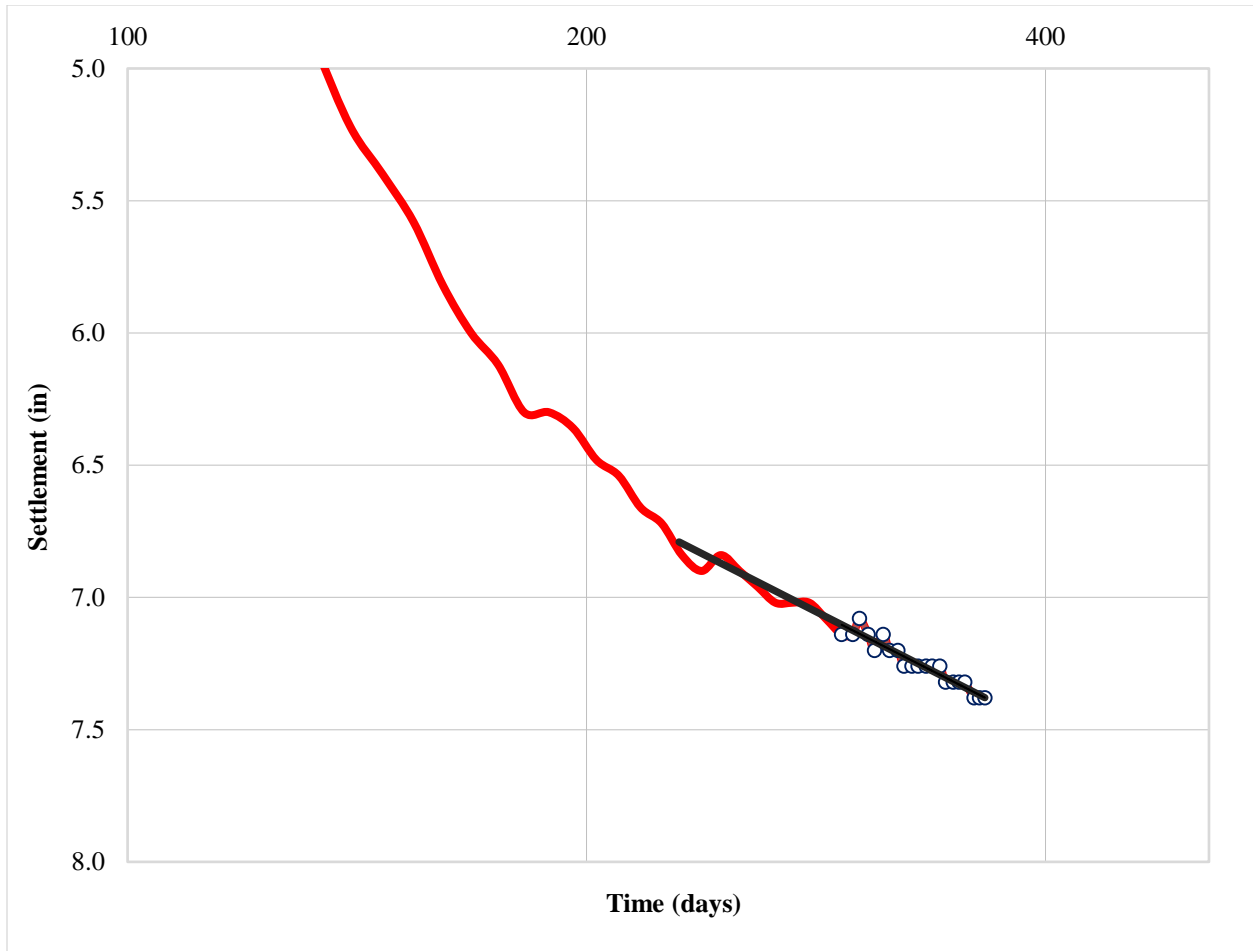
Figure C-5 Apparent log-linear behavior in the latter portion of fitted radial curve for the compression data between magnets 4 and 6 (M-2).
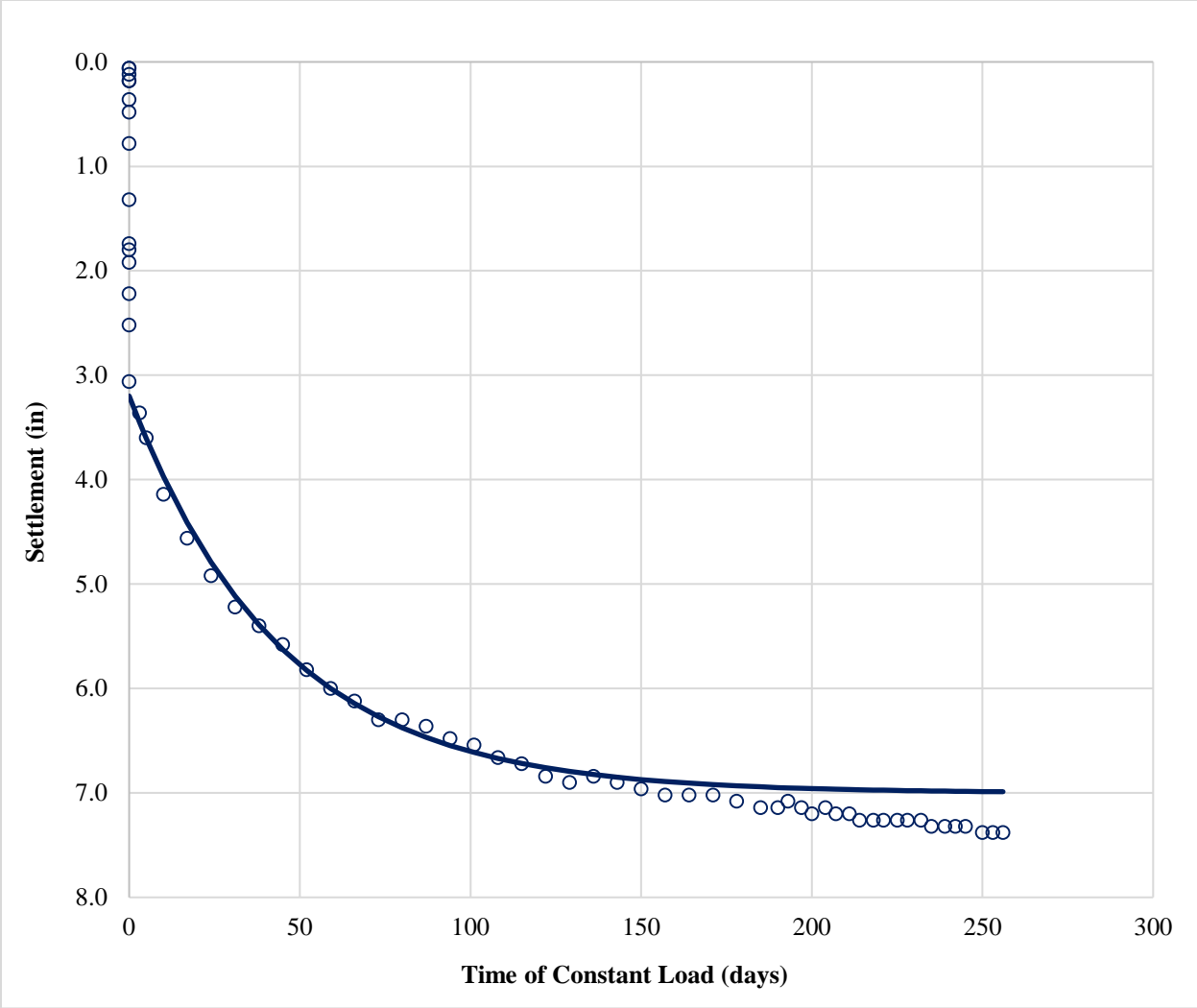
Figure C-6 Updated fitted curve for the compression data between magnets 4 and 6 (M-2) assuming end of primary consolidation settlement has already been reached.
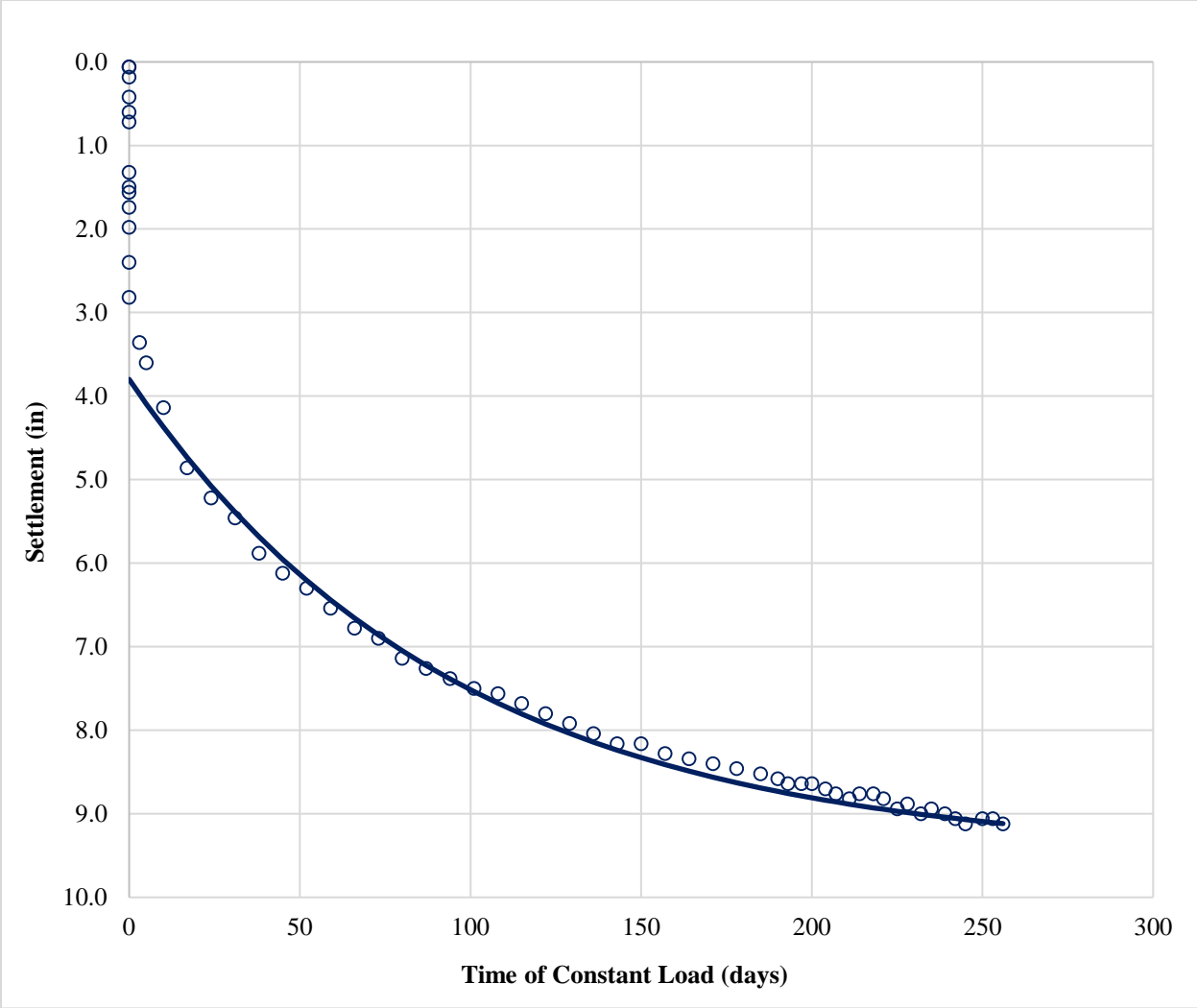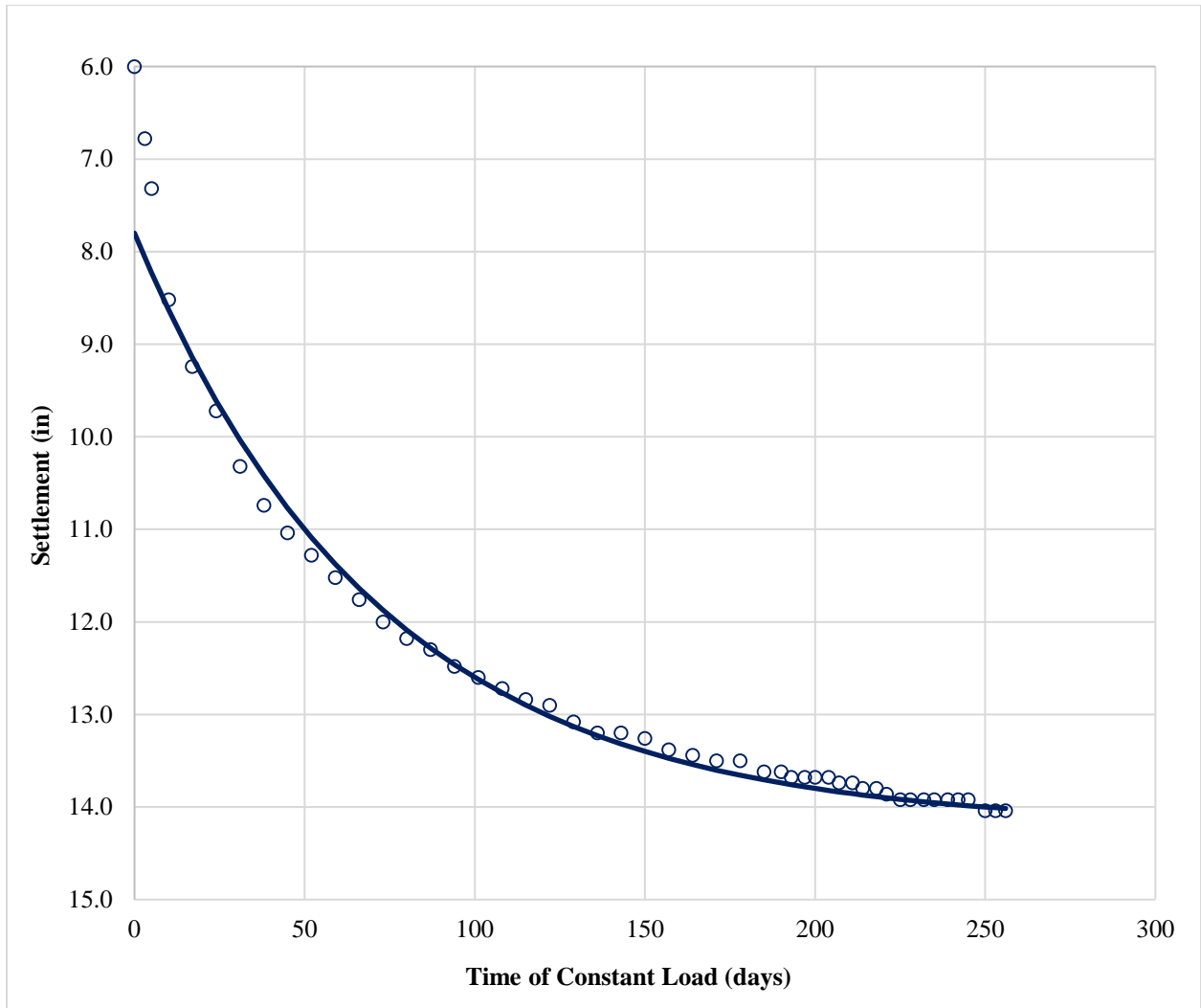
Figure C-7 Fitted radial curve for the compression data between magnets 2 and 4 (M-2).
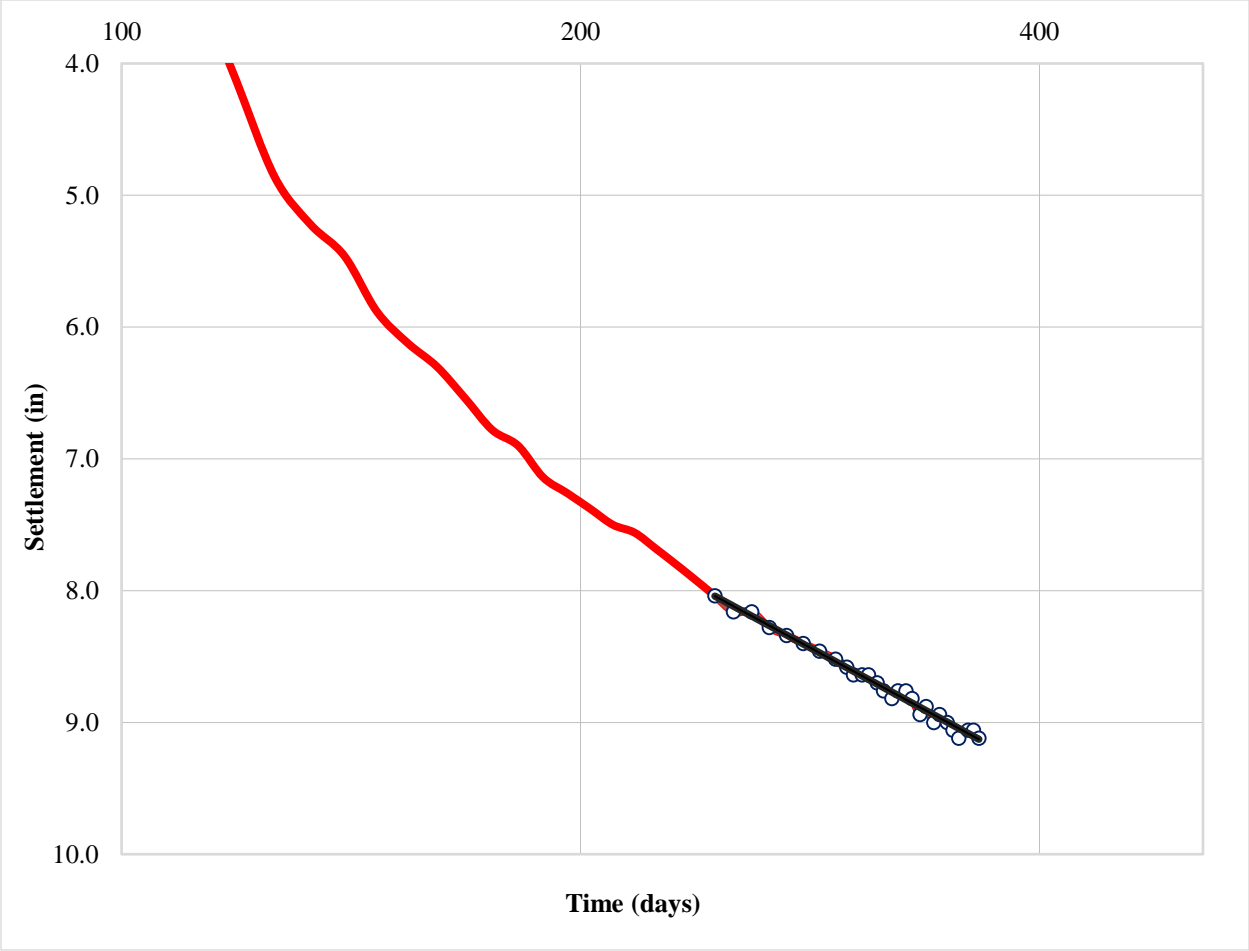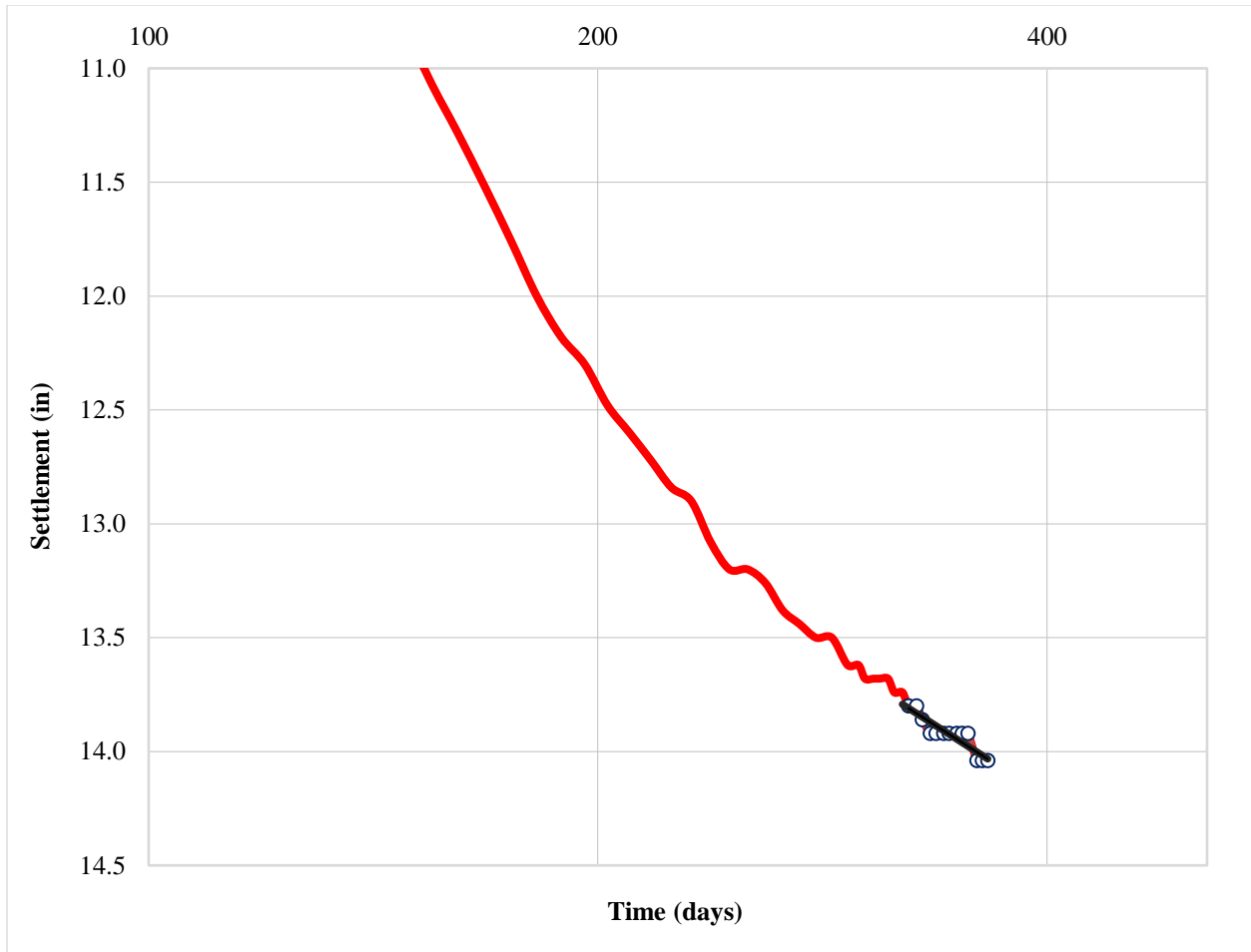
Figure C-8 Apparent log-linear behavior in the latter portion of fitted radial curve for the compression data between magnets 2 and 4 (M-2).
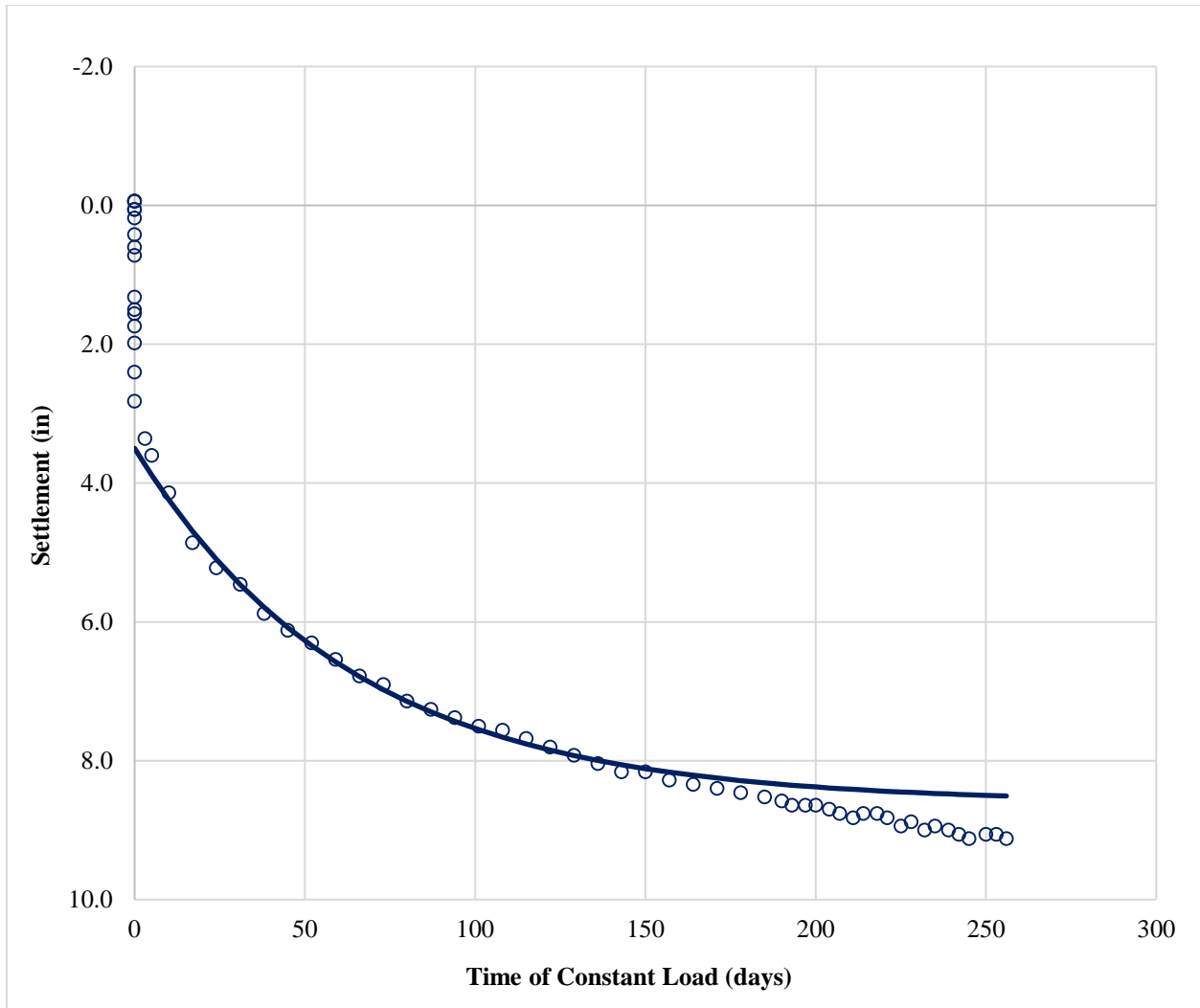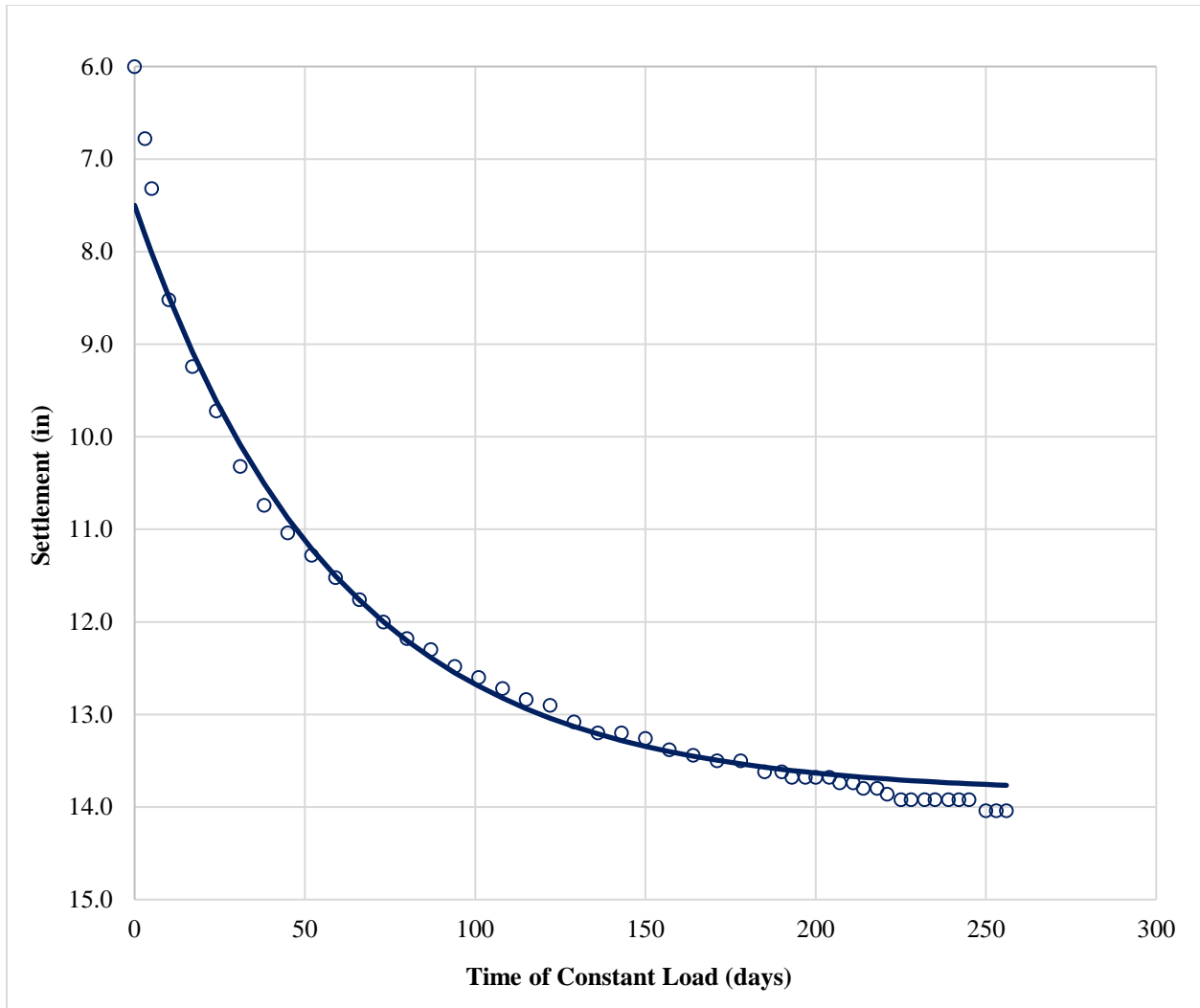
Figure C-9 Updated fitted curve for the compression data between magnets 2 and 4 (M-2) assuming end of primary consolidation settlement has already been reached.

Table C-2 Vertical drainage design variables for curve fitting field data for magnet extensometer M-2.

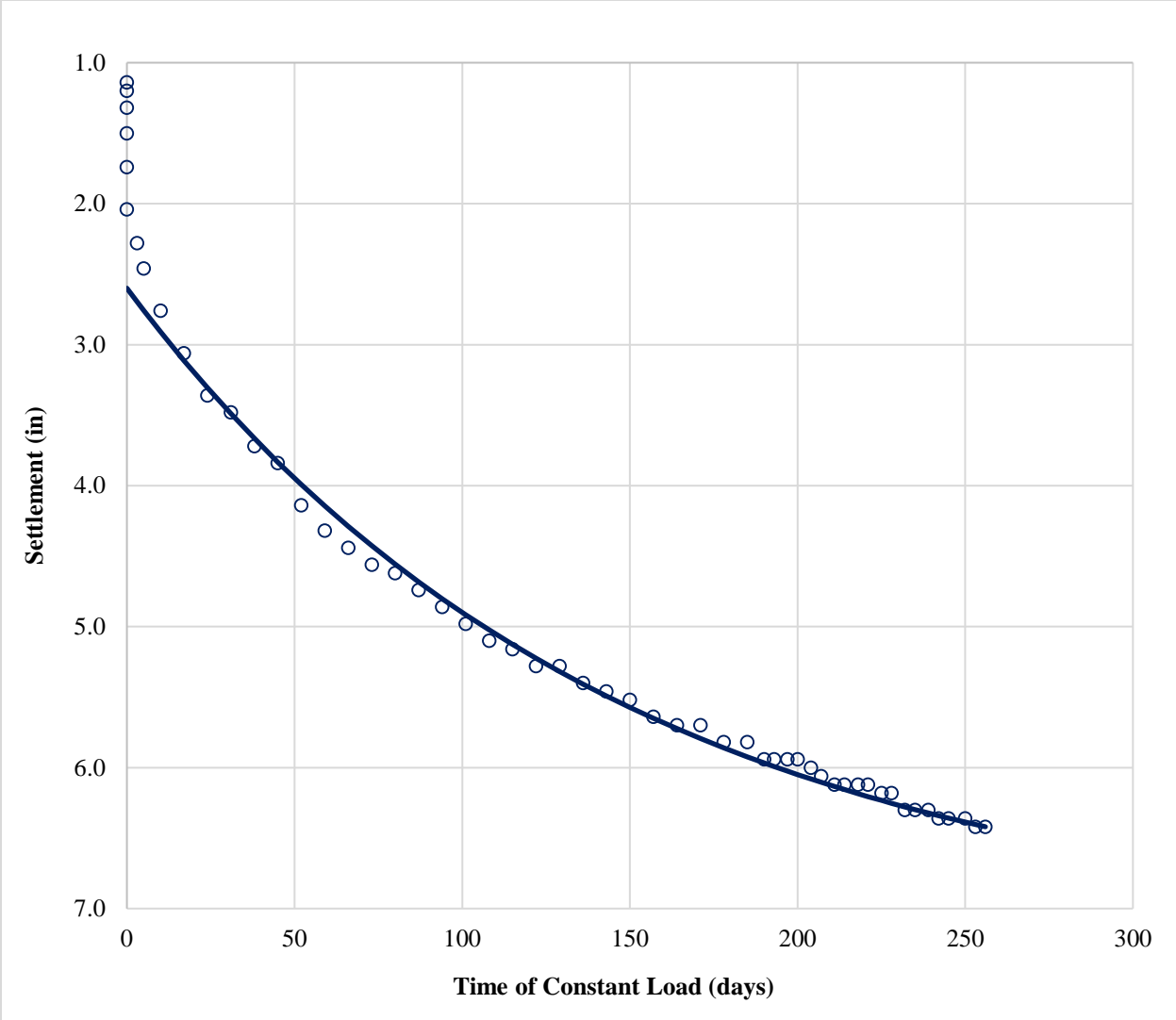| Magnet Interval	Day of Max Load	Settlement at start of curve (in)	Final settlement (in)	c_v/H^2
1-2	109	0.50	3.60	0.0017
0-1	109	0.52	3.50	0.0014
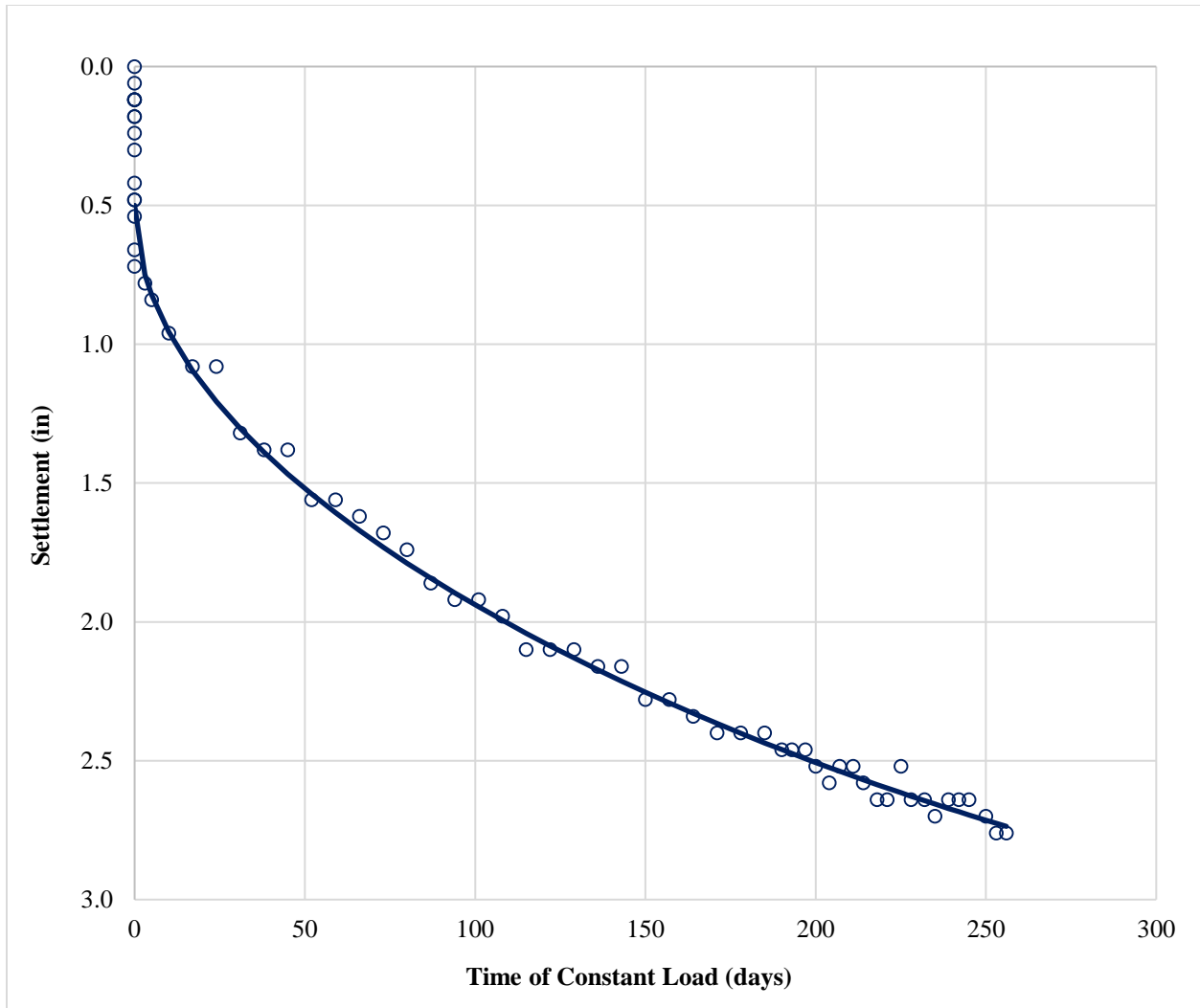
Figure C-10 Fitted vertical curve for the compression data between magnets 1 and 2 (M-2).
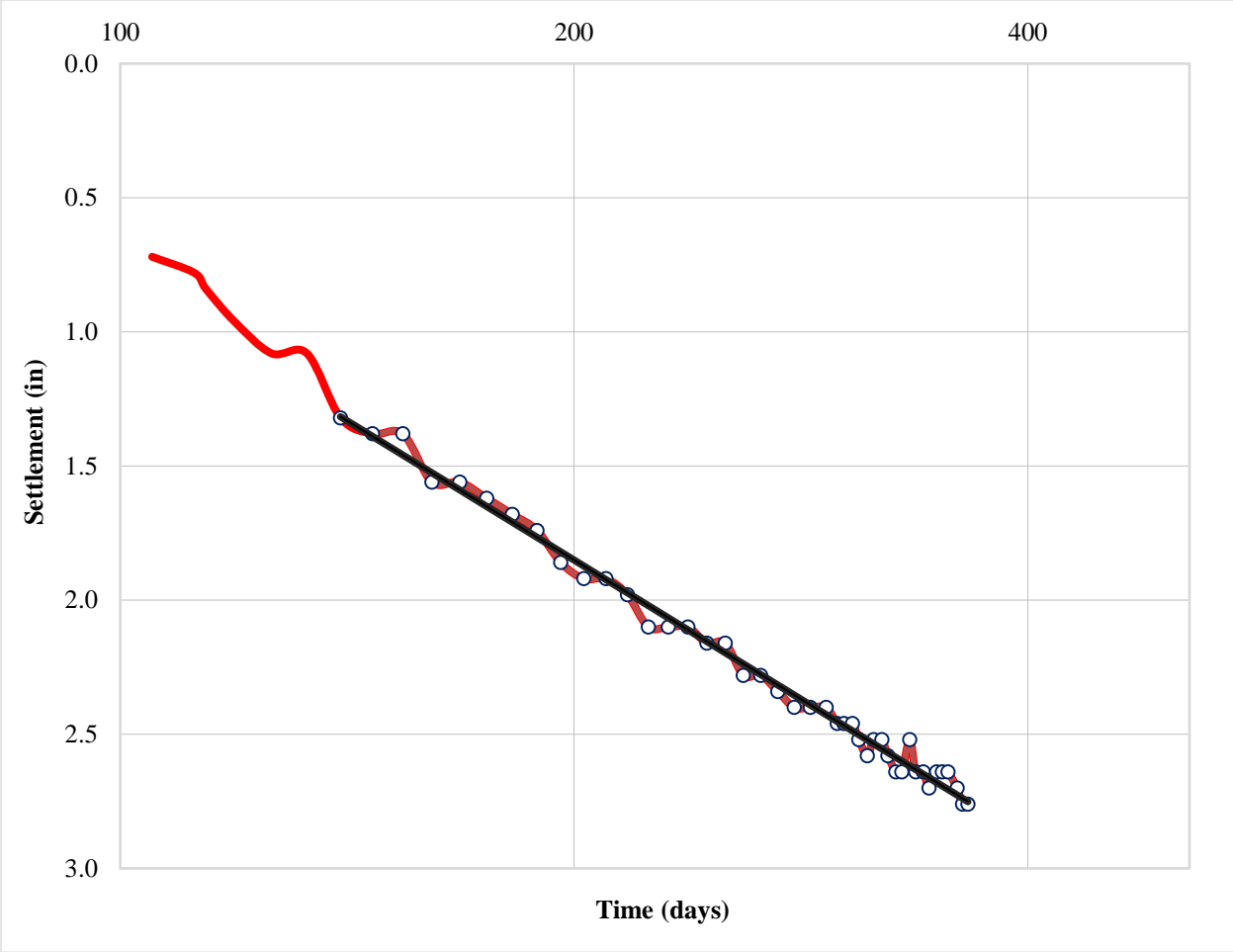
Figure C-11 Approximate log-linear center portion of the primary consolidation curve for the compression data between magnets 1 and 2 (M-2).
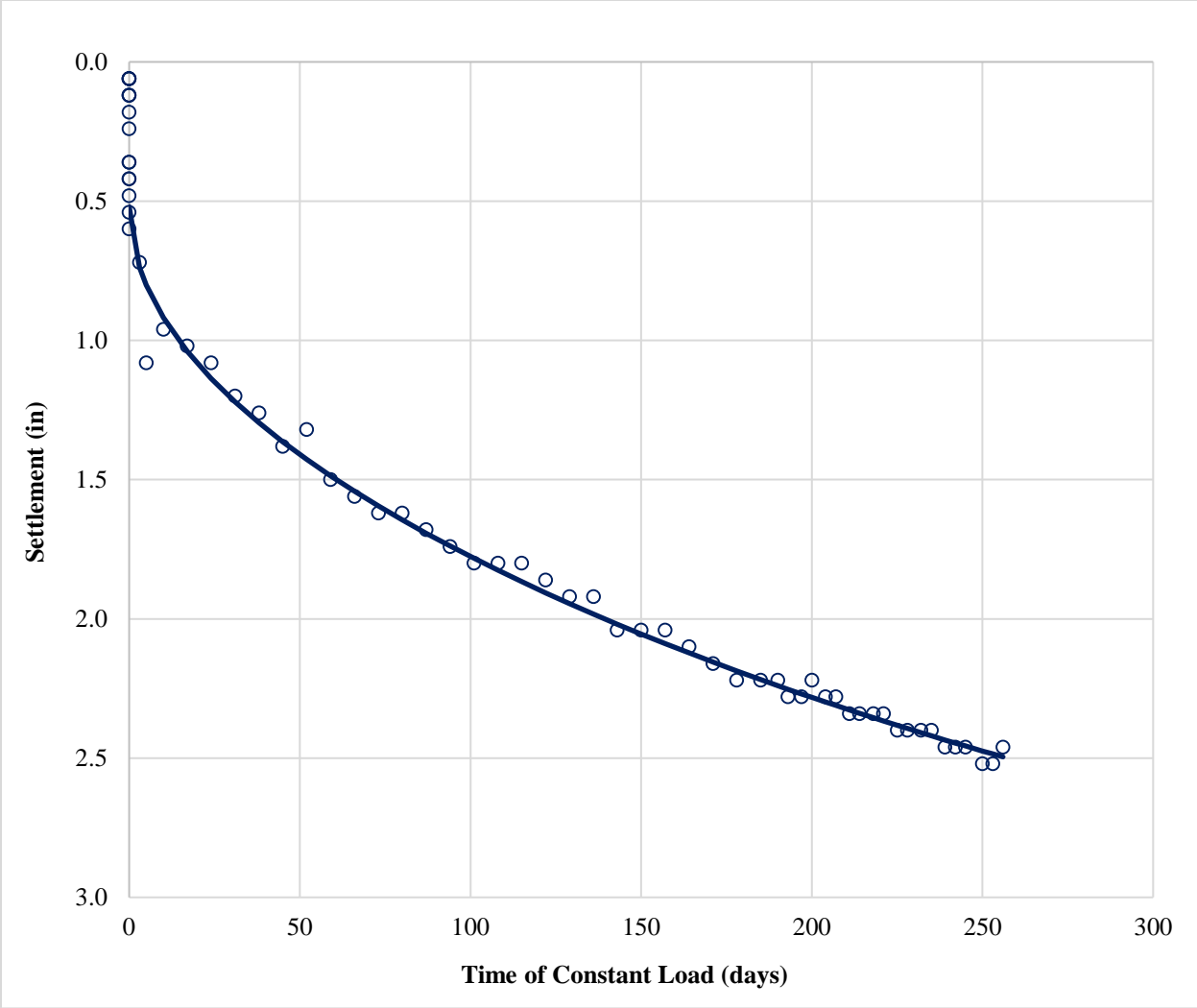
Figure C-12 Fitted vertical curve for the compression data between magnets 0 and 1 (M-2).
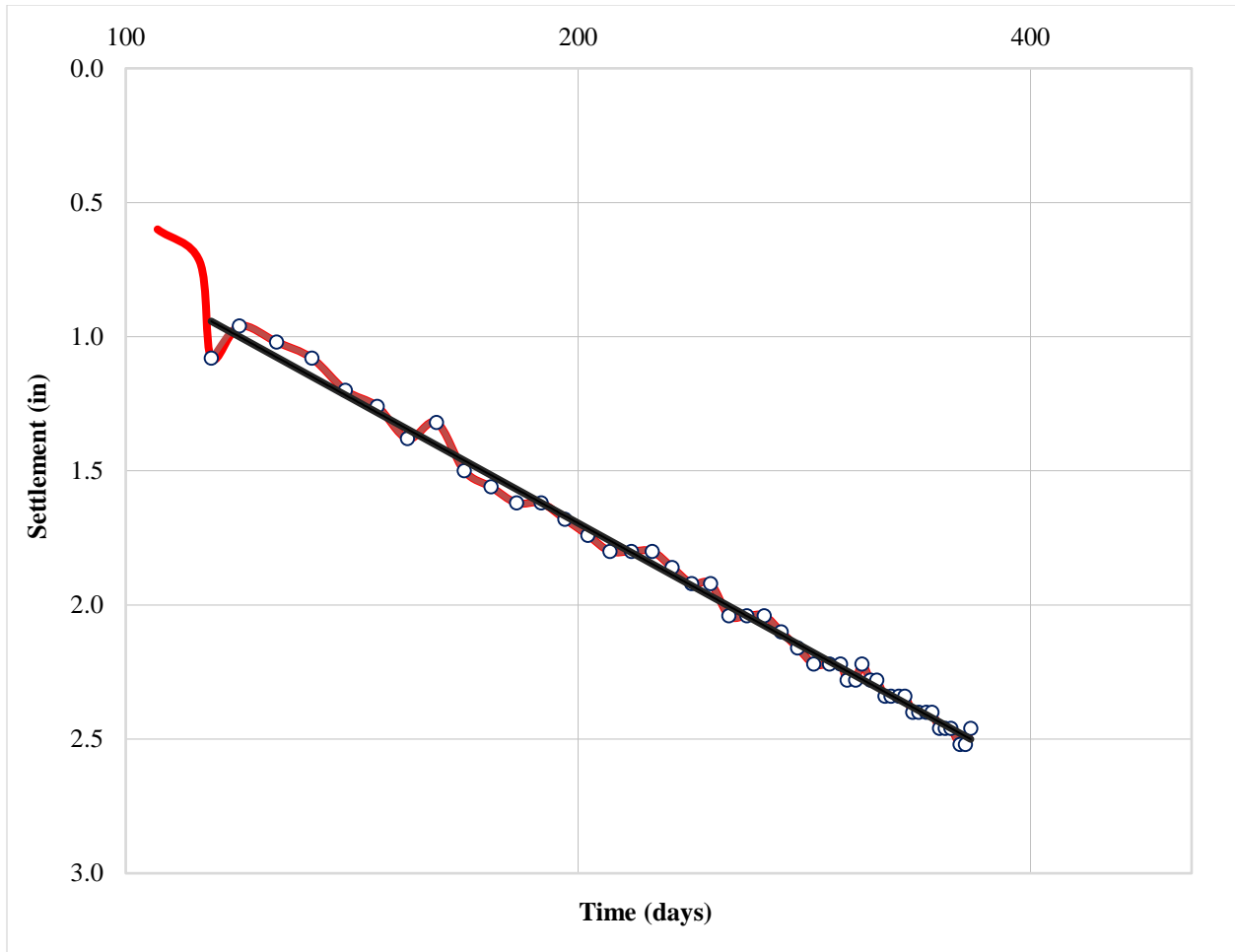
Figure C-13 Approximate log-linear center portion of the primary consolidation curve for the compression data between magnets 0 and 1 (M-2).

Table C-3 Radial drainage design variables for curve fitting field data for magnet extensometer M-2A.

Magnet Interval	Day of Max Load	Settlement at start of curve (in)	Final settlement (in)	c_h/d_e^2
2-3 w/out end of consolidation	109	7.80	14.20	0.0046
2-3 w/ end of consolidation	109	7.50	13.85	0.0056
1-2 w/out end of consolidation	109	2.60	7.20	0.0023
1-2 w/ end of consolidation	109	2.20	6.00	0.0044

Figure C-14 Fitted radial curve for the compression data between magnets 2 and 3 (M-2A).

Figure C-15 Apparent log-linear behavior in the latter portion of fitted radial curve for the compression data between magnets 2 and 3 (M-2A).
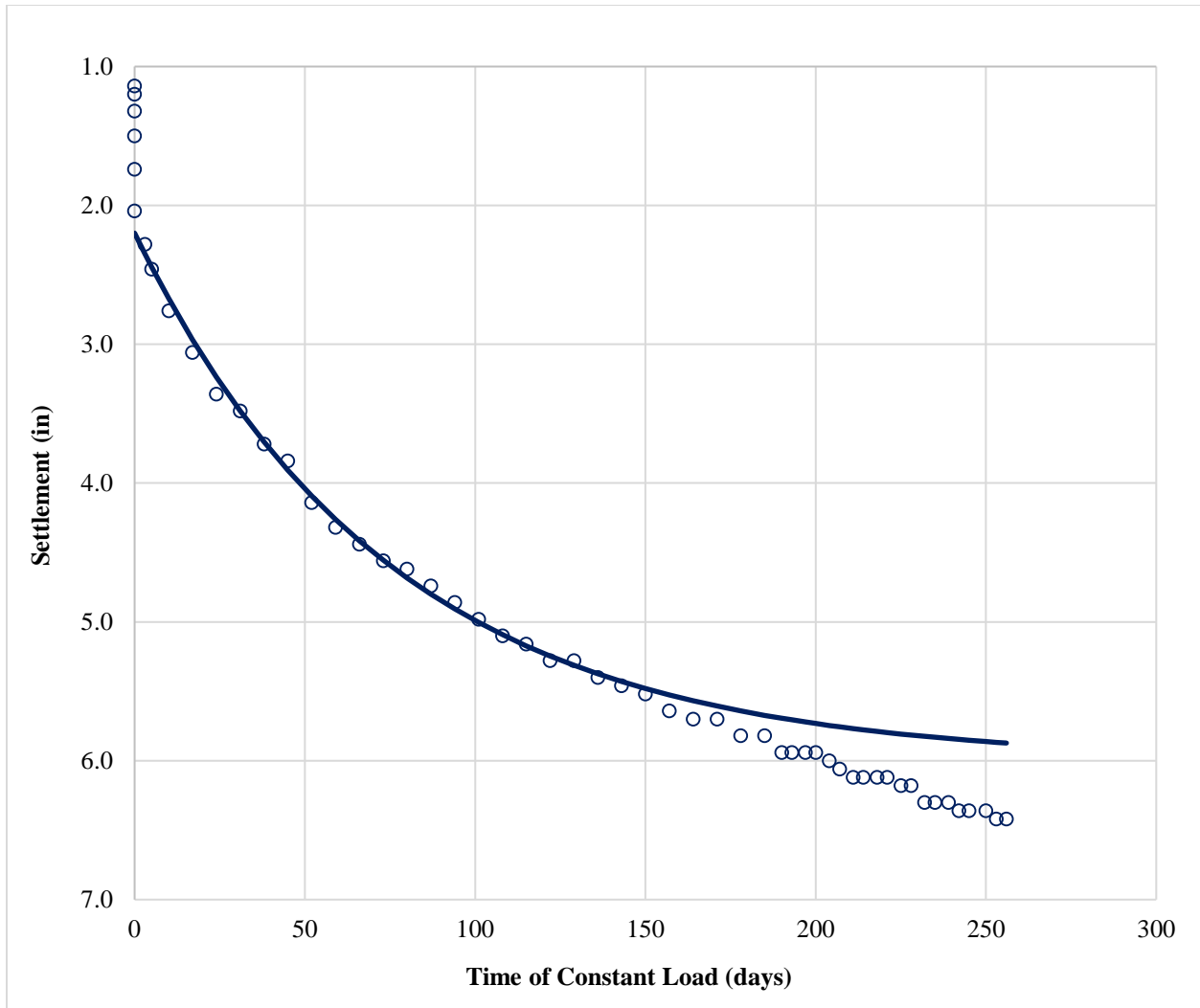
Figure C-16 Updated fitted curve for the compression data between magnets 2 and 3 (M-2A) assuming end of primary consolidation settlement has already been reached.
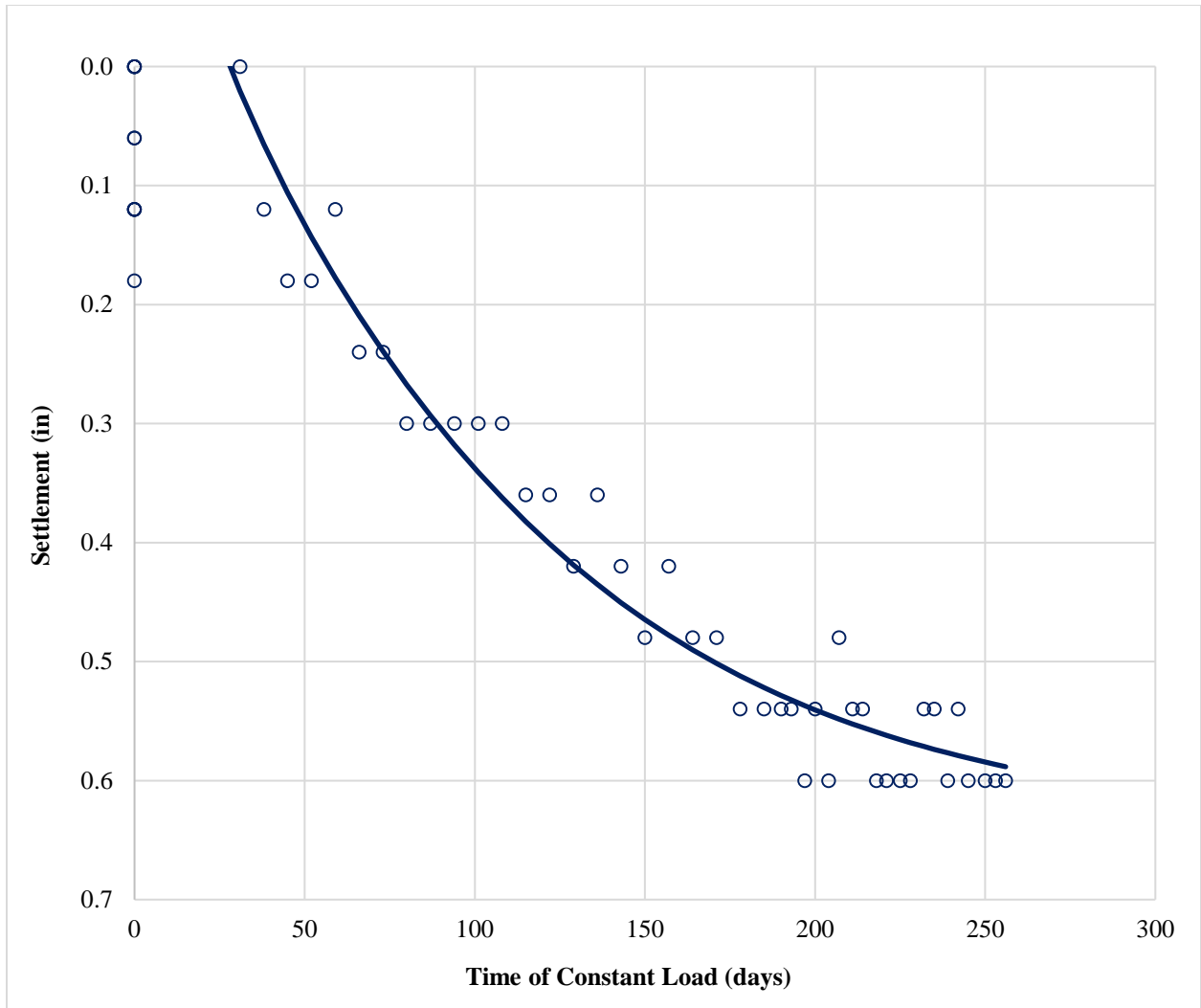
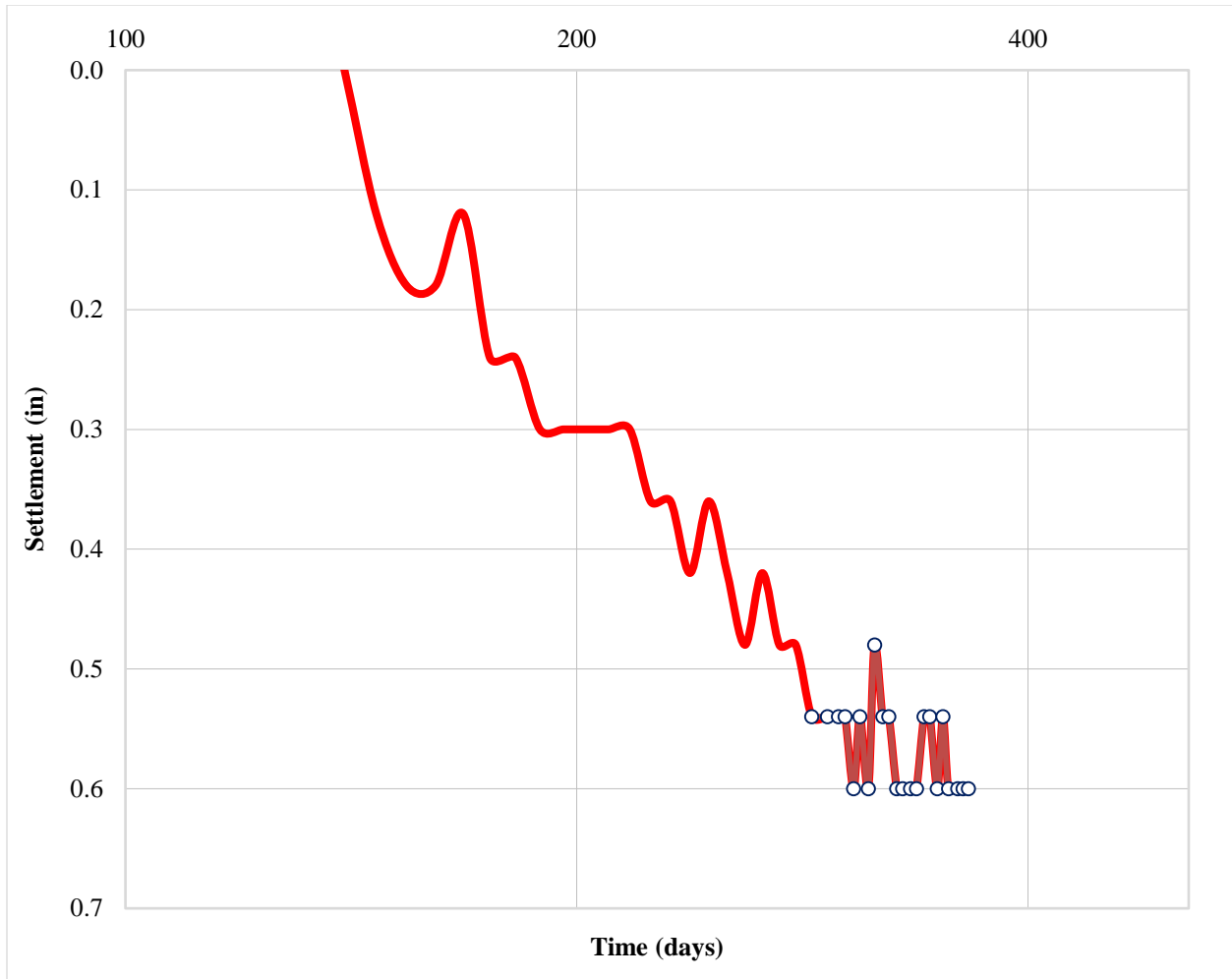**Figure C-17 Fitted radial curve for the compression data between magnets 1 and 2 (M-2A).**
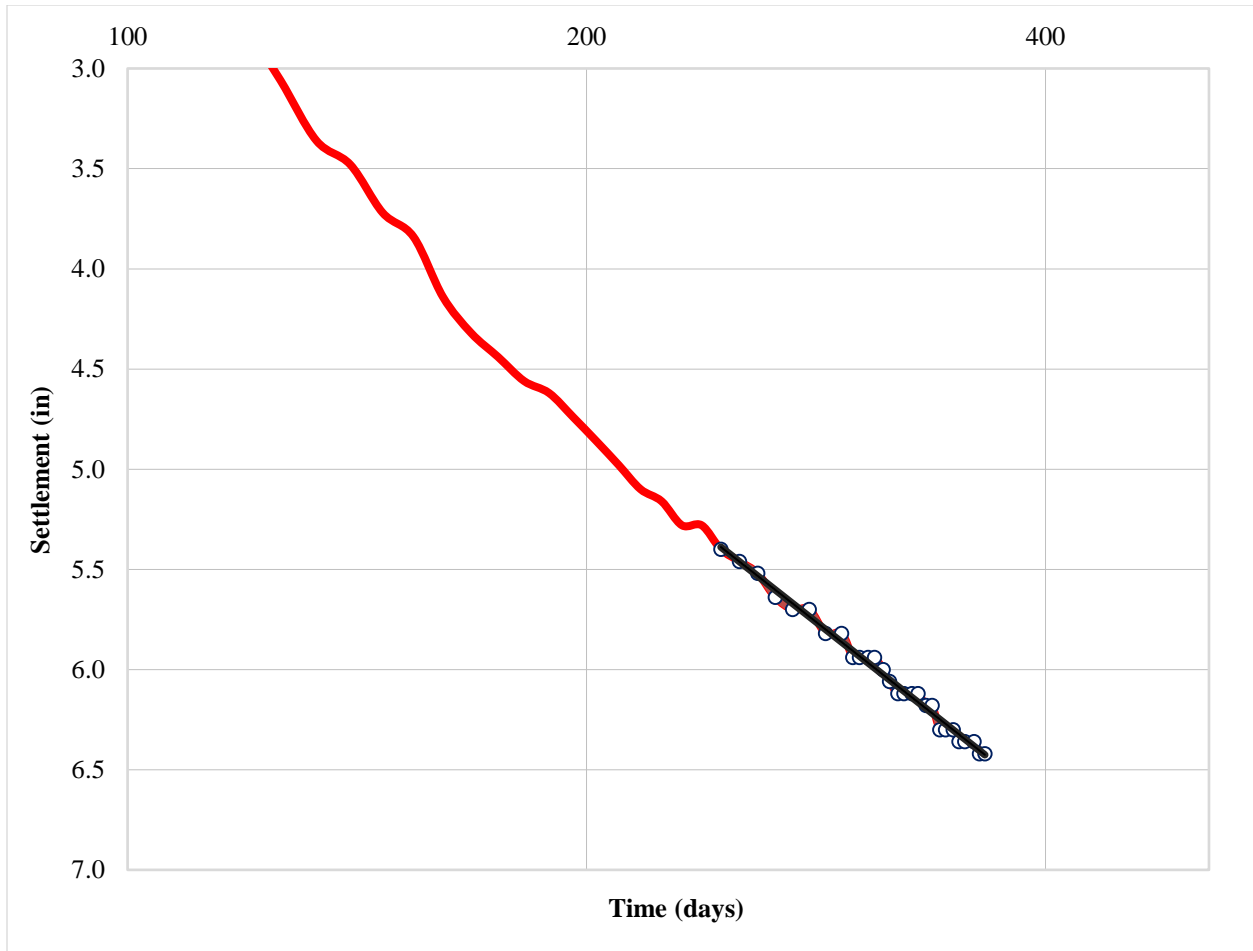
Figure C-18 Apparent log-linear behavior in the latter portion of fitted radial curve for the compression data between magnets 1 and 2 (M-2A).

Figure C-19 Updated fitted curve for the compression data between magnets 1 and 2 (M-2A) assuming end of primary consolidation settlement has already been reached.

Table C-4 Vertical drainage design variables for curve fitting field data for magnet extensometer M-2A.

Magnet Interval	Day of Max Load	Settlement at start of curve (in)	Final settlement (in)	c_v/H^2
1-2	109	0.50	3.60	0.0017
0-1	109	0.52	3.50	0.0014

Figure C-20 Fitted vertical curve for the compression data between magnets 0 and 1 (M-2A).

Figure C-21 Apparent log-linear behavior in the latter portion of fitted vertical curve for the compression data between magnets 0 and 1 (M-2A).

APPENDIX D: DATA AND FIGURES FOR FINITE DIFFERENCE METHOD

This appendix contains the finite difference fitted curves for the three different radial drainage intervals of magnet extensometer M-2.
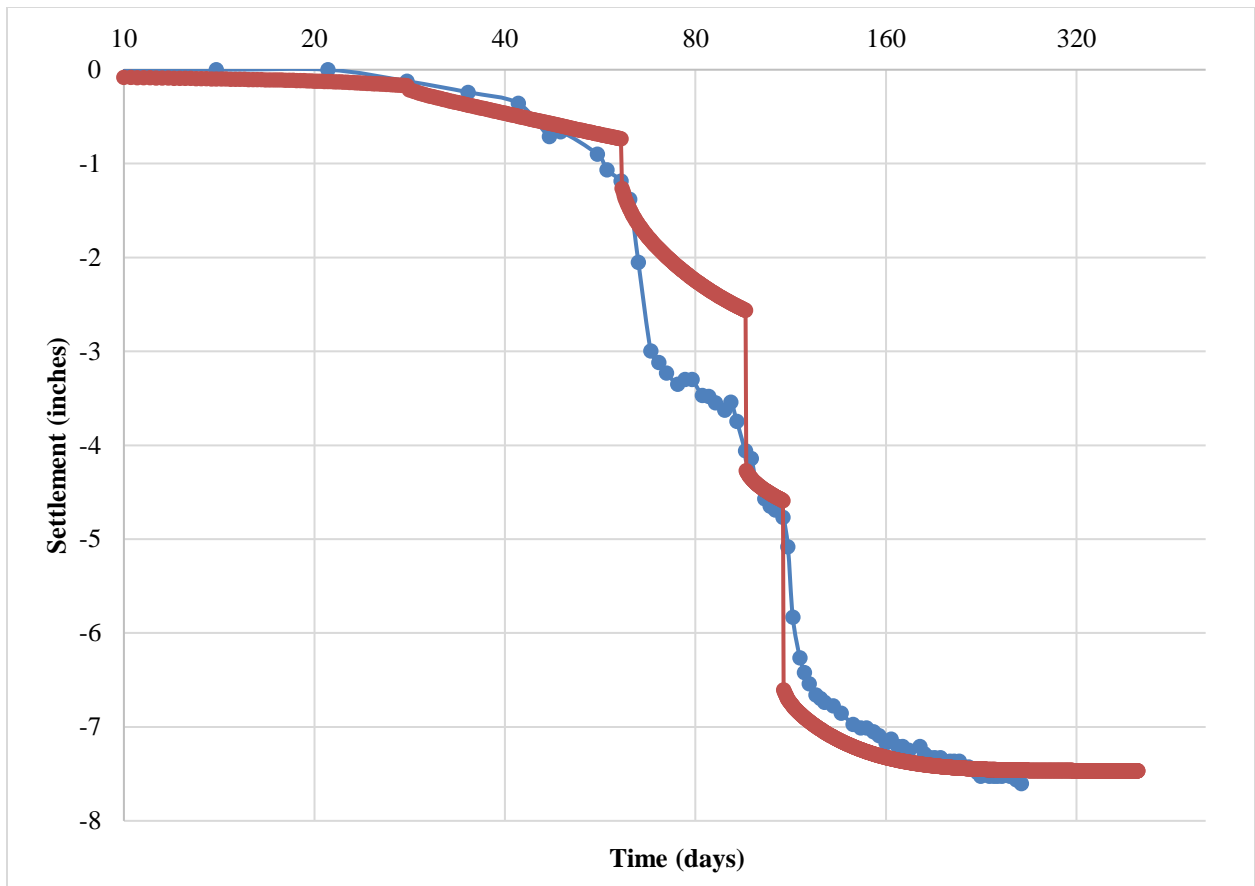
Figure D-1 Finite difference fitted curves with field data for settlement occurring between magnets 6 and 7 (M-2).
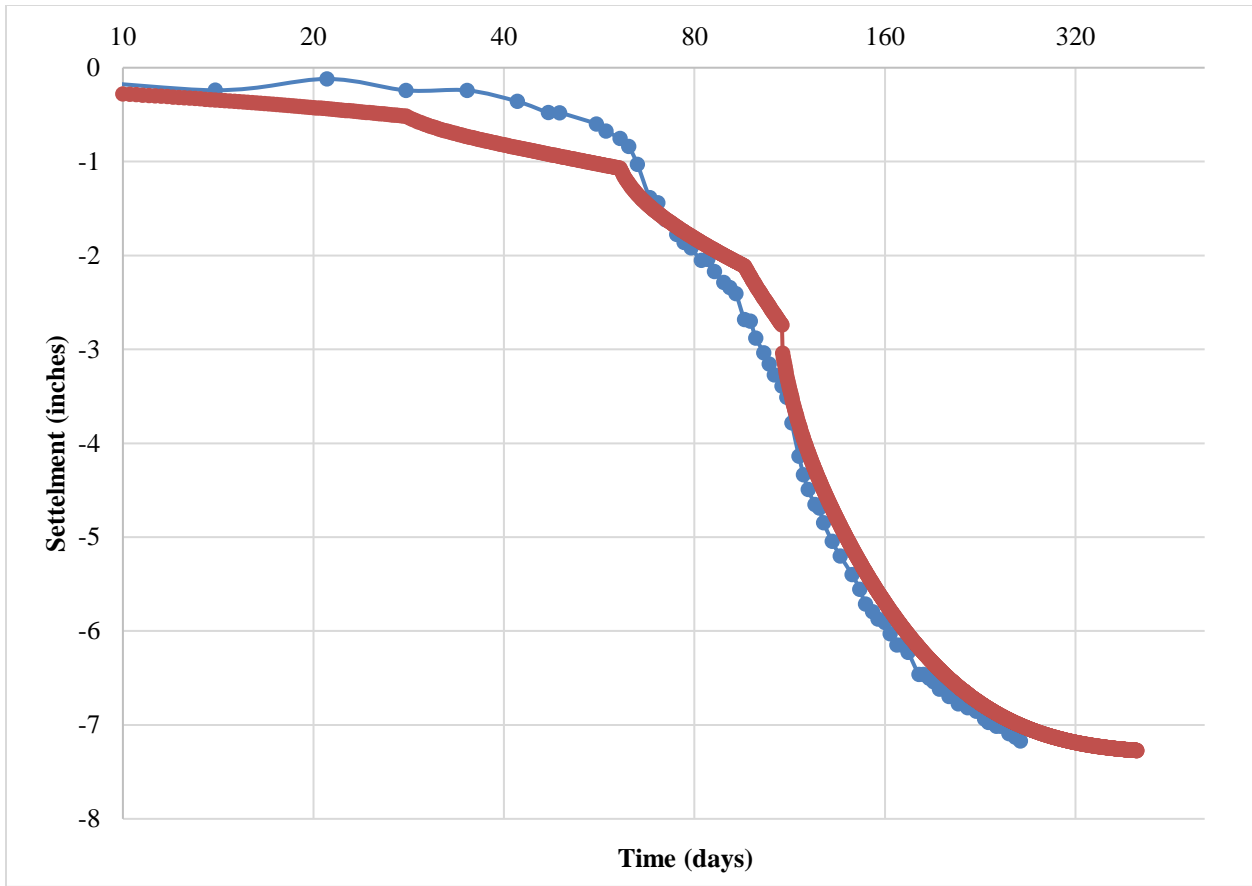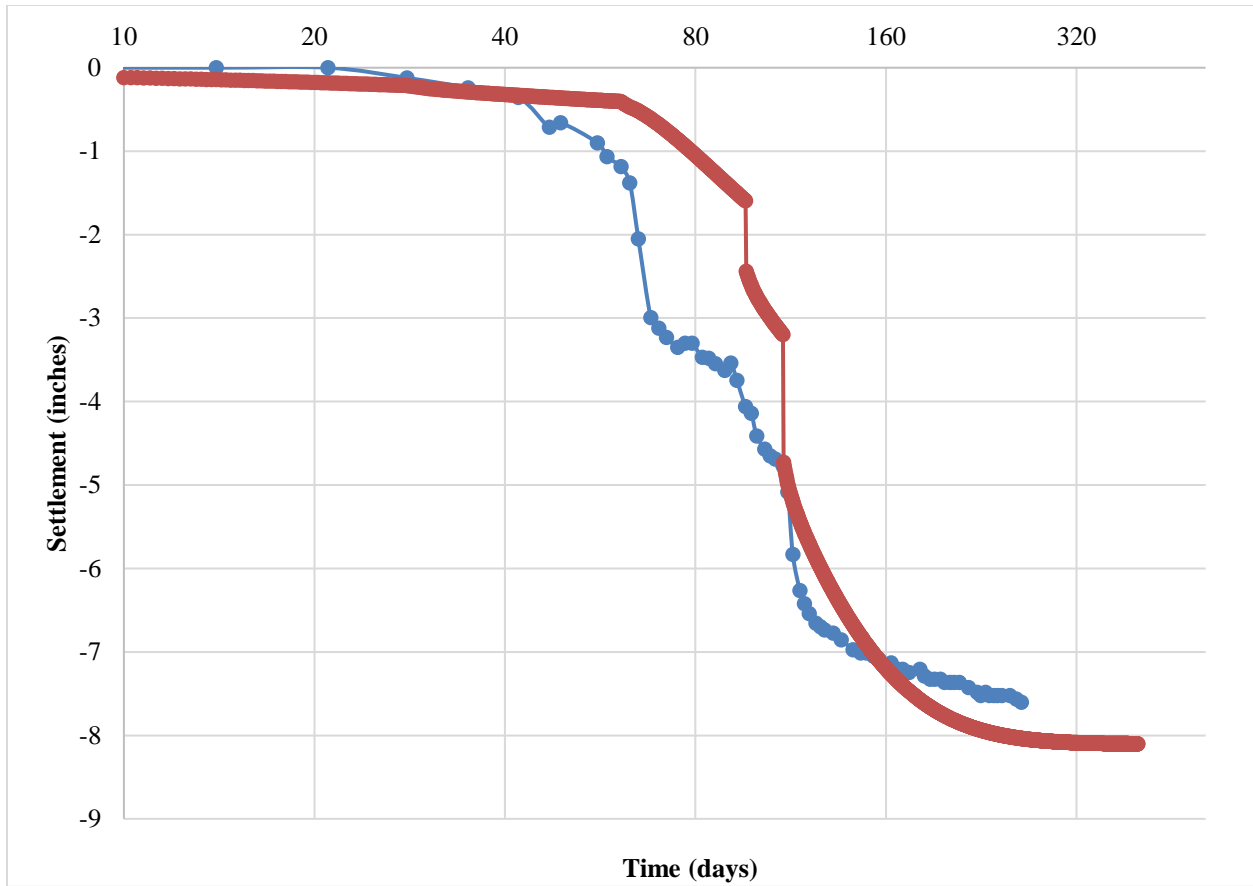
Figure D-2 Finite difference fitted curves with field data for settlement occurring between magnets 4 and 6 (M-2).

Figure D-3 Finite difference fitted curves with field data for settlement occurring between magnets 2 and 4 (M-2).